Study on Liposome Membrane Design for Recognition of Biomacromolecules and Control of Their Conformation

KEISHI SUGA

MARCH 2013

Study on Liposome Membrane Design for Recognition of Biomacromolecules and Control of Their Conformation

A dissertation submitted to

THE GRADUATE SCHOOL OF ENGINEERING SCIENCE

OSAKA UNIVERSITY

in partial fulfillment of the requirements for the degree of

DOCTOR OF PHILOSOPHY IN ENGINEERING

BY

KEISHI SUGA

MARCH 2013

PREFACE

This dissertation work was conducted under the supervision of Professor Hiroshi Umakoshi at the Division of Chemical Engineering, Graduate School of Engineering Science, Osaka University from 2007 to 2013.

The objective of this thesis is to establish the methodology to design the liposome membranes for the recognition of biomacromolecules, together with the control of their conformation and function. The physicochemical properties of liposome membranes and their interaction with biomacromolecules are investigated, especially focusing on the nano-domain formed at the membrane, in order to understand the key factors for the recognition of biomacromolecules.

The author hopes that this research would contribute to design the liposome membrane surface as a functional platform of the recognition of biomacromolecules and, also, control their functions. Utilization of the "*Bio-Inspired*" membranes will contribute to the development of innovative chemical and biochemical processes, such as *in vitro* synthesis of proteins, drug delivery system for transfection of polynucleotide.

KEISHI SUGA

Division of Chemical Engineering
Graduate School of Engineering Science
Osaka University

Contents

Summary

Liposome membrane is a self-assembly of phospholipid bilayer with a 5 nm thickness and affords an interface between polar surface and non-polar inner membrane. The liposome membrane has been reported to interact with the biomacromolecules, and can therefore be utilized as a platform of their accumulation and functionalization. In this study, the method to design the liposome membrane for the recognition of biomacromolecules and the control of their conformation was studied, focusing on the micro-phase separation and nano-domain on the liposome in order to utilize the liposome membrane as a platform of bio-/chemical processes.

In Chapter 1, the role of liposome membrane on the *in vitro* gene expression in an *E coli* cell-free translation system was studied, in order to find out the specific interaction of the lipid membrane with biomacromolecules. The charged liposomes were found to regulate GFP expression at the translation and folding steps via interaction with single-stranded RNA molecules and GFP polypeptides. Characterization of biomacromolecules indicated that the nascent mRNA and GFP polypeptide were unstable, and were likely to interact with the liposomes via electrostatic, hydrophobic, and hydrogen bonding interactions.

In Chapter 2, the physicochemical properties of 1,2-dioleoyl-*sn*-glycero-3-phosphocholine/1,2-dipalmitoyl-*sn*-glycero-3-phosphocholine (DOPC/DPPC) and DOPC/cholesterol (DOPC/Ch) binary lipid mixtures of large unilamellar vesicles (LUVs) were characterized, and nano-sized ordered domains were detected by using a newly-developed TEMPO quenching method. Analysis of membrane fluidity and polarity revealed the existence of immiscible "microscopic" segregated regions in the DOPC/DPPC binary lipid mixture of LUVs. The TEMPO quenching method clarified that the nano-sized ordered domains with 13-36 Å were formed in the DOPC/DPPC and DOPC/Ch liposomes. The phases diagram of the liposome membrane was clearly shown based on their physicochemical properties, focusing on fluidity, polarity, microscopic phase separation, and nano-sized domain.

In Chapter 3, the method to control the specific interaction of the liposomes with biomacromolecules was clarified, by selecting single-stranded RNAs (mRNA, tRNA) as case study. It was shown that mRNA was bound to the heterogeneous cationic liposome in an "active" state. Raman and Fourier transform infrared (FTIR) spectroscopic analysis clearly indicated that the nucleobases (A, G, C) in single-stranded RNAs interacted with the lipid molecules. Analysis of circular dichroism spectra indicated that the cationic liposome in disordered phase denatured the conformations of both the single-stranded loop (θ_{208}) and double-stranded (θ_{265}) regions in mRNA, while the heterogeneous cationic liposome partially denatured the mRNA conformation. The Ch-modified liposomes with the micro-domain were found to interact with the cytosine residue. The key of liposome membrane design for the biomacromolecular recognition can be understood as "co-induction" of multiple interactions, such as (i) electrostatic interaction, (ii) hydrophobic interaction, (iii) entropic forces with the dehydration of membrane surface, (iv) hydrogen bonding interaction, (v) micro-domain formation at the contacting surface.

In Chapter 4, the scheme of the liposome membrane design for the recognition of biomacromolecules was finally established, together with the control of their folding and function. The liposome membranes were, in practice, designed for recognition of biomacromolecules, such as hammerhead ribozyme (HHR) and tRNA. 1,2-Dioleoyl-*sn*-glycero-3-phoshoethanolamine/DPPC (DOPE/DPPC) (8/2) liposome was designed for the recognition of HHR, showing that HHR can bind at the interface regions. As a result, its conformational change was induced with the enhancement of its activity, despite of the absence of Mg^{2+}. In the case of tRNA, DOPC/sphingomyelin/Ch (4/3/3) with the nano-sized domain (48-76 Å) was found to recognize the stem and loop regions in tRNA, resulting in the induction of its conformational change.

A general strategy to design the liposome membrane as a platform for the recognition of biomolecules, accompanying with their folding and functionalization, was thus proposed based on the physicochemical properties of liposome membranes and their interaction with the single-stranded RNA and polypeptide molecules. The obtained results in this study were summarized in the general conclusions together with suggestions for future works.

General Introduction

A biomembrane can act both as a "physical boundary" that can enclose a variety of biomolecules and as an "active interface" that can transduce the signal across the membrane. A biomembrane, which consists of various kinds of phospholipid, membrane protein and other chemicals (**Fig. 1**), plays essential roles in permeability, signal transduction, membrane transport, and biogenesis (Luckey, 2008). It is in general known that the biomembrane of biological cell acts as a physical barrier that separates the biomolecules within a cell structure from the external environment. The biomembrane can therefore protect inner compartments from the environmental stresses, such as heat stress, pH changes, and oxidative stress. The typical characteristics of biomembranes are known as membrane fluidity, raft (micro-domain), surface charge density, *etc.*, which can be related to the interaction of the above membranes with biomacromolecules, such as proteins, enzymes, DNAs, and RNAs. It has been reported that the liposome, a model biomembrane with a variety of size (30 ~10000 nm), can regulate the biological reactions (Walde, 2010); the liposome reactivates the fragmented superoxide dismutase (SOD) under an oxidative condition in the presence of Cu^{2+} and Zn^{2+} (Tuan *et al.*, 2008); the liposome modified with Mn-PyP exerts both SOD activity and peroxidase activity (Umakoshi *et al.*, 2008); the liposome itself also affects the *in vitro* expression of green fluorescent protein (GFP) (Bui *et al.*, 2008). One of the essential roles of the biomembranes is to localize the functions of biomacromolecules on their membrane surfaces (*e.g.*, the ribosome can bind to the endoplasmic reticulum membrane). It is therefore important to understand their roles in recognition of biomacromolecules and functionalization of them.

A general design for novel biofunctional materials is definitely required in order to develop innovative bio-/chemical processes. A variety of specific recognition of biomacromolecules and chiral materials are known to be achieved in biological cellular

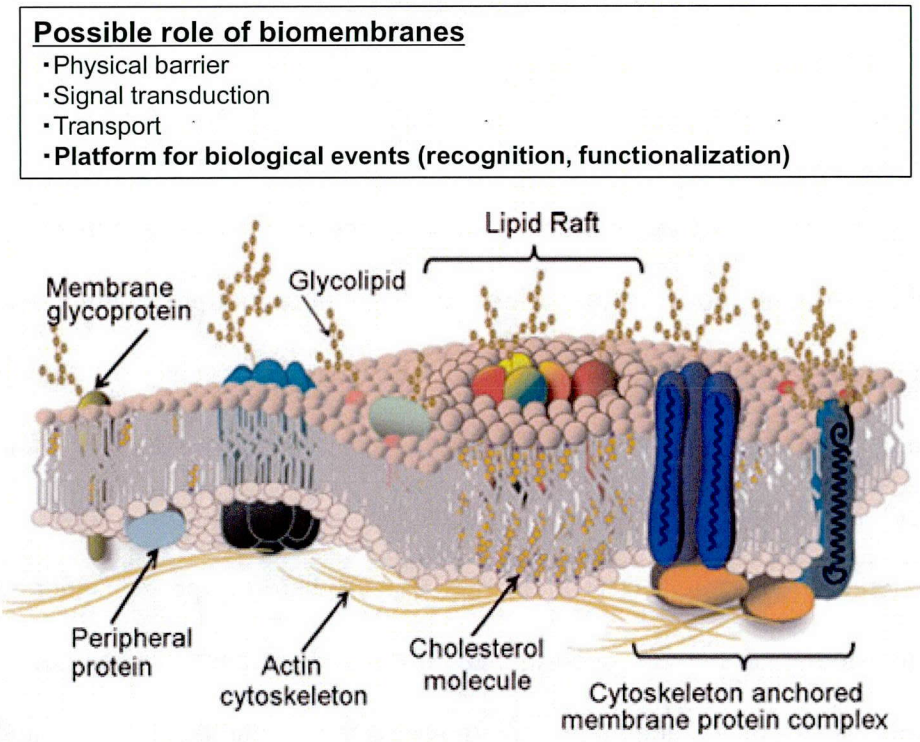

Fig. 1 Structure of biomembranes and their roles (Collawn *et al.*, 2008).

systems to maintain the cellular homeostasis through nano-machineries relating to metabolism and also gene expression (Tzareva *et al.*, 1994; Korostelev *et al.*, 2006). For example, RNA aptamers have been developed as molecular recognition tools, which recognize various kinds of biomolecules (*e.g.*, flavin mononucleotide (FMN), adenosine monophosphate (AMP), arginine, Tobramysin, and so on) (Patel *et al.*, 2000). However, there are some difficulties to perform the selective separation or molecular recognition in designing the above-mentioned artificial systems owing to their limited properties in physicochemical potentials. A key of the biofunctional design is a molecular recognition, which can act as a "*glue*" of different molecules and can induce an "*emergence*" on the self-assembly. As an example of "*Bio-Inspired*" materials, the molecular imprinting technology has been developed, where the self-assemblies, such as polymer matrixes with the micro- or nano-sized cavities fitting precisely to the template molecule, can recognize the target biomolecules (Caldorera-Moore *et al.*, 2009), as well as the "lock and key" model in enzyme and substrate. It is therefore

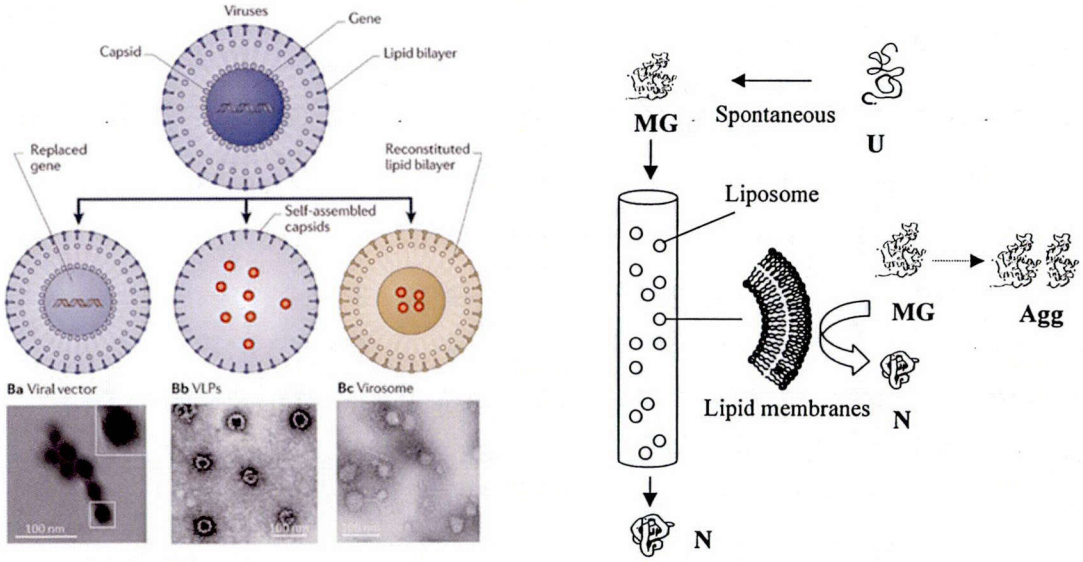

Viruses for DDS
(Yoo, *et al.*, 2008)

Liposome-immobilized chromatography
(Yoshimoto, *et al.*, 1998)

Fig. 2 "*Bio-Inspired*" materials utilizing their recognition potentials.

necessary to develop "*Bio-Inspired*" systems (Yoo *et al.*, 2011) by utilizing "self-assemblies" as effective platforms for recognition (**Fig. 2**).

There are various kinds of self-assemblies, which play fundamental roles in living cell systems. Lipid membranes, one of essential components of a cell, have also been utilized as "*Bio-Inspired*" materials for drug carrier, biosensor, and as platform of biochemical events (**Table 1**). Focusing on the molecular recognition, self-assembly systems play an important role on their interaction with target molecules (Borocci *et al.*, 2003; Banchelli *et al.*, 2007; Caldorera-Moore *et al.*, 2009). Based on the previous reports, the liposomes have been shown to recognize biomacromolecules through the combined interactions, such as electrostatic, hydrophobic, and hydrogen bonding forces; (i) the liposomes interacted with damaged proteins and fragmented enzymes (Yoshimoto *et al.*, 2000; Tuan *et al.*, 2008); (ii) the anionic liposomes induced spherulitic aggregation of amyloid β peptides (Shimanouchi *et al.*, 2012); (iii) the liposomes regulated the *in vitro* gene expression (Bui *et al.*, 2008; Bui *et al.*, 2009); (iv) the liposomes induced conformational change of single-stranded RNAs (Suga *et al.*,

Table 1 Self-assemblies utilized as "*Bio-Inspired*" systems

Reference	Lipid membrane type and its application
Yoshimoto *et al.*, 1998	Liposome-immobilized chromatography for detection of denatured proteins
Peetla *et al.*, 2009	Liposomes utilized as a model cell membrane for lipid-drug interaction
Yoo *et al.*, 2011	Design of the virus carriers for drug delivery
Shimanouchi *et al.*, 2010	Liposome-immobilized membrane chip analysis for the membrane-membrane interaction
Cerritelli *et al.*, 2007	Block copolymer vesicles for intracellular drug delivery
Caldorera-Moore *et al.*, 2009	Molecular imprinting polymers as intelligent and responsive biomaterial-based systems
Sugaya *et al.*, 2010	Liposome-immobilized hollow fiber membrane module for dialysis of damaged protein

2011). It is therefore suggested that the liposomes can be regarded as the "*Bio-Inspired*" self-assemblies, and can be utilized as functional platforms for recognition and functionalizing of target biomacromolecules.

The basic structure of a lipid membrane is the lipid bilayer at a 5 nm thickness with the interface between polar membrane surface and non-polar inner membrane, where lipid molecules can freely diffuse, depending on the phase state of the lipid membrane (Jeon *et al.*, 2012). The typical characteristics of lipid membranes, such as liposome systems, are known as (i) "macroscopic" characteristics as "system", (ii) "microscopic" characteristics as "lipid molecules", and the (iii) "dynamic behavior" of the membrane in the variation of surrounding condition and in the interaction with a variety of biomacromolecules (**Fig. 3**). Several techniques have been developed to understand the phase state of lipid membranes as summarized in **Table 2**. Sphingomyelin (SM) and cholesterol (Ch) are typical components that can form the raft domains in liquid-disordered (l_d) membranes (De Almeida *et al.*, 2005). Because the formation of membrane domains depends on the lipid composition and surrounding environment (*e.g.*, temperature), the phase diagrams of membranes in binary and ternary lipid mixtures have been systematically studied as summarized in **Table 3**. The

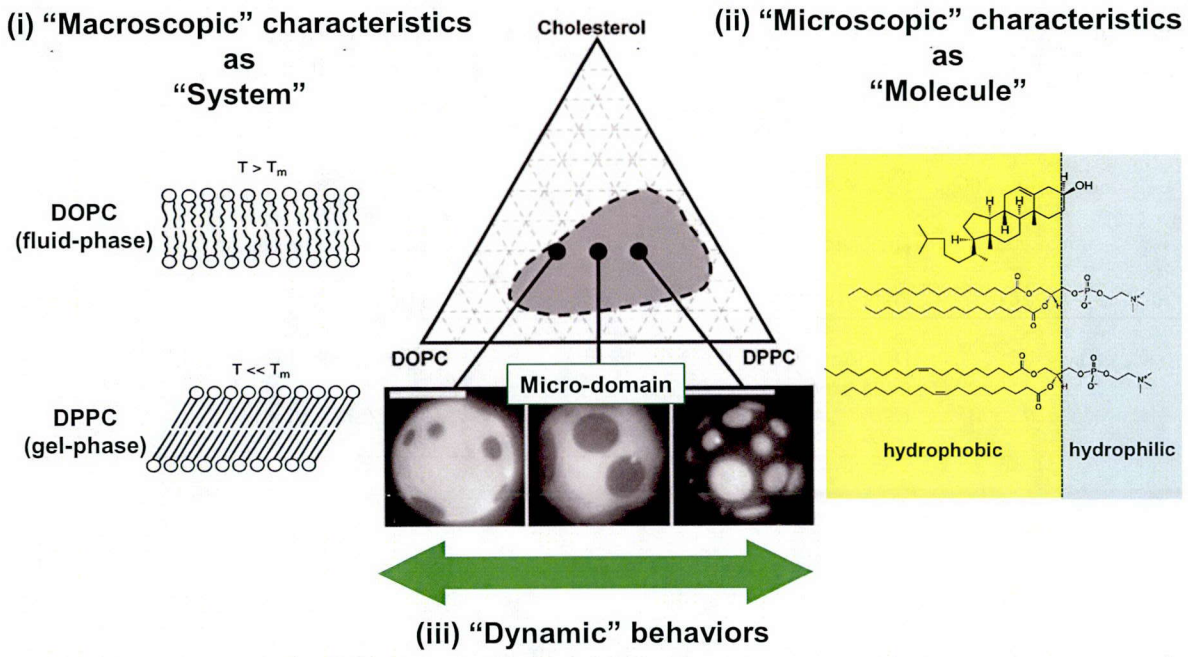

Fig. 3 Characteristics of lipid membranes.

Table 2 Summary of the phase diagram of the lipid membranes

Reference	Components	Method	Existing phases *
Veatch *et al.*, 2005	DOPC/PSM/Chol DOPC/DPPC/Chol	Fluorescence microscopy	One-liquid (L_α, L_o), two-liquids (L_α+L_o), liquid-solid (L_α+S_o)
Juhasza *et al.*, 2011	DOPC/DPPC	Confocal fluorescence microscopy	L_d, gel, fibril
Fox *et al.*, 2007	DPPC	DSC, Raman spectroscopy	L_α, P_β', L_β, L_c
De Almeida *et al.*, 2003	POPC/PSM/Chol	Fluorescence microscopy, FRET	L_d, L_d+L_o, L_o, S_o, L_d+S_o, L_o+S_o, L_d+L_o+S_o
de Lange *et al.*, 2007	DPPC/Chol	Raman spectroscopy	L_d, L_o, S_o, L_d+S_o, L_o+S_o
Schmidt *et al.*, 2009	DOPC/DPPC	^{2}H NMR	L_α, gel, sub-gel, L_α+gel, L_α+sub-gel, L_α+gel+sub-gel

* Phase state of lipid membrane
L_α, L_d : disordered liquid crystalline; liquid-disordered phase
L_o : ordered liquid crystalline; liquid-ordered phase with Ch and sphingolipids
L_β, S_o, gel : lamellar orthorhombic; solid-ordered phase
L_c, sub-gel: lamellar crystalline orthorhombic; sub-gel phase
P_β' : hexagonal periodical; ripple-gel phase

Table 3 Summary of the membrane domain size

Reference	Liposome/vesicle	Domain size (method)
Parasassi *et al.*, 1995	DMPC/Ch Ch 30~70 mol%	20 ~ 50 [Å] (fluorescence)
Pathak *et al.*, 2011	bSM/POPC/Ch (1/1/1)	~150 [Å]/ 80 ~100 [Å]/ < 40 [Å] (FRET)
De Almeida *et al.*, 2005	PSM/POPC/Ch	> 75 ~ 100 [nm] (Microscopy and FRET), < 20 [nm] (FRET only)
Veatch *et al.*, 2005	DOPC/PSM/Ch	1 ~ 5 [μm] (Microscopy)
Heberle *et al.*, 2010	DSPC/DOPC/Ch	~ 5 [nm] (ESR)
Šachl *et al.*, 2011	DOPC/SM/Ch/DOPG/DPPE/biotine (29/39/25/5/2)	< 20 [nm] (FRET)
Kiskowski *et al.*, 2007	DOPC/DPPC/Ch (40/40/20)	6 [nm] (Simulation)

membrane characteristics, which can be observed by a microscopy, are herein defined as "macroscopic" properties, although these techniques can clarify the "visible" information of membranes. The "micro-"domains, which are almost smaller than 100 nm and cannot be visualized by a microscope, are observed by using a fluorescence resonance energy transfer (FRET) technique, where the domain size has been reported to be ca. 20 nm (De Almeida *et al.*, 2005). However, conventional techniques are known to have some restrictions on hardware for the analysis (*e.g.*, a high-quality microscope) and have not yet enabled us to detect nano-sized domains smaller than < 5 nm. It is therefore important to characterize "microscopic" properties of lipid membranes and detect "nano-"sized domains in order to understand the behaviors of lipid molecules and utilize the lipid membrane as a platform of the recognition and functionalization of biomacromolecules.

For explaining the essential roles of lipid membranes, it is important to consider the localization of functions on the membranes through the binding of biomacromolecules (Walde, 2010). It seems that the binding of biomacromolecules can be well related with the "macroscopic" and "microscopic" properties of the lipid membrane. It has been previously

reported that lipid membranes affect not only the recognition of proteins and enzymes but also the conformation and function of them (Umakoshi *et al.*, 2009; Ngo *et al.*, 2010; Umakoshi *et al.*, 2012), where the "micro-"domains formed in the liposomes can contribute to recognition, folding, and functionalization. In most cases, a protein folding process is irreversible, while a folding of polynucleotide is reversible. In both cases, the conformational stability of biomacromolecules is absolutely-required factors to induce and regulate their functions (**Figs. 4** and **5**). According to Janas *et al.*, specific RNAs can bind to ordered phospholipid bilayers. They observed that the 1,2-dioleoyl-*sn*-glycero-3-phosphocholine (DOPC)/SM/Ch (60/30/10) liposome effectively interacted with RNA 10 (~15% binding), whereas DOPC/SM (70/30) and DOPC/SM/Ch (40/30/30) did not (<5% binding). These reports suggest that the design of physicochemical properties of the lipid membranes, such as surface charge density, membrane fluidity, membrane polarity, micro-domain structure, are extremely important for recognition

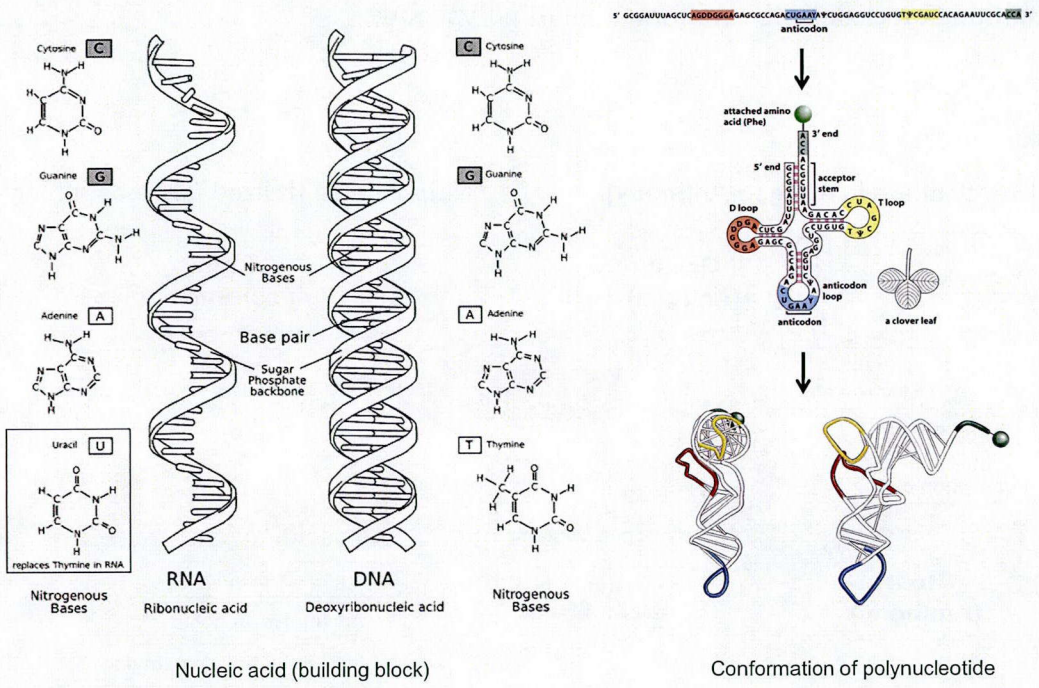

Fig. 4 Building blocks and the conformation of polynucleotides.

of biomacromolecules through (i) electrostatic interaction, (ii) hydrophobic interaction, (iii) interactions driven by entropic forces, (iv) hydrogen bonding interaction, (v) van der Waals forces caused by the matching of the contact surfaces (**Fig. 6**). Based on the strategy, the

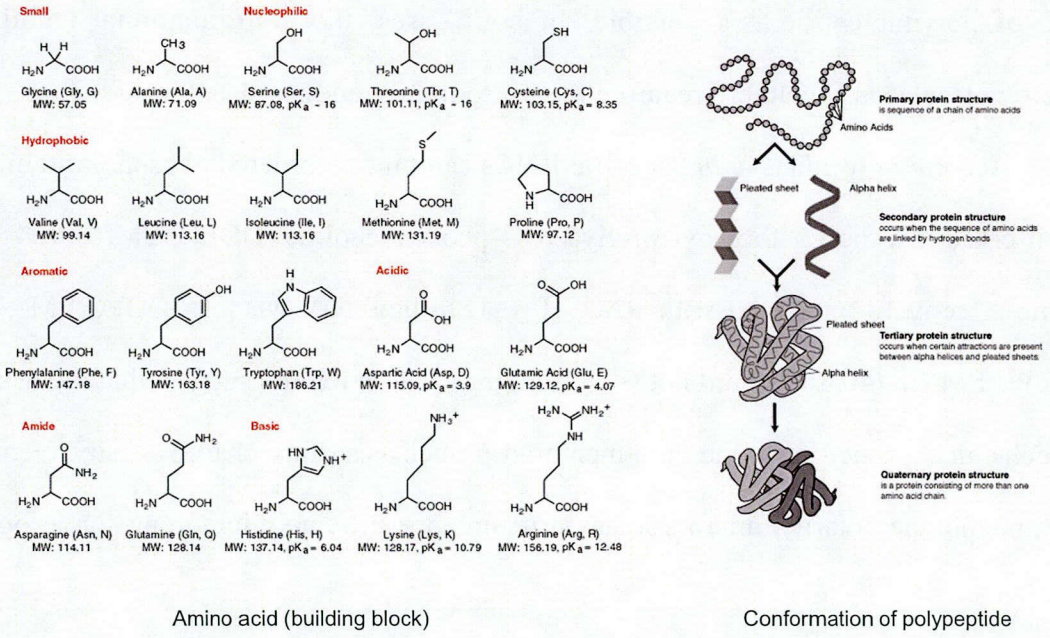

Fig. 5 Building blocks and the conformation of polypeptide.

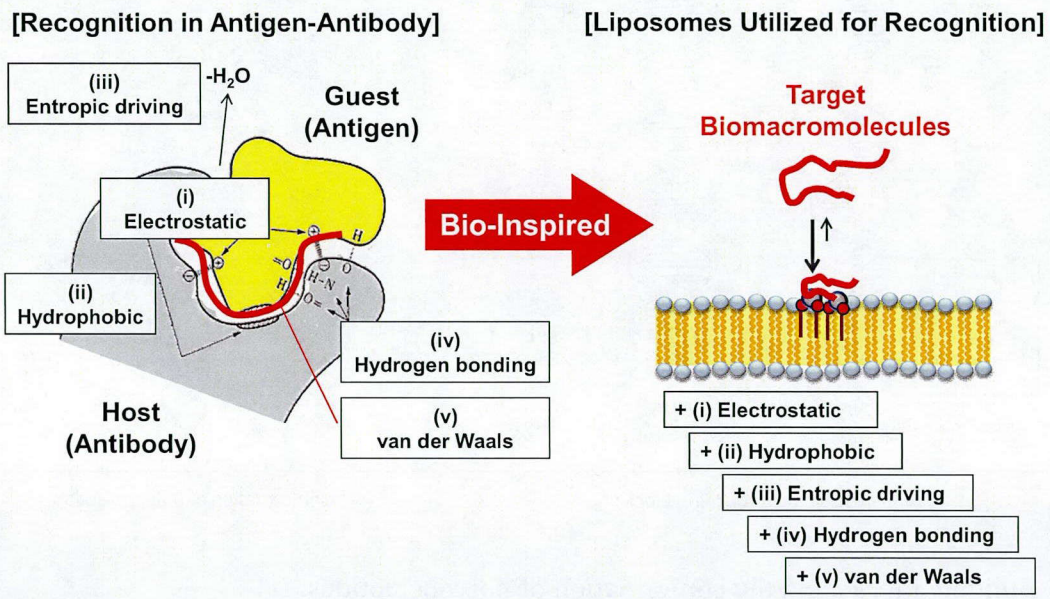

Fig. 6 Strategy for the design of liposome membranes.

strong interaction between liposomes and biomacromolecules can be expected, as well as, the molecular recognition in the antigen-antibody or the base-pair formation in nucleic acids.

A central dogma in molecular biology shows that the gene expression process is constructed from at least three sequential steps, such as (i) transcription, (ii) translation, and (iii) folding (**Fig. 7**). The development of the cell-free translation (CFT) system enables us to synthesize proteins in a test tube, with a mixture of enzymes and substrates (the plasmid DNA, T7 RNA polymerase, ribosome, transfer RNA (tRNA), nucleotide triphosphates (NTPs), amino acids, and so on) (Spirin *et al.*, 1988). Using the CFT systems, high-throughput production of the target protein can be achieved within several hours, excluding a risk of biohazards or unexpected products, although there have been still some limitations of protein expression due to mRNA stability or misfolded intermediates. Further improvement has been needed for the CFT systems. One of the most ideal environments for protein synthesis is cell compartment. The lipid membranes have been reported to play important roles such as molecular localization (Walde, 2010). The liposomes have been utilized in CFT system as the

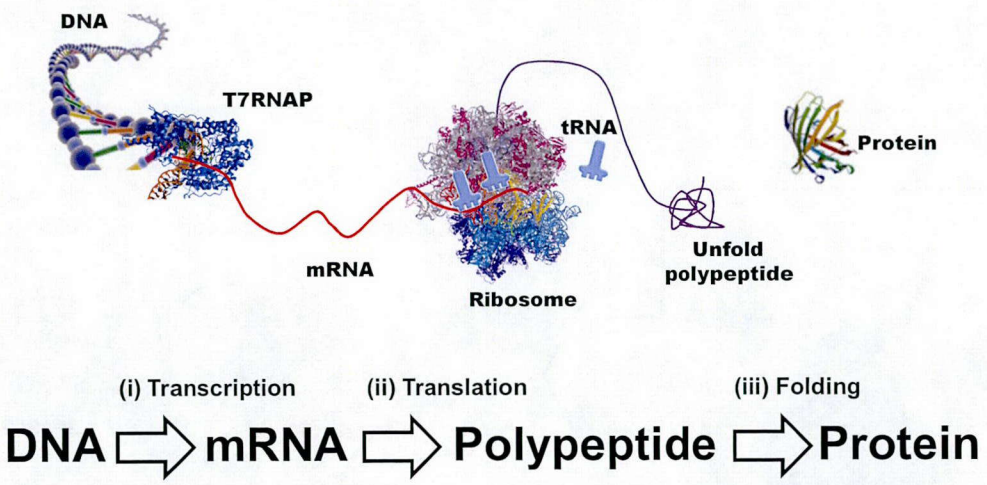

Fig. 7 Central dogma in molecular biology. A cell-free translation system has been developed based on this scheme.

cell-like reactors. Functional protein synthesis has been reported to be performed inside the liposome (Yu, *et al.*, 2001; Ishikawa, *et al.*, 2004; Kuruma, *et al.*, 2009). Therefore, the combination of CFT system and liposomes that mimic the cell-like environment can bring us an innovation to the *in vitro* protein synthesis. Although much information from the viewpoint of genome and proteome has been accumulated, the role of liposome membranes on the gene expression has not been clarified yet.

A possible breakthrough, which overcomes such problems in the CFT systems, is to understand the role of liposome membranes, focusing on the recognition of biomacromolecules included in the CFT systems and the functionalization of them on the lipid membranes (**Fig. 8**). In the previous reports, it has been reported that the liposomes externally added to the CFT system can also regulate the *in vitro* expression of GFP (Bui *et al.*, 2008). It is also shown that the liposomes affect the biological reactions (*e.g.*, transcription, translation, and folding), although the key parameters for regulation strategies of biomacromolecules have been still unclear. From the viewpoint of "molecular recognition", it is possible to assess the idea that the liposomes specifically interacted biomacromolecules in the CFT system. Therefore, it is important to find out the key biomacromolecules that can be "recognized" by liposomes.

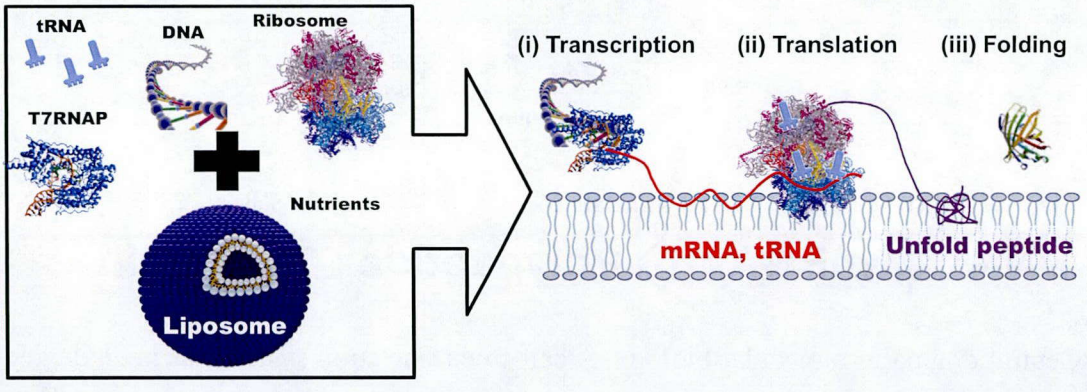

Fig. 8 *In vitro* gene expression on the surface of liposome membrane.

The final purpose of this thesis is to establish the methodology to design the liposome membranes for the recognition of biomacromolecules and the control of their conformation in order to utilize the liposome membrane surface as a platform of bio-/chemical processes. The physicochemical properties of liposome membranes and their interaction with biomacromolecules are investigated in order to understand the key factors for the recognition of biomacromolecules, together with their folding and functionalization. The framework and flow chart of the present study are schematically shown in **Figs. 9** and **10**, respectively.

In Chapter 1, the role of liposomes in an *Escherichia coli* cell-free translation (CFT) system was studied, focusing on their specific interaction with biomacromolecules at elementary steps, such as (i) transcription, (ii) translation, and (iii) folding. It was shown that the surface characteristics of liposome membranes (*e.g.*, surface charge density, phase state) were key factors to regulate (ii) translation and (iii) folding steps; the interaction between liposome and biomacromolecule is defined as "*Biomembrane Interference*", wherein the liposomes specifically interact with the biomacromolecules, and thus regulate their folding and function. The target biomacromolecules to be recognized and regulated on the lipid membranes were selected through the analysis of PDB data, together with the partition method using aqueous two-phase system (ATPS) for the evaluation of surface hydrophobic properties. It was found that the single-stranded RNAs and the nascent GFP polypeptide were unstable, in other words, they were possible to interact with the liposomes. Based on these findings, the polynucleotides (RNAs) and polypeptides were found to be key biomacromolecules, which can specifically interact with lipid membranes.

In Chapter 2, the liposome membranes were characterized, focusing on "microscopic" phase separation and "micro-domains" formed in the DOPC/1,2-dipalmotoyl-*sn*-glycero-3-phoshocholine (DOPC/DPPC) and DOPC/Ch binary lipid mixtures. The fluorescent

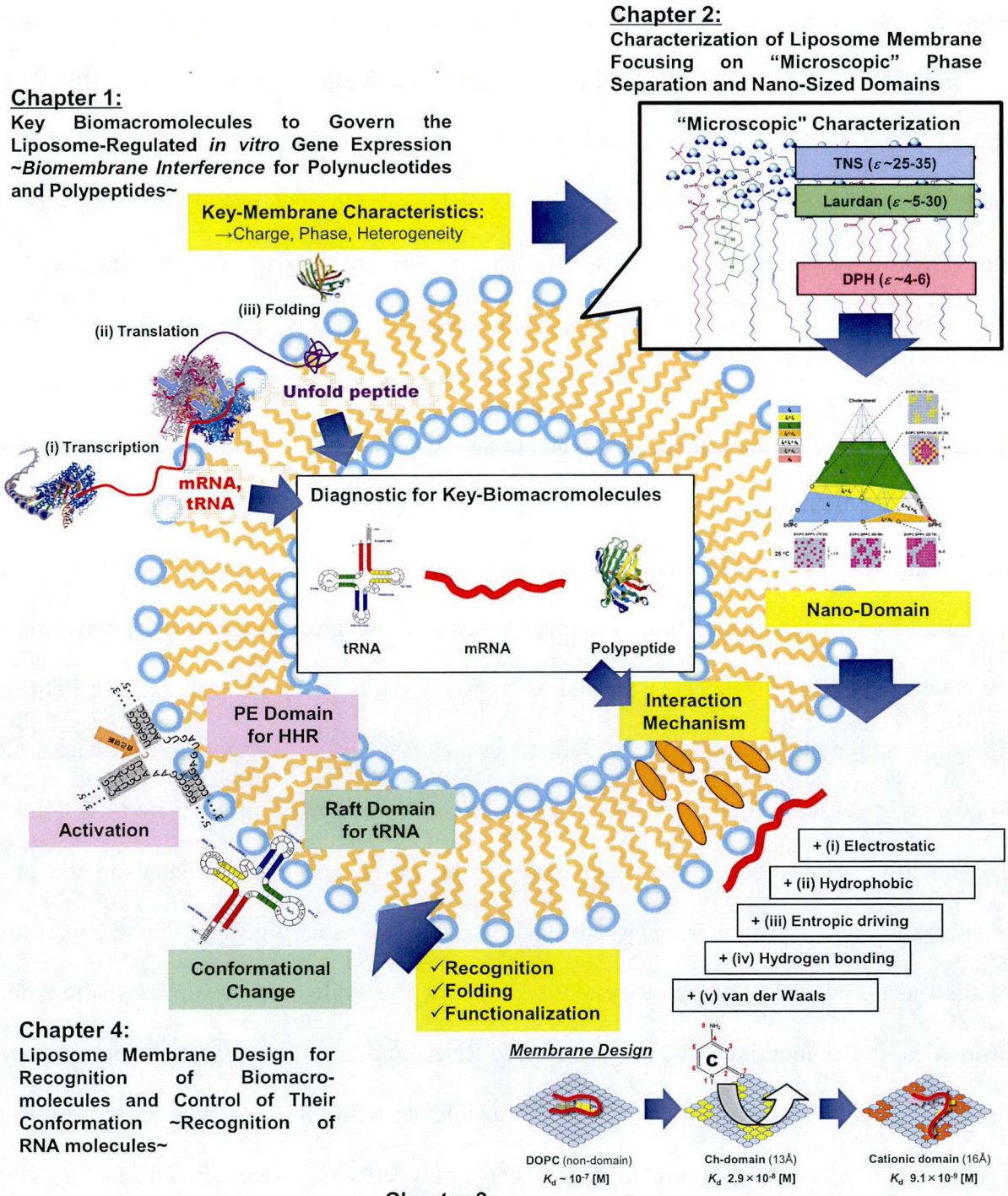

Fig. 9 Framework of the present study.

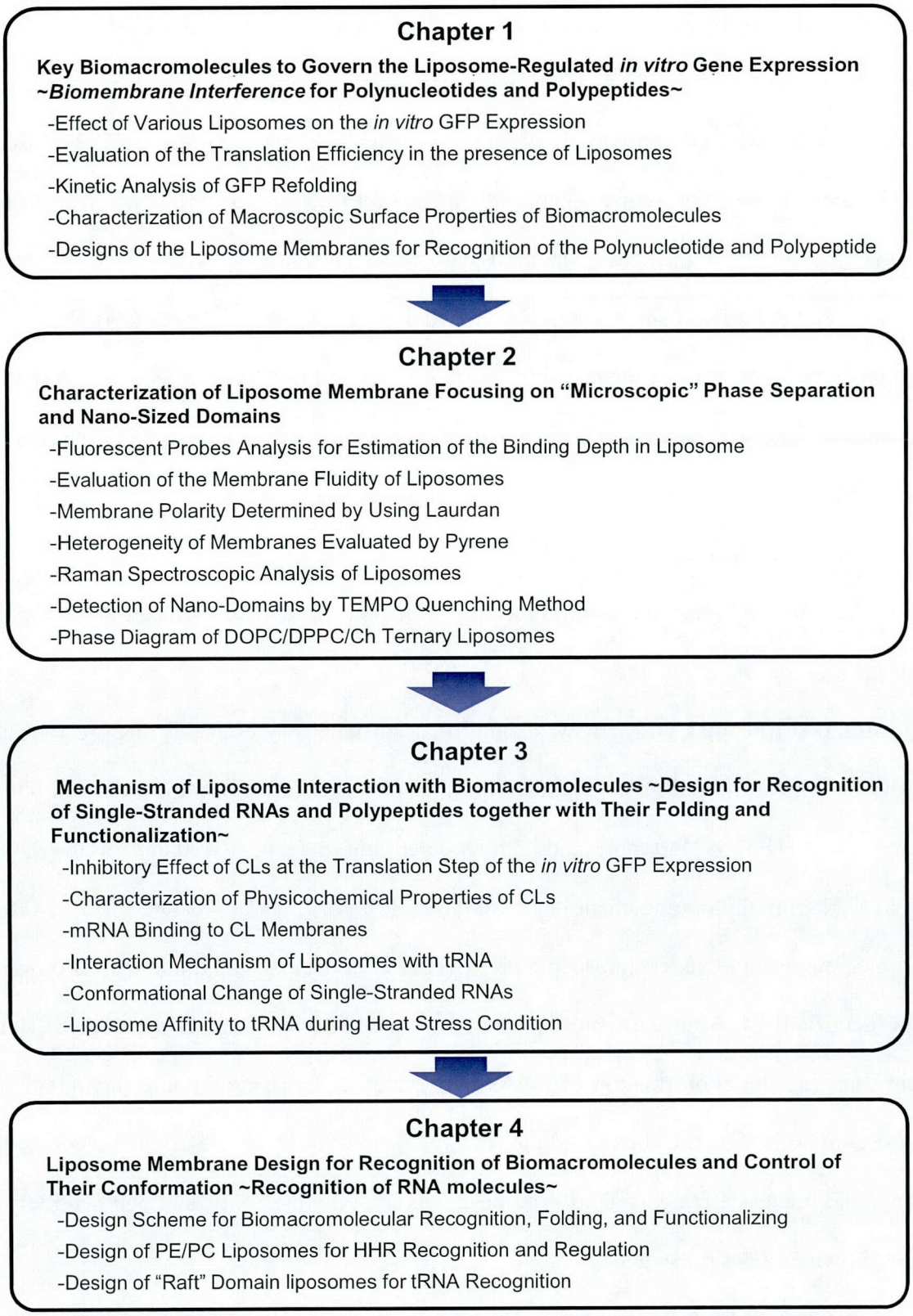

Fig. 10 Flow chart of the present study.

probes, such as 1,6-diphenyl-1,3,5-hexatriene (DPH), 6-lauroyl-2-dimethylaminonaphthalene (Laurdan), and 6-(p-toluidino)-naphthalene-2-sulfonate (TNS), were used in order to measure the membrane fluidity, polarity, and hydrophobicity, respectively. "Macroscopic" properties of liposomes were also determined by Raman spectroscopy, because Raman spectroscopic analysis depends on microscopy techniques. In order to investigate the nano-sized ordered domains, the TEMPO quenching method was newly developed, where DPH molecules present in both disordered and ordered (liquid-ordered, (l_o) or solid-ordered, (s_o)) phases were quenched by (2,2,6,6-tetramethylpiperidin-1-yl)oxyl (TEMPO), which preferentially distributes in the l_d phase membranes. Based on the above results, phase diagrams of DOPC/DPPC/Ch liposomes at various temperatures were finally shown as the basic information for the membrane design.

In Chapter 3, the interaction mechanism of liposomes with biomacromolecules was investigated, focusing on the recognition, folding, and functionalization by selecting single-stranded RNAs as target. It was found that an inhibitory effect of mRNA translation was dependent on the phase state of cationic liposomes. Laurdan spectra indicated both an ordered phase (Em = 440 nm) and a disordered phase (Em = 490nm) in the DOPC/ 3β-[N-(N',N'-dimethyl-aminoethane)-carbamoyl]cholesterol (DOPC/DC-Ch) (70/30) liposome, suggesting that a microscopic phase separation occurs. The binding sites of mRNA were identified by Laurdan analysis, Raman, and Fourier transform infrared (FTIR) spectroscopies. The conformation of RNAs was evaluated by using circular dichroism (CD) spectroscopy. Based on the above findings, the key factors for liposome design for recognition, folding, and functionalizing of biomacromolecules (*i.e.*, polynucleotide and polypeptide) were finally shown as a design scheme.

In Chapter 4, the liposome membranes were designed based on the schemes, together with schemes described in **Chapters 1**, **2**, and **3**, by selecting a Hammerhead ribozyme and tRNA as the target biomacromolecules. In the case of HHR, phosphoethanolamine/

phosphocholine (PE/PC) (8/2) liposomes were optimized by modifying acyl chain lengths. The role of 1,2-dioleoyl-*sn*-glycero-3-phosphoethanolamine/DPPC (DOPE/DPPC) (8/2) itself on HHR was also determined in the absence of Mg^{2+}, showing that the liposomes can directly interact with HHR and regulate its conformation and activity. In the case of tRNA, the interaction between DOPC/SM/Ch liposomes and tRNA were investigated, focusing on the "raft" domain size. The TEMPO quenching method was carried out to detect nano-sized ordered domains in DOPC/SM/Ch membranes. The binding moieties of tRNA was evaluated by using SYBR Green I (SGI) and SYBR Green II (SGII), which binds to double-stranded stem regions and single-stranded loop regions, respectively.

The results obtained in this work are summarized in the General Conclusions section. Suggestions for Future Work are described as extension of the present thesis.

Chapter 1

Key Biomacromolecules to Govern the Liposome-Regulated *in vitro* Gene Expression ~*Biomembrane Interference* for Polynucleotides and Polypeptides~

1. Introduction

Biomembranes play crucial roles through their interaction with various biomacromolecules in biological systems. Recent studies have investigated that the surface of biomembranes can be a functional platform in biological reactions (Brown *et al.*, 1998; Lingwood *et al.*, 2010). Artificial lipid membranes, such as liposomes, Langmuir-Blodgett monolayers, and so on, have been studied as model biomembranes that mimic biological interfaces (Oberholzer *et al.*, 1999; Brezesinski *et al.*, 2003). One of the essential roles of lipid membranes is to localize the functions on the membranes through their binding with biomacromolecules (Walde, 2010). For example, biomacromolecules existing in an *Escherichia coli* (*E. coli*) cell exist under crowded condition (300-400 mg/ml, in growth phase (Zimmerman *et al.*, 1991)), and, therefore, they can exhibit their functions due to localization. From the viewpoint of the synthetic cell biology, it has been conventionally reported that the roles of biomembrane can be explained by a compartment effect (Stano *et al.*, 2011; Kato *et al.*, 2012) and, furthermore, the functionalization of biomacromolecules at the membrane surface (Walde, 2010). It is therefore important to understand the role of lipid membrane, focusing on the specific interaction with biomacromolecules.

The cell-free translation (CFT) system has been developed as a powerful tool for the *in vitro* protein synthesis (Spirin *et al.*, 1988; Spirin *et al.*, 2004). Using the CFT systems,

high-throughput production of the target protein can be achieved within several hours, excluding a risk of biohazards or unexpected products. The CFT systems coexisting with various kinds of liposomes been studied to model the gene expression in a real biological environments. As an example, the functional protein synthesis has been reported inside the liposome to investigate the "compartment" effect of liposome membrane (Yu, *et al.*, 2001; Ishikawa, *et al.*, 2004; Kuruma, *et al.*, 2009). Therefore, the combination of the CFT systems and liposomes that mimic cell-like environments can bring us novel insights into the deeper understanding on the roles of lipid membranes. In our previous reports, the liposomes externally added to the CFT system have been shown to regulate the *in vitro* expression of green fluorescent protein (GFP) (Bui *et al.*, 2008; Bui *et al.*, 2009). These results indicate that the lipid membranes themselves can interact with biomacromolecules and regulate their functions, although the key factors which are necessary for recognition of key biomacromolecules have not been clarified yet.

In this chapter, the role of liposomes in an *E. coli* CFT system was studied, focusing on their specific interaction with biomacromolecules (*i.e.*, polynucleotide, polypeptide) at elementary steps, such as (i) transcription, (ii) translation, and (iii) folding (**Fig. 1-1**). Because an *in vitro* gene expression is a sequential process, the possible variation (promotion or inhibition) of each step is due to the liposome interaction with key biomacromolecules. Using 1-palmitoyl-2-oleoyl-*sn*-glycero-3-phosphocholine (POPC) liposomes modified with cholesterol (Ch) or charged lipids, it was shown that the surface characteristics of liposome membranes (*e.g.*, surface charge density, phase state) were key factors to regulate the (ii) translation and (iii) folding steps; the interaction between liposome and biomacromolecule can herewith be defined as "*Biomembrane Interference*" (Suga *et al.*, 2011), wherein the liposome specifically interact with the biomacromolecules, and then regulate their folding and functions (*cf., RNA interference*; Hannon, 2002). It has been previously reported that the liposomes can interact with various kinds of biomacromolecules, such as DNA, RNA, protein,

and enzyme (Thomas *et al.*, 2005; Janas *et al.*, 2006; Tuan *et al.*, 2007; Bui *et al.*, 2009; Kato *et al.*, 2009; Umakoshi *et al.*, 2012). Because an *E. coli* CFT system contains more than 40 kinds of biomacromolecules, including messenger RNA (mRNA), transfer RNAs (tRNAs), and, of course, nascent polypeptide as a gene product (Murtas *et al.*, 2007; Stano *et al.*, 2011), the target biomacromolecules to be recognized and regulated on the lipid membranes were selected through the analysis of PDB data, together with the partitioning method by using aqueous two-phase system (ATPS) for the evaluation of surface hydrophobic properties from a macroscopic viewpoint. It was found that the single-stranded RNAs and the nascent GFP polypeptide were unstable and, in other words, they were possible to interact with the liposomes. Based on these findings, the polynucleotides (RNAs) and polypeptides were found to be key biomacromolecules, which can specifically interact with lipid membranes. As a summary of this chapter, a general strategy to specify the "key biomacromolecules" to be recognized on the lipid membranes was shown as a scheme.

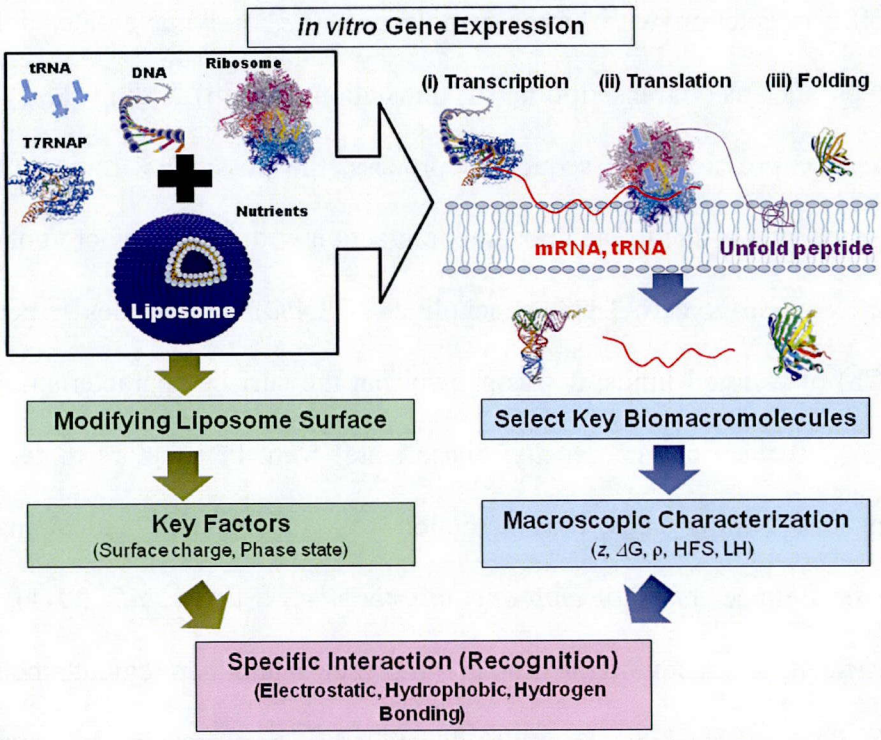

Fig. 1-1 Conceptual illustration of Chapter 1.

2. Materials and Methods

2.1 Materials

1-Palmitoyl-2-oleoyl-*sn*-glycero-e-phosphocholine (POPC), 1,2-dipalmitoyl-*sn*-glycero-3-phoshocholine (DPPC), 1,2-dioleoyl-3-trimethylammonium propane (DOTAP), and 1-palmitoyl-2-oleoyl-*sn*-glycero-3-phospho-(1'-*rac*-glycerol) (POPG) were purchased from Avanti Polar Lipids, Inc. (Alabaster, AL, USA). Ch, transfer RNA (tRNA) originating from *E. coli*, nucleotide monophosphate (NMP; AMP, UMP, CMP, and GMP) were purchased from Sigma-Aldrich (St. Louis, MO, USA). A Rapid Translation System RTS 100 *E. coli* HY Kit (RTS-Kit) was purchased from Roche Diagnostics (Indianapolis, IN, USA). T7 RiboMAX™ Expression Large-scale RNA Production System and SV Total RNA Isolation System were purchased from Promega (Madison, WI, USA). Custom-synthesized poly-(dA) and poly-(dT) were purchased from Life Technologies Japan Ltd. (Tokyo, Japan). Other chemicals were purchased from Wako Pure Chemical (Osaka, Japan) and were used without further purification.

2.2 Liposome Preparation

A solution of phospholipids in chloroform was dried in a round-bottom flask by rotary evaporation under vacuum. The obtained lipid films were dissolved in chloroform and the solvent evaporated. The lipid thin film was kept under high vacuum for at least 3 h, and then hydrated with distilled water at room temperature. The vesicle suspension was frozen at -80 °C and then thawed at 50 °C to enhance the transformation of small vesicles into larger multilamellar vesicles (MLVs). This freeze-thaw cycle was repeated five times. MLVs were used to prepare large unilamellar vesicles (LUVs) by extruding the MLV suspension 11 times through two layers of polycarbonate membrane with a mean pore diameter of 100 nm using an extruding device (Liposofast; Avestin Inc., Ottawa, Canada). Liposomes with different compositions were also prepared by using the same method. Surface charge densities of

liposomes were calculated assuming unilamellarity, spherical shape, a bilayer thickness of 3.7 nm, and a mean head group area of POPC, POPG, and SA were 0.72, 0.72, and 0.20 nm^2, respectively (Taran *et al.*, 1996; Korner *et al.*, 1994), and considering that the phosphate group of POPG and SA are fully ionized at pH 8.0 (Tocanne *et al.*, 1990; Ptak *et al.*, 1980).

2.3 Transcription and Purification of mRNA

pIVEX control vector GFP (Roche) was used as the plasmid DNA. The plasmid DNA was treated once with the restriction enzyme *ApaL* I for one hour incubation at 37 °C in order to cleave the *Amp*R gene and to obtain line DNA fragments harboring the GFP gene before its transcription. The transcription of the mRNA encoding the GFP gene (861 bp) was carried out by using T7 RiboMAX™ Expression Large Scale RNA Production System (Promega, Madison, WI, USA), which includes T7 RNA polymerase as a transcriptional enzyme. Transcription was performed for 30 min at 37 °C. The obtained mRNA was recovered and purified with the SV total RNA Isolation Kit (Promega, Madison, WI, USA). The mRNA products were quantified from the absorbance at 258 nm and the electrophoresis on 1 % of agarose gel.

2.4 Evaluation of GFP Expression Using *E.coli* CFT System

GFP expression was performed by using *E. coli* CFT system, RTS-Kit. GFP was expressed in the presence of liposomes, where gene vectors were pIVEX control vector GFP (plasmid DNA) or the transcribed mRNA. In the case of evaluation at translation step, liposomes and mRNA were pre-incubated at 30 ° for 15 min, and then added to the RTS-Kit. GFP expression was performed for 6 h at 30 °C, and the obtained GFP was kept at 4 °C for 24 h. The amount of GFP synthesized by using the RTS-Kit was evaluated by SDS-PAGE analysis and the fluorescence of GFP (Ex = 395 nm, Em = 509 nm), based on the previously-published methods (Bui *et al.*, 2008).

2.5 Total RNA Isolation: Evaluation of Transcription

mRNA synthesis in the presence of liposomes was performed for 3 h at 30 °C, using RTS-Kit without amino acids. Synthesized RNA was purified with SV Total RNA Isolation System (Promega) (Kobs, 1998; Otto *et al.*, 1998). The reaction solution containing RNA was diluted in lysis buffer, and then RNA was denatured for 3 min at 70 °C. The denatured RNA in solution was separated by a centrifuge ($14000 \times g$) for 10 min, and then the upper phase was added to a spin column assembly. RNA binding to spin column was eluted in nuclease-free water. The purity of isolated RNA was determined by absorbance ratio of A_{260} $/A_{280}$, and isolated RNA was analyzed by UV absorbance A_{260} using a UV spectrophotometer (UV-1800, SHIMADZU, Kyoto, Japan). The amount of RNA transcribed without liposomes was defined as 100 %.

2.6 Kinetics Analysis of GFP Refolding: Evaluation of Folding

Recombinant GFP (nature GFP) was completely denatured in 5.4 M guanidine HCl (GdnHCl) for 3 h at 30 °C for kinetic measurements, the reactions were initiated by the manual mixing of denatured GFP and diluent solutions; unfolded GFP (5.4 M GdnHCl) was diluted 100-fold in refolding buffer containing 0.25 mM of liposomes. The final concentration of GFP was 0.001 mg/ml. The mixing resulted in a jump in the concentration of GdnHCl from 5.4 M to 0.05 M. Time course of GFP fluorescence at 509 nm was measured with an excitation of 395 nm. The refolding kinetics and refolding yield were analyzed for 20 min. The kinetic data were fitted by nonlinear least squares using the following equation:

$$A(t) = A(\infty) - \sum \Delta A_i \, e^{-kit},$$

where A(t) and $A(\infty)$ are the fluorescence intensities at time t and the infinite time, respectively; in addition, ΔA_i and k_i are the amplitude and the apparent rate constant of the i-th phase, respectively (Enoki *et al.*, 2004).

2.7 Evaluation of Surface Properties of GFP and tRNA Using ATPS Method

The surface properties of various kinds of biomolecules have previously been evaluated in our previous works (Kuboi *et al.*, 1994; Kuboi *et al.*, 2004; Umakoshi *et al.*, 2008). The partition coefficient of molecules in ATPS is defined as follows:

$$\ln K = K_{\text{elctrostatic}} + K_{\text{hydrophobic}} + K_{\text{salt}} + K_{\text{ligand}} + \ldots,$$

where $K_{\text{elctrostatic}}$, $K_{\text{hydrophobic}}$, K_{salt}, and K_{ligand} represent the contribution by electrostatic, hydrophobic, salt, and ligand effect, respectively. Under the *pI* and low ionic strength condition, the values of $K_{\text{hydrophobic}}$ and K_{salt} can be ignored (Albertsson, 1970), thus the partition of biomolecules is simply dependent on the hydrophobicity:

$$\ln K = K_{\text{hydrophobic}}$$

The hydrophobicity of ATPS was determined based on the partitioning behaviors of amino acids. The hydrophobicity differences between two phases in ATPS can herewith be defined as hydrophobicity factor, *HF*:

$$\ln K = HF \text{ x } (RH + B),$$

where *RH* is the relative hydrophobicity determined based on the Nozaki-Tanford value (Nozaki *et al.*, 1971) and *B* is the normalization constant defined as the ratio of the partition coefficient and the hydrophobicity of glycine, $\ln K_{\text{Gly}}/\Delta G_{\text{Gly}}$. The *HF* values of various kinds of ATPS, determined based on partitioning behaviors of amino acids, are reported (Kuboi *et al.*, 2004). A liner relationship can be obtained between *HF* and $\ln K$, where the surface net hydrophobicity (*HFS*) of biomacromolecules is defined:

$$\ln K = HFS \times HF$$

The local hydrophobicity (*LH*) is determined by the partitioning behaviors of biomacromolecules in ATPSs with and without a hydrophobic ligand-modified PEG, Triton X-405:

$$LH = \Delta \ln K = \ln K_{(+)\text{Triton}} - \ln K_{(-)\text{Triton}},$$

where $\ln K_{(+)\text{Triton}}$ and $\ln K_{(-)\text{Triton}}$ are the partition coefficients in the presence and absence of 1

mM Triton X-405 in PEG6000/Dex ATPS, respectively. The total concentration of tRNA in ATPS was 1.4 μM.

2.8 Statistical Analysis

Results are expressed as mean ± standard deviation. All experiments were performed at least three times. The distribution of data was analyzed, and statistical differences were evaluated using the Student's t-test. A P-value of <5% was considered significant.

3. Results and Discussion

3.1 Effect of Various Liposomes on the *in vitro* GFP Expression

The GFP gene was expressed in an *E. coli* CFT system in the presence of various kinds of liposome in order to study the possible role of the liposome membrane surface in the recognition of biomacromolecules relating to the gene expression.

3.1.1 Enhanced Effect of Zwitterionic Liposomes on GFP Expression

It has been reported that POPC and DPPC liposomes at 100 nm diameters most effectively enhanced GFP expression (Bui *et al.*, 2008). The surface characteristics of liposomes have been reported to depend on the composition of lipid and the surrounding temperature (De Almeida *et al.*, 2003). Phosphocholine lipids which have unsaturated aliphatic chains (*e.g.*, POPC, 1,2-dioleoyl-*sn*-glycero-3-phosphocholine (DOPC)) are in liquid-disordered phase (l_d) with higher fluidities, while those having saturated aliphatic chains (*e.g.*, DPPC, 1,2-distearoyl-*sn*-glycero-3-phosphocholine (DSPC)) are in solid-ordered phase (s_o) with lower fluidities (Boggs *et al.*, 1987; Ichimori *et al.*, 1990). Cholesterol molecules make a membrane surface rigid, which is known as liquid-ordered phase (l_o) (Jeon *et al.*, 2012). Using the zwitterionic liposomes with different phase states, the effect of the liposomes on GFP expression was first investigated at 30 °C (**Fig. 1-2**). Both POPC and DPPC enhanced the GFP expression to 140 %, although they are in different phase states. POPC/Ch (70/30), which is in heterogeneous (l_d + l_o) phase, most effectively enhanced the GFP expression. Bui *et al.* reported that POPC/Ch (70/30) enhanced GFP expression at transcription, translation and folding steps, showing that the phase state of liposome can play important roles in the enhancement of the *in vitro* GFP expression.

3.1.2 Inhibitory Effects of Charged Liposomes on GFP Expression

The effect of charged liposomes on GFP expression was evaluated (**Fig. 1-3**), by

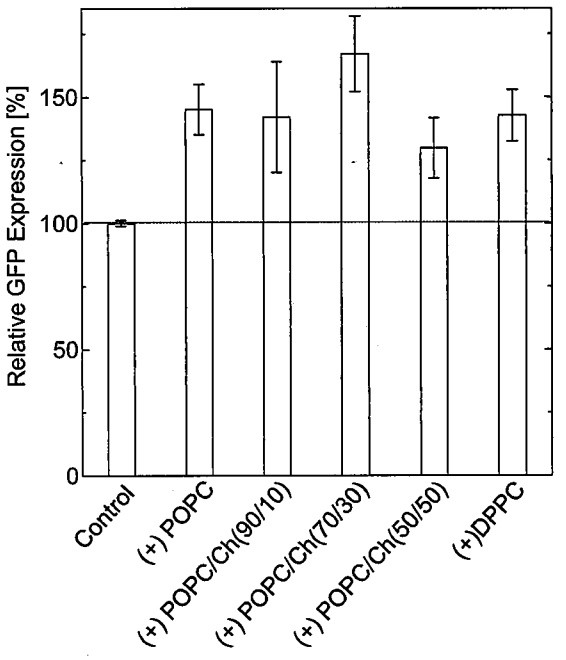

Liposome	Phase state*
POPC	l_d
POPC/Ch (90/10)	l_d
POPC/Ch (70/30)	$l_d + l_o$
POPC/Ch (50/50)	l_o
DPPC	s_o

* Phase state of liposome (De Almeida *et al.*, 2003)
l_d :liquid-disordered
l_o :liquid-ordered
$l_d + l_o$:mixed
s_o :solid-ordered

Fig. 1-2 Effect of zwitterionic liposomes on GFP expression. Table show the phase state of liposomes at 30 °C (De Almeida *et al.*, 2003).

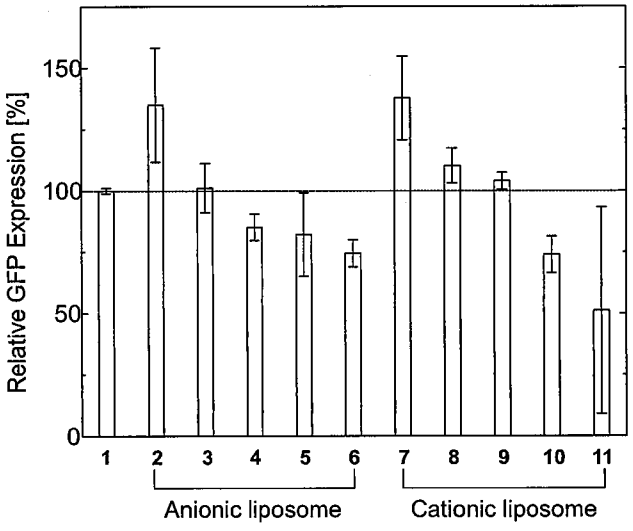

Entry	Liposome	Surface charge density [C/nm²]
1	Control	-
2	POPC/POPG (95/5)	-0.07
3	POPC/POPG (93/7)	-0.10
4	POPC/POPG (90/10)	-0.14
5	POPC/POPG (70/30)	-0.42
6	POPG	-1.4
7	POPC/SA (95/5)	0.07
8	POPC/SA (90/10)	0.15
9	POPC/SA (88/12)	0.18
10	POPC/SA (70/30)	0.53
11	POPC/SA (50/50)	1.08

Fig. 1-3 Effect of charged liposomes on GFP expression. The phase states of these liposomes were estimated to be in l_d phases through the membrane fluidity analysis.

using the same method as described in above sections. The expression of GFP decreased with an increase in the molar ratio of charged lipids. The cationic DOTAP liposome at 3 mM completely inhibited the GFP expression (Bui *et al.*, 2008; Bui *et al.*, 2009). The amount of

GFP expressed in the presence of anionic POPC/POPG (93/7) and cationic POPC/SA (88/12) was almost the same with the control (without liposome). It has been reported that the negatively-charged liposomes inhibited the *in vitro* GFP expression due to their effect on the folding step (Bui *et al.*, 2009); positively-charged liposomes inhibited the *in vitro* gene expression at the translation step (Tachibana *et al.*, 2002); charged vesicles affected the production rate of GFP (Kato *et al.*, 2012). It is therefore shown that the liposomes regulate the *in vitro* GFP expression, depending on their surface characteristics.

In order to study the role of liposomes at the (i) transcription, total RNA in the expression mixture was isolated for the evaluation of the RNA transcribed from DNA (data not shown). In the presence of the liposomes, the amount of isolated RNA increased in spite of the variation of the surface charge density of liposomes. It has been reported that both the cationic and anionic liposomes can interact with polynucleotides (Patil *et al.*, 2000; Liu *et al.*, 2007; Milani *et al.*, 2009; Klein *et al.*, 2010), suggesting that the liposomes can also interact with RNA molecules via electrostatic, hydrophobic, and hydrogen bonding interactions. Detail mechanisms of liposome-RNA interaction are discussed in **Chapter 3**. It is therefore shown that liposomes can interact with RNAs (*e.g.*, nascent mRNA of GFP (861 bp), tRNA (75 bp)) and the nascent polynucleotide, and can regulate the (ii) translation and (iii) folding steps.

3.2 Evaluation of the Translation Efficiency in the presence of Liposomes

The translation is the most influent step in the whole process of gene expression (Sawasaki *et al.*, 2002). It is therefore expected that liposomes can be significantly affect the (ii) translation step. The direct translation of mRNA was performed by SDS-PAGE analysis, in order to determine the effect of liposomes at the (ii) translation step (**Fig. 1-4(A)**). The GFP band at 27 kDa was observed in the presence of POPC/Ch (70/30), while that was not observed in the presence of the cationic DOTAP liposome. It was thus demonstrated that the

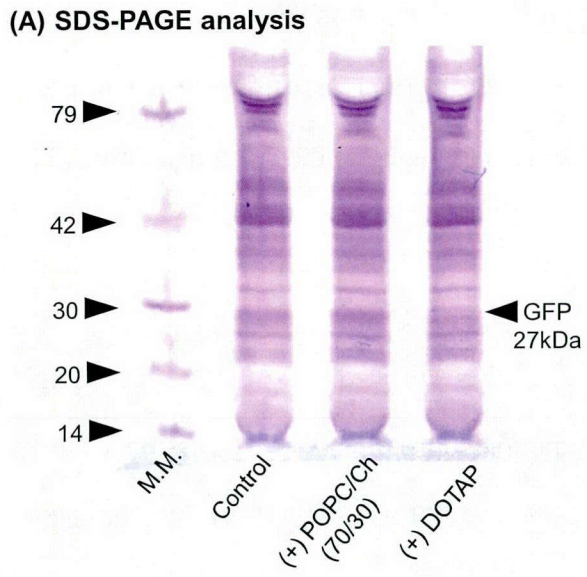

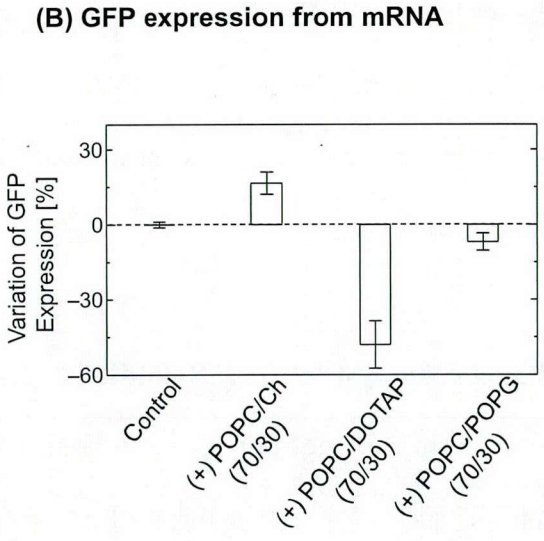

	mRNA binding [%] (1)	GFP expression [%] (2)	Relative activity [-] {[(2)-[100-(1)]} / [100-(1)]
POPC/Ch (70/30)	64	117	1.26
POPC/DOTAP (70/30)	100	52	0.52
POPC/POPG (70/30)	50	93	0.86

Fig. 1-4 Direct translation of mRNA in the presence of charged liposomes. (A) SDS-PAGE analysis for GFP peptide synthesis. (B) Fluorescence analysis for the amount of folded GFP. Table shows the relative activity of mRNA.

cationic liposomes inhibited mRNA translation. The analysis of GFP fluorescence indicated that POPC/Ch (70/30) enhanced the translation and folding steps, while POPC/POPG (70/30) inhibited the folding step (**Fig. 1-4(B)**) (Bui *et al.*, 2009). In order to estimate the relative activity of mRNA on the translation step, mRNA adsorption was determined by ultracentrifugation method (**Fig. 1-4** (Table)). The calculated values of the relative activity of mRNA binding to the liposome also indicated that POPC/Ch (70/30) activated mRNA via liposome binding. Because the cationic liposomes form their complexes with polynucleotides, so called as lipoplex (Klein *et al.*, 2010), strong interaction between cationic liposomes and RNAs interferes the translation step (Tachibana *et al*, 2002; Bui *et al.*, 2009). Although previous researchers reported only RNA bindings to lipid membranes (Janas *et al.*, 2006;

Michanek *et al.*, 2010), the detail mechanisms in RNA interaction and regulation have not been clarified yet. The liposome-RNA interactions were further investigated in **Chapter 3**. Based on the above results, it is shown that liposomes can regulate the (ii) translation step via interaction with mRNA.

3.3 Kinetic Analysis of GFP Refolding

From the viewpoint of synthesis of functional proteins, the expression of folded proteins is also required in the CFT systems (Swartz, 2006). Using the GFP fluorescence assay for the evaluation of the expressed GFP amount, it is shown that liposomes can affect the *in vitro* GFP expression, including the (ii) translation and (iii) folding steps. The GFP fluorescence is deeply relating to its conformation (folding), because GFP has its fluorescence when the chromophore is completely formed (Zimmer, 2002). It is therefore expected that the liposomes can also affect at the (iii) folding step of the nascent GFP polypeptide. The GFP refolding was performed in order to evaluate the effect of liposomes at the (iii) folding step (**Fig. 1-5**). The GFP in a native state was fully denatured by 5.4 M GdnHCl, where the denatured GFP had no fluorescence at 509 nm. The refolding kinetics of the denatured GFP was observed by the recovery of GFP fluorescence. The refolding yield of GFP without liposome was 0.8, revealing that the GFP refolding was not fully achieved in the test tube environment (Fukuda *et al.*, 2000). In contrast, the denatured GFP was fully refolded in the presence of POPC, indicating that the protein folding can be promoted in the lipid membrane environment. DPPC liposomes slightly enhanced the GFP refolding (refolding yield: 0.85), while the anionic liposomes inhibited it. It has been previously reported that the refolding of proteins and enzymes can be assisted by hydrophobic environments, such as detergents, micelles, and liposomes (Zardeneta *et al.*, 1994); the refolding of lysozyme was enhanced in the presence of zwitterionic and anionic liposomes; (Kuboi *et al.*, 2000); the refolding of carbonic anhydrase (CAB) was enhanced by immobilized liposome chromatography

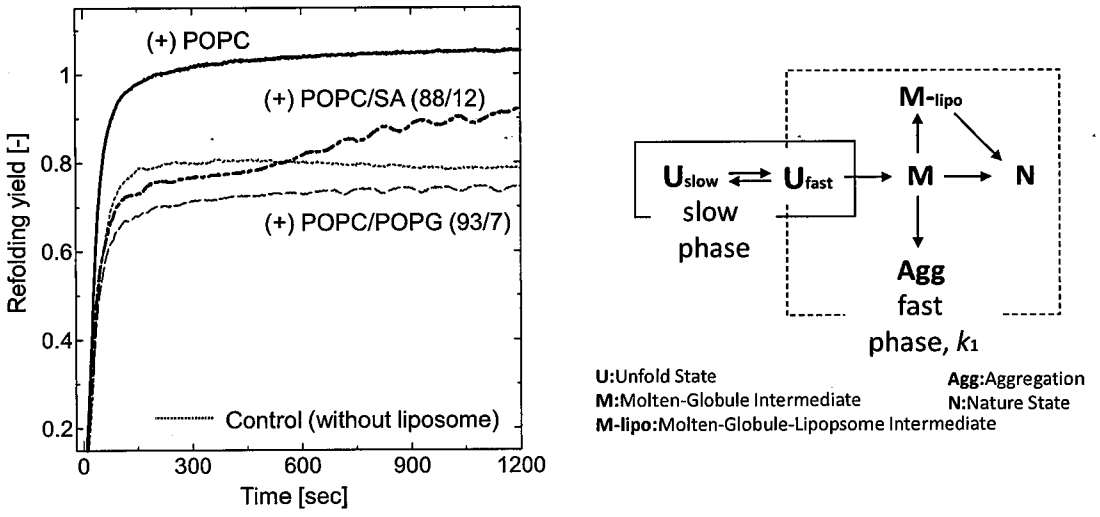

	k_1 [s^{-1}]	Refolding yield [-]
Control	1.25×10^{-2}	0.80
POPC	1.73×10^{-2}	1.03
POPC/POPG (93/7)	1.30×10^{-2}	0.73
POPC/SA (88/12)	1.17×10^{-2}	0.93

Fig. 1-5 Kinetics of GFP refolding and obtained refolding yield.

(Yoshimoto *et al.*, 1998); the oxidized and damaged superoxide dismutase was recognized and reactivated by the liposomes. The refolding kinetics was also analyzed by a time course measurement of GFP fluorescence (**Fig. 1-5** (Table)). GFP is a typical molten-globular protein (MG) (Enoki *et al.*, 2004). Based on the hydropathy plot calculation (Abraham *et al.*, 1978), the unfolded GFP peptide tends to induce self-aggregation (Enoki *et al.*, 2006). In the presence of the anionic liposomes, the electrostatic repulsion could keep a denatured GFP molecule away from membrane, which induced the aggregation of MG intermediates. On the other hand, the MG intermediate, which has negative charge in net, strongly interacted with the cationic liposome membranes. The aggregation was observed in POPC/SA (70/30), while it was not observed in the case of other liposome samples, suggesting that the cationic liposomes inhibited the GFP refolding due to the membrane fusion, based on the membrane

fusion model (Yoshimoto *et al.*, 1998). It is therefore shown that liposomes, which have optimal surface charge densities, enhanced the refolding of GFP, indicating that liposomes can control the (iii) folding step of the nascent polypeptides during the *in vitro* GFP expression process.

3.4 Characterization of Macroscopic Surface Properties of Biomacromolecules

Based on the above results, it is shown that liposomes can interact with biomacromolecules in the CFT system, especially with the mRNA and nascent polypeptide. The electrostatic, hydrophobic, and hydrogen bonding interactions were expected as possible driving forces between liposomes and biomacromolecules. It is thus important to understand the surface properties of polynucleotides and polypeptides in order to understand the role of liposomes in the recognition of biomacromolecules. In this section, the surface properties of biomacromolecules were determined, focusing on the PDB data analysis, together with the partition method using ATPS. In our previous reports, the surface characteristics of biomacromolecules in RTS-Kit were calculated: the surface net charge (z), hydrophobicity (ΔG), hydrogen bonding stability (ρ), using their amino acid sequences (**Table 1-1**). The protein- and enzyme-liposome interactions have been reported; the possible driving forces are electrostatic (z), hydrophobic (ΔG), and hydrogen bonding interactions (ρ) (Yoshimoto *et al.*, 1998; Yoshimoto, PhD thesis (1999); Yoshimoto, PhD thesis (2005); Yoshimoto *et al.*, 2006). Because nucleic acids have hydrophilic backbones and hydrophobic nucleobases (Sasaki *et al.*, 1987; Shih *et al.*, 1998), such hydrophobic molecules are expected to interact with lipid membrane via hydrophobic and hydrogen bonding interactions. It has also been reported that the rRNA helix 59 (H59 domain) in *E. coli* ribosome can directly contact with negatively-charged POPG molecules (Frauenfeld *et al.*, 2011). It is therefore important to evaluate the hydrophobic properties of biomacromolecules, such as the surface net hydrophobicity (*HFS*) and the local hydrophobicity (*LH*).

As indicators of the surface hydrophobicity of tRNA and GFP, the *HFS* and *LH* values were evaluated (**Table 1-2**), based on the PEG/Dex ATPS method (Kuboi *et al.*, 1994; Kuboi *et al.*, 2004). The *HFS* and *LH* values of biomacromolecules are summarized in **Figs. 1-6** and **1-7** (Kuboi *et al.*, 2004; Umakoshi *et al.*, 2008; Shimanouchi *et al.*, 2010). It was found that the surface of tRNA was hydrophilic at physiological temperature (30 °C), while it turned to be hydrophobic at 70 °C. Because the melting temperature (T_m) of tRNA was reported as 52 °C (Carmona *et al.*, 1999), tRNA is expected to be denatured at a higher temperature. It was also shown that the nucleotide monophosphates (NMPs), such as AMP, GMP, CMP, and UMP, were hydrophobic than tRNA, revealing that the denatured tRNA with exposed nucleobases turned to be hydrophobic. These results indicate that the single-stranded RNAs can interact with the liposomes via hydrophobic interaction. The *LH* values of tRNA were also analyzed at various temperatures. The higher *LH* values indicate the intensity of the hydrophobicity pockets on the local domain in the molecule surface, and their number (Shimanouchi *et al.*, 2010). The *LH* values of tRNA were maximal within a temperature range of 20-40 °C, indicating that tRNA has a larger number of clustered hydrophobicity pockets, in contrast to those at 50-80 °C. The obtained results in **Table 1-2** also indicated that the surface hydrophobic properties of GFP varied, depending on its conformation. According to the previous reports, a protein or enzyme in a partly-denatured state, known as MG, shows a higher *LH* value, and it has high affinity with molecular assemblies (Yoshimoto *et al.*, 1998; Yoshimoto *et al.*, 2000), such as molecular chaperone (*i.e.*, GroES). The *HFS* and *LH* values are possible indexes to reflect the driving force in their interaction with liposomes. Based on the ATPS analysis, it is shown that tRNA and GFP at partially-denatured states are likely to interact with liposome membranes through hydrophobic attraction forces. In the *in vitro* GFP expression process, the nascent mRNA and GFP polypeptide vary their conformation and the relating physicochemical properties, indicating that the liposomes can selectively interact with such unstable biomacromolecules during the (ii) translation and (iii) folding steps.

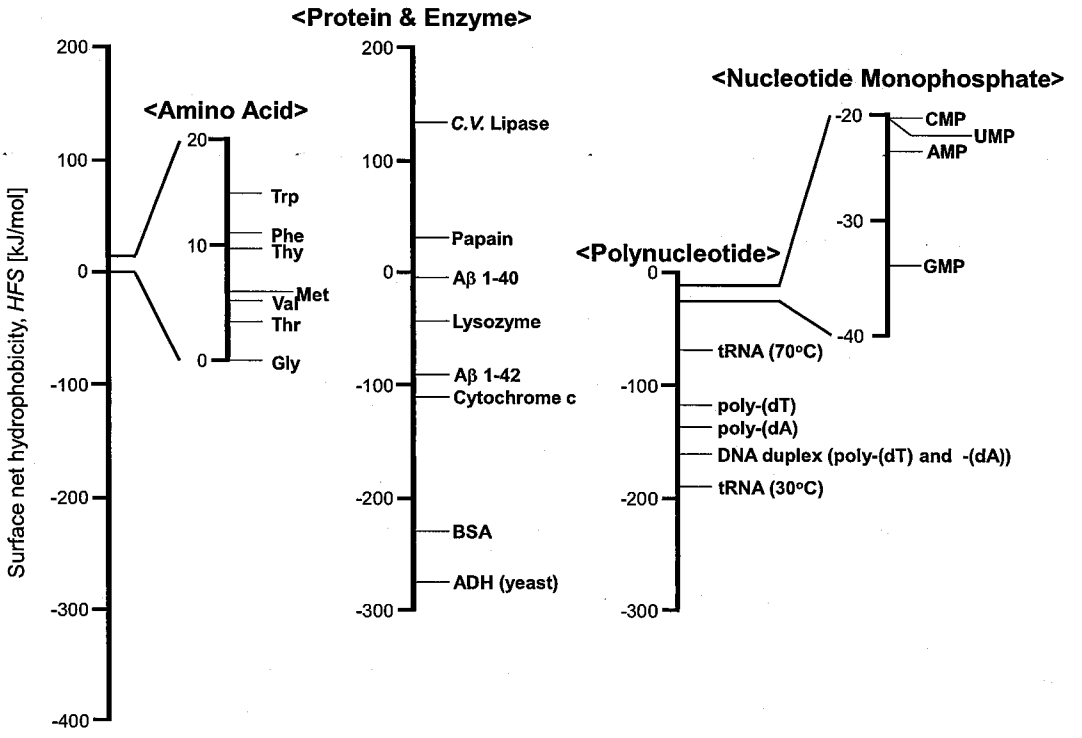

Fig. 1-6 *HFS* values of various biomacromolecules (Kuboi *et al.*, 2004).

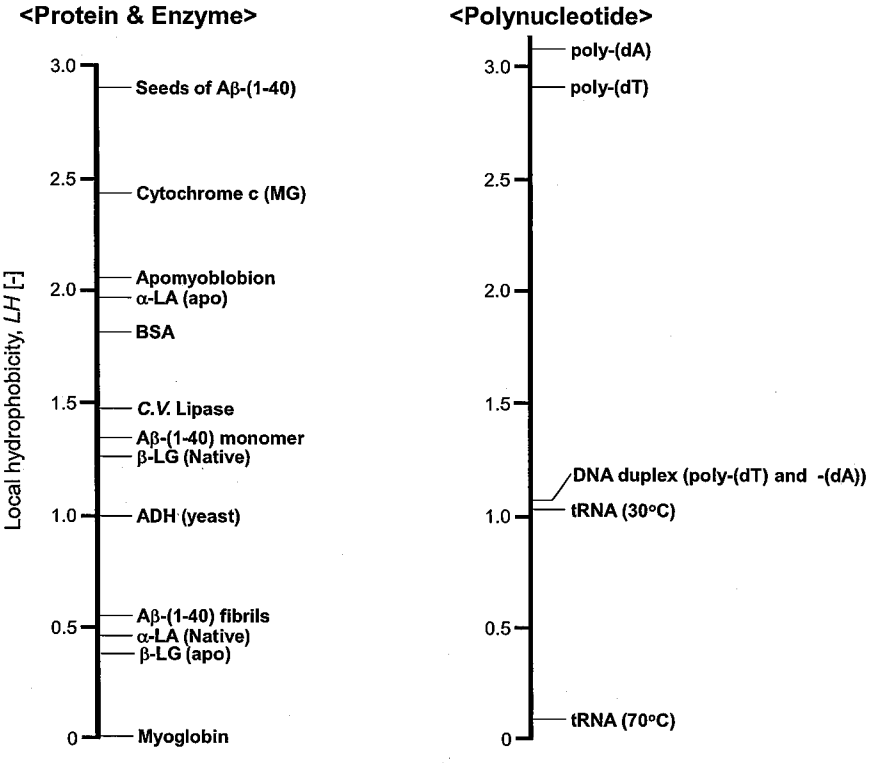

Fig. 1-7 *LH* values of various biomacromolecules (Umakoshi *et al.*, 2008; Shimanouchi *et al.*, 2010).

Table 1-1 Surface properties of biomacromolecules (Bui *et al.*, 2008)

	Structure	M_w [kDa]	Surface net charge, z [C/nm^2]	Hydrophobicity ΔG [kJ/mol/nm^2]	*HFS* [kJ/mol]	*LH* [-]	ρ [-]
DNA	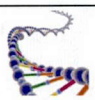	2795 (4235bp)	-3.78	-	-	-	-
T7RNA polymerase	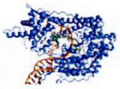	98.8	-0.01	-1.16	-	-	6.88
mRNA		284.1 (861bp)	-1.62	-	-	-	-
70S ribosome	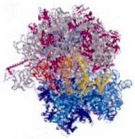	~ 2.7×10^6					
16S rRNA		521.6 (~1500bp)	-0.75	-	-	-	-
ribosomal protein		252	0.13	-1.23	-	-	6.55
POPC/Ch (70/30)		~ 2.4×10^5	0 (zwitterionic)	-0.05	~ -150*1	~ 0.4*1	-

*1 The *HFS* and *LH* values of liposomes have been reported by Yoshimoto' s PhD thesis (1999)

Table 1-2 Surface properties of tRNA and GFP (in this study)

	Structure	M_w [kDa]	Surface net charge, z [C/nm^2]	Hydrophobicity ΔG [kJ/mol/nm^2]	*HFS* [kJ/mol]	*LH* [-]	ρ [-]
tRNA (folded)		25.8	-0.68	-	-192	1.03	-
tRNA (unfolded)					-100	0.17	
GFP (folded)		26.7	-0.06	-6.73	-86.9	0.01	6.76
GFP (unfolded)					-59.1	0.32	

3.5 Designs of the Liposome Membranes for Recognition of the Polynucleotide and Polypeptide

Based on the above results, it is indicated that the liposome membranes can interact with the specific biomacromolecules in the *in vitro* gene expression process, where the polynucleotides (mRNA, tRNA) and polypeptides (nascent GFP polypeptide) were shown as

key biomacromolecules which were recognized and regulated by the liposome membranes. It is therefore shown that the liposomes can regulate the (ii) translation and (iii) folding steps through their specific interaction (recognition) with the key biomacromolecules. In order to design the liposome membrane for the recognition and regulation of biomacromolecules, the "key diagnostic scheme" is established, based on the obtained results in this chapter **(Fig. 1-8)**. This scheme was constructed, assuming that the liposomes do not inhibit the (i) transcription step, because the previous report indicated that the (i) transcription step was not inhibited in the presence of liposomes (Bui *et al.*, 2008; Bui *et al.*, 2009). As an example of the case of cationic liposomes, the relative GFP expression decreased (*else*); the total RNA synthesis increased (*else*); mRNA translation was inhibited (*inhibition*); and the z and *LH* values of tRNA were found to be -0.68 and 1.03, respectively (z <0, *LH* >0.5). It is therefore shown that the cationic liposomes can specifically interact with the single-stranded RNAs, including mRNA and tRNA in an *E. coli* CFT system, and the (ii) translation step was thus inhibited due to their strong interaction with the cationic liposomes. In the case of anionic liposomes, mRNA translation was not inhibited (*else*); the GFP refolding was inhibited (*inhibition*); and the *HFS* and *LH* values of unfolded GFP polypeptide (denatured GFP) were found to be -59.1 and 0.32, respectively (*HFS* >-100, *LH* >0.5), showing that the anionic liposomes can specifically interact with the nascent GFP polypeptide (Bui *et al.*, 2009), and the (iii) folding step was thus inhibited in the presence of the anionic liposomes. It is therefore concluded that the liposomes can specifically recognize the biomacromolecules, such as polynucleotides (mRNA, tRNA) and the nascent GFP polypeptide.

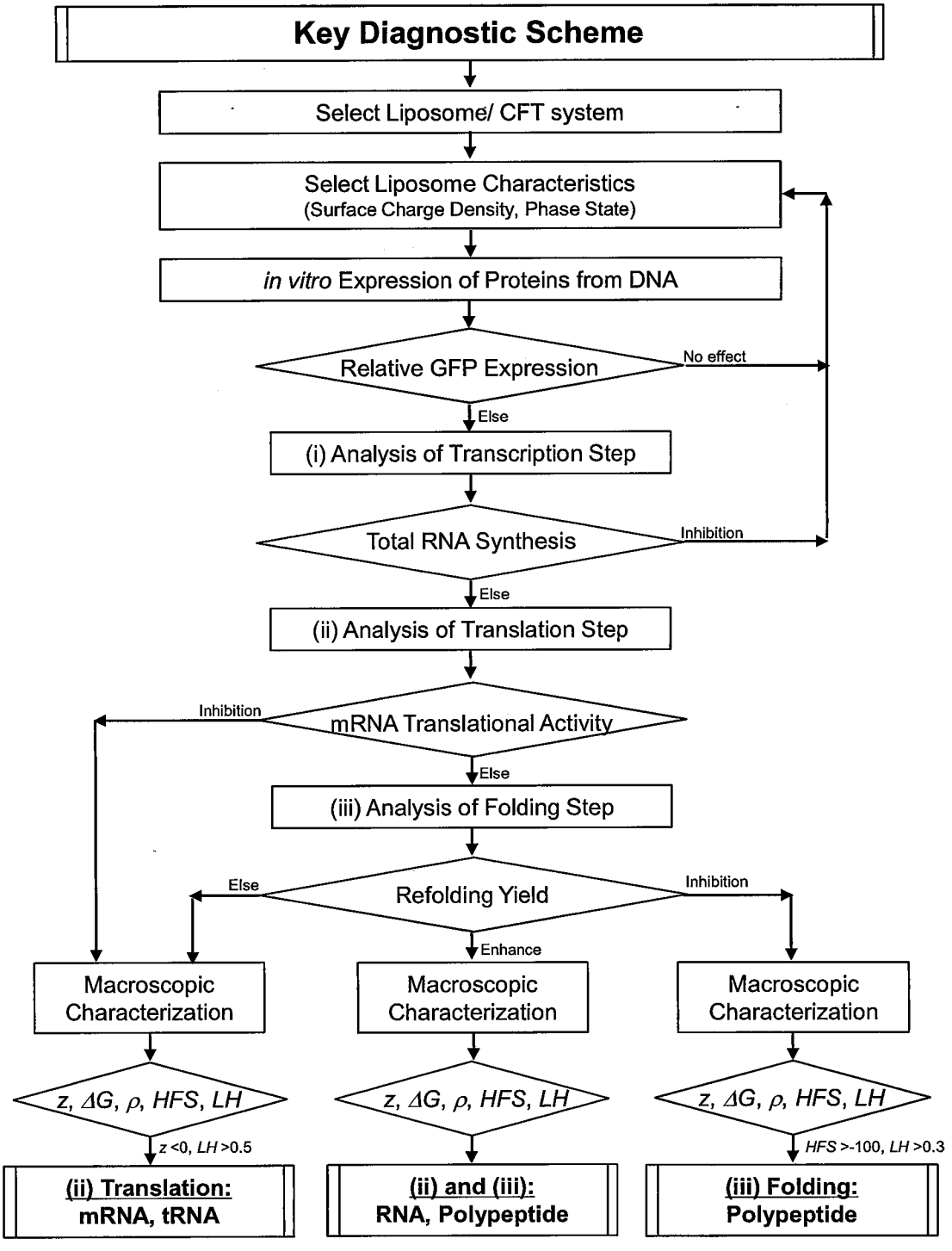

Fig. 1-8 Key diagnostic scheme for designs of the liposome membranes for recognition of biomacromolecules and control of their functions in the *in vitro* gene expression process.

4. Summary

The effect of the liposome addition on the *in vitro* gene expression in an *E coli* CFT system was determined in order to find out the specific interaction of lipid membrane with biomacromolecules. It was shown that GFP expression was effectively enhanced by POPC/Ch (70/30) in ($l_d + l_o$) phase, while it was inhibited by the charged liposomes at the (ii) translation and (iii) folding steps via interaction with RNA molecules and GFP polypeptides. Based on the SDS-PAGE analysis, the cationic liposomes inhibited the (ii) translation steps, revealing that cationic liposomes can recognize mRNA and other RNA molecules due to electrostatic interaction. The zwitterionic liposomes enhanced the folding step, while the anionic liposomes and POPC/SA (50/50) inhibited, suggesting that the nascent GFP polypeptide is also a key biomacromolecule to be recognized by the liposomes. Characterization of biomacromolecules indicated that the nascent mRNA and GFP polypeptide were unstable, and were likely to interact with liposomes via electrostatic, hydrophobic, and hydrogen bonding interactions. It is therefore concluded that the liposomes can recognize the polynucleotides and the nascent GFP polypeptide in the *in vitro* GFP expression process of an *E. coli* CFT system.

The (ii) translation step was found to be significantly regulated by the liposomes, depending on their characteristics (*e.g.*, surface charge density, phase state), suggesting that the liposomes can *interfere* with RNA molecules. Focusing on the POPC/Ch liposomes, POPC/Ch (70/30) liposomes effectively enhanced the (ii) translation step because it can interact with RNA molecules via hydrophobic and hydrogen bonding interaction (Janas *et al.*, 2006; Michanek *et al.*, 2010). It has been reported that the raft domain on the membrane plays important role in biological systems (Brown *et al.*, 1998). These results suggest that the surface properties of liposome (*i.e.*, fluidity, polarity, and heterogeneity (domain)) are also key factors to regulate liposome-biomacromolecule interaction.

Based on the above findings, a diagnostic scheme to find out key biomacromolecules

was finally proposed. In **Chapter 1**, the "macroscopic" analysis is mainly discussed in relation to the specific interaction with liposome and biomacromolecule. In the following chapters, the details in the physicochemical properties of liposome membranes (**Chapter 2**) and in the interaction mechanisms of liposome membranes with biomacromolecules (**Chapter 3**) were discussed focusing on "microscopic" behaviors.

Chapter 2

Characterization of Liposome Membrane Focusing on "Microscopic" Phase Separation and Nano-Sized Domains

1. Introduction

Insights into the possible effect of surrounding environment on the conformation and function of enzymes and nucleic acids are important to clarify the *in vivo* mechanisms of biomacromolecules. The formation of membrane lipid domains ("rafts") in cells has attracted much attention because of its implications for membrane-related processes, including bacterial and viral infection, signal transduction, and so on (Pathak *et al.*, 2011). Recent studies have also revealed that the lipid membranes can activate the biomacromolecules and regulate their functions (Walde, 2010; Umakoshi *et al.*, 2012). Liposomes, which are self-assemblies of various kinds of phospholipids, have been intensely studied as a biomimetic environment of lipid bilayers. Previous studies have also found that the polynucleotides can accumulate on the micro-domains of lipid membranes (Janas *et al.*, 2006; Kurz *et al.*, 2006). From the viewpoint of membrane-protein (or enzyme) interaction, the large unilamellar vesicles (LUVs) modified with a positively charged cholesterol derivative show enhanced the accumulation and enzymatic activity of hexokinase (Umakoshi *et al.*, 2012). It is therefore important to understand the physicochemical properties of LUVs, such as their phase state, micro-phase separation, and domain formation on the membrane.

Lipid membranes composed of natural lipid molecules exhibit several important dynamic behaviors, such as thermal undulation, morphological change of the entire lipid membrane (*e.g.*, fusion/fission), (transient) pore formation, and formation of heterogeneous structures (*i.e.*, phase separation/domain formation) (Yeagle, 2005; Shimanouchi *et al.*, 2011).

Sphingomyelin (SM) and cholesterol (Ch) are typical components that can form the raft domains in liquid-disordered (l_d) membranes (De Almeida *et al.*, 2005). Because the formation of membrane domains depends on the lipid composition and surrounding environment (*e.g.*, temperature), the phase diagrams of membranes in binary and ternary lipid systems have been systematically studied (De Almeida *et al.*, 2003; Veatch *et al.*, 2005; Schmidt *et al.*, 2009; Heberle *et al.*, 2010). Fluorescence microscopy and fluorescence resonance energy transfer (FRET) assays have been developed to detect domains in living membranes. However, despite advances in far-field optical microscopy, subwavelength lipid domains have never been directly visualized, although their sizes are predicted to be <20 nm (Eggeling *et al.*, 2009). FRET is therefore often used to characterize these nano-sized domains (Heberle *et al.*, 2010), because it can detect the nature of nano-domains even if they are transient (Šachl *et al.*, 2011). The phase diagrams and lipid domains have been studied by using microscopy (Veatch *et al.*, 2003; Veatch *et al.*, 2005; De Almeida *et al.*, 2005), FRET (De Almeida *et al.*, 2003; Brown *et al.*, 2007; Šachl *et al.*, 2011; Pathak *et al.*, 2011), ^{2}H NMR spectroscopy (Schmidt *et al.*, 2007), ESR spectroscopy (Heberle *et al.*, 2010), molecular dynamics (Monte Carlo method) (Kiskowski *et al.*, 2007), and fluorescent probes (Parasassi *et al.*, 1995), as summarized in **Table 2-1**. Membrane characteristics, which can be observed by a microscopy, are herein defined as "macroscopic" properties. "Micro-"domains are known to be observed by using FRET, where the domain size has been reported to be ca. 20 nm (De Almeida *et al.*, 2005). Because there have however been little reports about "nano-"sized domains (<5 nm) formed in the lipid membranes, it is therefore important to characterize "microscopic" properties of lipid membranes and detect "nano-"sized domains.

In this chapter, liposome membranes were characterized, focusing on "microscopic" phase separation and "nano-domains" formed in the DOPC/DPPC and DOPC/Ch binary lipid mixtures (**Fig. 2-1**). The fluorescent probe, 1,6-diphenyl-1,3,5-hexatriene (DPH), was used to monitor lipid order and motion in liposome bilayers (Lentz *et al.*, 1976; Lentz *et al.*, 1993).

Table 2-1 Summary of the domain size

Liposome/vesicle	Vesicle	*T* [°C]	Domain size (method)	Reference
DMPC/Ch Ch 30~70 mol%	MLV	20	20 ~ 50 [Å] (fluorescence)	Parasassi *et al.*, (1995)
bSM/POPC/Ch (1/1/1)	LUV (100 nm)	10/ 23/ 45	~150 [Å]/ 80 ~100 [Å]/ < 40 [Å] (FRET)	Pathak *et al.*, (2011)
PSM/POPC/Ch	LUV	23	> 75 ~ 100 [nm] (Microscopy and FRET), < 20 [nm] (FRET only)	De Almeida *et al.*, (2005)
DOPC/PSM/Ch	GUV	25	1 ~ 5 [μm] (Microscopy)	Veatch *et al.*, (2005)
DSPC/DOPC/Ch	GUV	22	~ 5 [nm] (ESR)	Heberle *et al.*, (2010)
DOPC/SM/Ch/ DOPG/ DPPE/biotine (29/39/25/5/2)	GUV	-	< 20 [nm] (FRET)	Šachl *et al.*, (2011)
DOPC/DPPC/Ch: (40/40/20)	MLV	30	6 [nm] (Simulation)	Kiskowski *et al.*, (2007)
DOPC/DPPC (50/50) DOPC/Ch (70/30)	LUV (100 nm)	25	13.9 [Å] (TEMPO quenching) 13.2 [Å] (TEMPO quenching)	This study

Another fluorescent probes, 6-lauroyl-2-dimethylaminonaphthalene (Laurdan) and 6-(p-toluidino)-naphthalene-2-sulfonate (TNS), were used to study the dipolar relaxation of liposome membranes (Parasassi *et al.*, 1991; Niu *et al.*, 1992; Parasassi *et al.*, 1995; Parasassi *et al.*, 1998). The physicochemical properties of LUVs were analyzed by using DPH, Laurdan, and TNS as molecular probes. "Macroscopic" properties of liposomes were also determined by Raman spectroscopy, because Raman spectroscopic analysis depends on microscopy techniques. Laurdan spectra indicated both an ordered phase (Em = 440 nm) and a disordered phase (Em = 490 nm) in the DOPC/DPPC (50/50) liposome, which suggests that the microscopic phase separation occurs. Heterogeneity of liposomes was analyzed by 1-pyrene-dodecanoic acid (Pyrene), where a dimer of Pyrene molecules shows the excimer

fluorescence at 475 nm (Pillot *et al.*, 1996). To investigate the nano-sized ordered domains, DPH molecules present in both disordered and ordered (liquid-ordered (l_o) or solid-ordered (s_o)) phases were quenched by (2,2,6,6-tetramethylpiperidin-1-yl)oxyl (TEMPO), which preferentially distributes in the (l_d) phase. Because of the Förster radii of DPH (36 Å) and TEMPO (12 Å), the maximum size of the DPPC domain is expected to be about 48 Å. Based on the remaining DPH fluorescence, $Q_{liposome}$, nano-sized ordered domains can be detected in the DOPC/DPPC/Ch ternary lipid mixture.

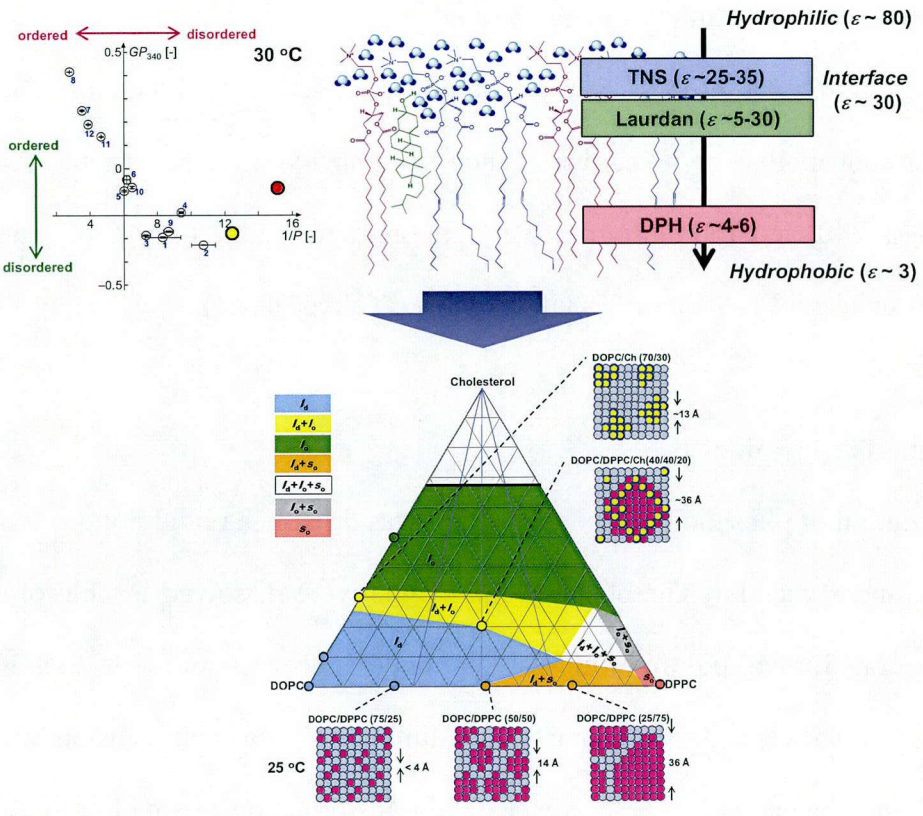

Fig. 2-1 Conceptual illustration of Chapter 2.

2. Materials and Methods

2.1 Materials

1-Palmitoyl-2-oleoyl-*sn*-glycero-3-phosphocholine (POPC), 1,2-dipalmitoyl-*sn*-glycero-3-phosphocholine (DPPC), 1,2-dioleoyl-*sn*-glycero-3-phosphocholine (DOPC), and 1,2-dimirystoyl-*sn*-glycero-3-phosphocholine (DMPC) were purchased from Avanti Polar Lipids, Inc. (Alabaster, AL, USA). Ch was purchased from Sigma-Aldrich (St. Louis, MO, USA). Other chemicals were purchased from Wako Pure Chemical (Osaka, Japan) and were used without further purification.

2.2 Characterization of Fluorescent Probes

The fluorescent probes, 6-(p-toluidino)naphthalene-2-sulfonate (TNS), 6-lauroyl-2-dimethylaminonaphthalene (Laurdan), and 1,6-diphenyl-1,3,5-hexatriene (DPH), were excited at 340, 340, and 360 nm respectively. Fluorescent spectra in water/dioxane solutions were monitored using FP-6500 or FP-8500; JASCO, Tokyo, Japan).

2.3 Liposome Preparation

A solution of phospholipids in chloroform was dried in a round-bottom flask by rotary evaporation under vacuum. The obtained lipid films were dissolved in chloroform and the solvent evaporated. The lipid thin film was kept under high vacuum for at least 3 h, and then hydrated with distilled water at room temperature. The vesicle suspension was frozen at -80 °C and then thawed at 50 °C to enhance the transformation of small vesicles into larger multilamellar vesicles (MLVs). This freeze-thaw cycle was repeated five times. MLVs were used to prepare large unilamellar vesicles (LUVs) by extruding the MLV suspension 11 times through two layers of polycarbonate membrane with a mean pore diameter of 100 nm using an extruding device (Liposofast; Avestin Inc., Ottawa, Canada). Liposomes with different compositions were also prepared by using the same method.

2.4 Evaluation of the Membrane Fluidity of Liposomes

The inner membrane fluidity of the liposomes was evaluated in a similar manner to previous reports (Yoshimoto *et al.*, 2007; Hayashi *et al.*, 2011). Fluorescent probe DPH was added to a liposome suspension with a molar ratio of lipid/DPH = 250/1; the final concentrations of lipid and DPH were 100 and 0.4 μM, respectively. The fluorescence polarization of DPH (Ex = 360 nm, Em = 430 nm) was measured using a fluorescence spectrophotometer (FP-6500 or FP-8500; JASCO, Tokyo, Japan) after incubation at 30 °C for 30 min. The sample was excited with vertically polarized light (360 nm), and emission intensities both perpendicular ($I_{\perp}$) and parallel ($I_{\parallel}$) to the excited light were recorded at 430 nm. The polarization (P) of DPH was then calculated by using the following equations:

$$P = (I_{\parallel} - GI_{\perp}) / (I_{\parallel} + GI_{\perp})$$

$$G = i_{\perp} / i_{\parallel},$$

where $i_{\perp}$ and $i_{\parallel}$ are emission intensity perpendicular and parallel to the horizontally polarized light, respectively, and G is the correction factor. The membrane fluidity was evaluated based on the reciprocal of polarization, $1/P$.

2.5 Evaluation of the Polarity of the Membrane Surface Using Laurdan

The fluorescent probe Laurdan is sensitive to the polarity around itself, which allows the surface polarity of lipid membranes to be determined (Parasassi *et al.*, 1998; Hirsch-Lerner *et al.*, 1999; Viard *et al.*, 1997). Laurdan emission spectra exhibit a red shift caused by dielectric relaxation. Thus, emission spectra were calculated by measuring the general polarization (GP_{340}) for each emission wavelength as follows:

$$GP_{340} = (I_{440} - I_{490}) / (I_{440} + I_{490}),$$

where I_{440} and I_{490} are the emission intensity of Laurdan excited with 340 nm light. The final concentrations of lipid and Laurdan in the test solution were 100 and 2 μM, respectively.

2.6 Raman Spectroscopic Analysis

Raman spectra of liposomes were measured by using a confocal Raman microscope (LabRAM HR-800; HORIBA, Ltd., Kyoto, Japan) at a wavelength of 532 nm, with laser power of 100 mW and a total data accumulation time of 30 s. For each sample, the background signal of the solution was removed, and then the baseline was corrected. The peak intensities at 2882 and 2930 cm^{-1} were evaluated according to previous reports (Batenjany *et al.*, 1994; de Lange *et al.*, 2007):

$$R = I_{2882} / I_{2930},$$

where R indicates the packing density of lipids. The final concentration of lipid in Raman samples was 100 mM.

2.7 Evaluation of Heterogeneity of Liposomes Using Pyrene

Pyrene shows a monomer emission peak at 398 nm and an excimer emission peak at 475 nm, when it is excited at 346 nm. An excimer peak increases when the pyrene molecules form dimer. Heterogeneity of the membranes was estimated by measuring the excimer/monomer peak ratio E/M, as follows:

$$E/M = I_{470} / I_{395},$$

where I_{475} and I_{395} are the emission intensity of Pyrene excited with 340 nm light. The final concentrations of lipid and Pyrene in the test solution were 100 and 1 μM, respectively.

2.8 Fluorescence Quenching of DPH by TEMPO

The quenching of fluorescence from DPH by TEMPO was measured (Bakht *et al.*, 2007; Pathak *et al.*, 2011). Liposome suspensions (1 mL) containing lipid (1 mM) and DPH (0.025 μM) were incubated for 30 min at room temperature (25 °C) to complete the insertion of DPH into the lipid membrane. A solution of TEMPO in ethanol (0-10 mM, 20 μL) was added to each sample. After incubation for 10 min, the fluorescence of DPH (Ex = 360 nm,

Em = 430 nm) was measured. The $Q_{liposome}$ value was then calculated by using the following equation:

$$Q_{liposome} = F / F_0,$$

where F and F_0 are the fluorescence intensity of DPH in the presence and absence of TEMPO, respectively.

2.9 Calculation of Domain Radius

The minimum size of each ordered domain was estimated by using an excess of TEMPO against DPH. Based on $Q_{liposome}$, the domain radii of ordered phases (s_o and l_o) were calculated. TEMPO molecules prefer to bind to (l_d) domains (Bakht *et al.*, 2007), whereas DPH is distributed evenly over both disordered and ordered domains (Lentz *et al.*, 1976; Ahmed *et al.*, 1997). Therefore, TEMPO strongly quenches the fluorescence from DPH in disordered domains, but only weakly quenches fluorescence from DPH in ordered domains. The Förster radii of DPH and TEMPO, R_{DPH} and R_{TEMPO}, are 36 and 12 Å, respectively. Based on these principles, it is considered that $Q_{liposome}$ depends on the size of the ordered domains. The domain radius, X, can thus be calculated according to **Eq. (1)**.

$$X = [R_{DPH} + R_{TEMPO}] \times [(Q_{liposome} - Q_{DOPC}) / (Q_{DPPC} - Q_{DOPC})] \qquad \textbf{Eq. (1)},$$

where Q_{DOPC} and Q_{DPPC} are the remaining fluorescence from DPH in DOPC and DPPC liposomes, respectively, in the presence of TEMPO. The geometry of each domain was assumed as circular area at the 2D-interface of lipid membrane. The number of lipid molecules per domain (N) is calculated by using **Eq. (2)** and **(3)**.

$$N = S / [48 \times (x_{,DPPC} / (x_{,DPPC} + x_{,Ch}) + 40 \times (x_{,Ch} / (x_{,DPPC} + x_{,Ch})] \qquad \textbf{Eq. (2)}$$

$$N_{rel.} = N_{liposome} / N_{DPPC} \qquad \textbf{Eq. (3)},$$

where S is the calculated domain area, $x_{,DPPC}$ and $x_{,Ch}$ are the mole fractions of DPPC and Ch, respectively, and N_{DPPC} is the number of lipid molecules in a DPPC domain with a size of 48 Å. The number of lipid molecules per single liposome was calculated to be ca. 40000, where

the liposome was spherical shape, 100 nm of diameter, and the mean head group area of 72 Å2 (Liu *et al.*, 2004; Luckey, 2008). The areas of the head groups of DPPC and Ch are 48 and 40.3 $Å^2$, respectively (Marrink *et al.*, 2004; De Meyer *et al.*, 2009). Calculations were performed under the conditions: lipids (1 mM), DPH (0.025 μM), TEMPO (6 mM), 25 °C.

2.10 Statistical Analysis

Results are expressed as mean ± standard deviation. All experiments were performed at least three times. The distribution of data was analyzed, and statistical differences were evaluated using the Student's t-test. A *P*-value of <5% was considered significant.

3. Results and Discussion

3.1 Analysis of Fluorescent Probes which Bind to the Different Depth in Liposome Membrane

Fluorescence probes are sensitive to the surrounding environment. DPH, Laurdan, and TNS have been used as micro-polarity-sensitive probes for lipid membranes (Edelman *et al.*, 1968; Lentz, 1993; Parasassi *et al.*, 1991). Because lipid membranes have a hydrophobicity gradient in the vertical direction of lipid bilayers (Cevc, 1990), fluorescent probes reflect the micro-environmental information, depending on their binding depth. The emission spectra of TNS (Ex = 340 nm), Laurdan (Ex = 340 nm), and DPH (Ex = 360 nm) are shown in **Fig. 2-2**, where the dielectric constants of solvents were controlled with water/dioxane mixtures (Critchpield *et al.*, 1953). The halftone area in each column shows the

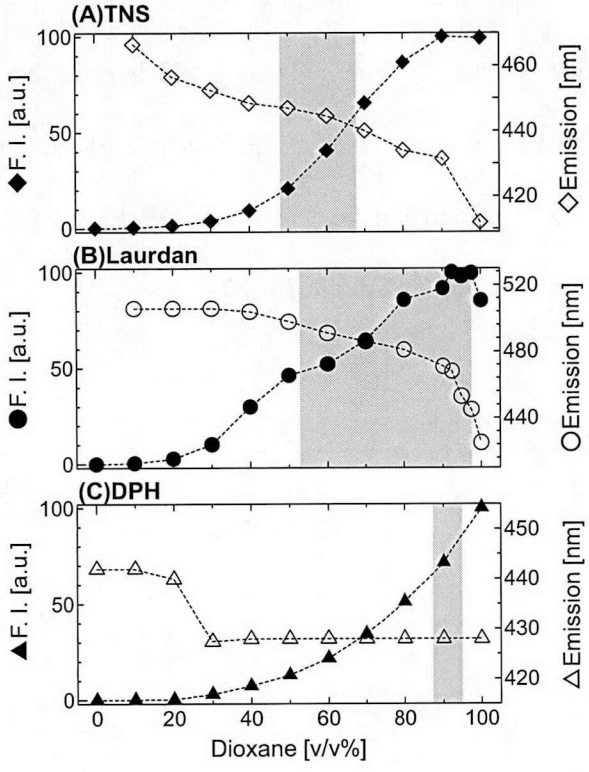

Dioxane [v/v%]	ε [-]
0	76.72
10	68.74
20	60.38
30	51.91
40	43.33
50	34.81
60	26.45
70	18.58
80	11.58
90	5.96
92.5	5.40
95	4.24
97.5	3.06
100	2.20

Fig. 2-2 Characterization of fluorescent probes, (A) TNS, (B) Laurdan, and (C) DPH in water/dioxane solutions. Table shows the dielectric constant of solutions.

ranges of emission wavelength of the fluorescent probe in liposome solutions (DOPC, POPC, and DPPC). Because TNS and Laurdan are polar probes, their emission peaks were blue shifted and their fluorescence intensities increased in proportion to the hydrophobicity of solvents. In the presence of liposomes, the ranges of TNS emission wavelength of TNS were 438-446 nm, indicating that TNS are inserted at water-membrane interface regions (ε: 25-35). Furthermore, the intensity of TNS fluorescence was higher value in DOPC liposome, while that was lower in DPPC liposome at 25 °C, indicating that the membrane surface of DOPC was more hydrophobic than that of DPPC. It is therefore shown that the fluorescence intensity of TNS can be an indicator of the hydrophobicity of lipid membrane. In the case of Laurdan, the binding regions are estimated to be at $5 < \varepsilon < 30$, which is slightly hydrophobic region than that of TNS. On the other hand, DPH, which is non-polar probe, showed no peak shifts in hydrophobic solvents (ε <50), and its fluorescence intensity increased in proportion to the hydrophobicity of solvent. DPH inserted into liposome membranes indicated the emission peak at 428 nm and its fluorescence intensity is ca. 70, showing that DPH is inserted into hydrophobic regions (ε: 4-6). It is concluded that the surface properties of liposome membranes can be monitored using TNS (ε: 25-35), Laurdan (ε: 5-30), and DPH (ε: 4-6), and the characteristics of each probe was summarized in **Table 2-2** and **Fig. 2-3**.

Table 2-2 Characteristics fluorescent probes in the presence of liposomes

Probe	Structure	Ex [nm]	Em [nm]	Dielectric constant, ε [-]	Binding region (depth [nm])
TNS	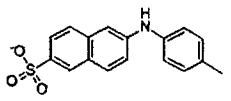	340	438-446	25-35	interface (~1nm)
Laurdan	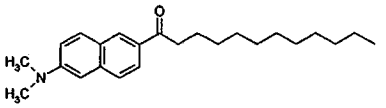	340	440-490	5-30	interface (~1nm)
DPH	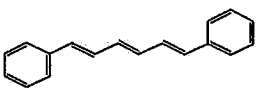	360	430	4-6	inner membrane (~2nm)

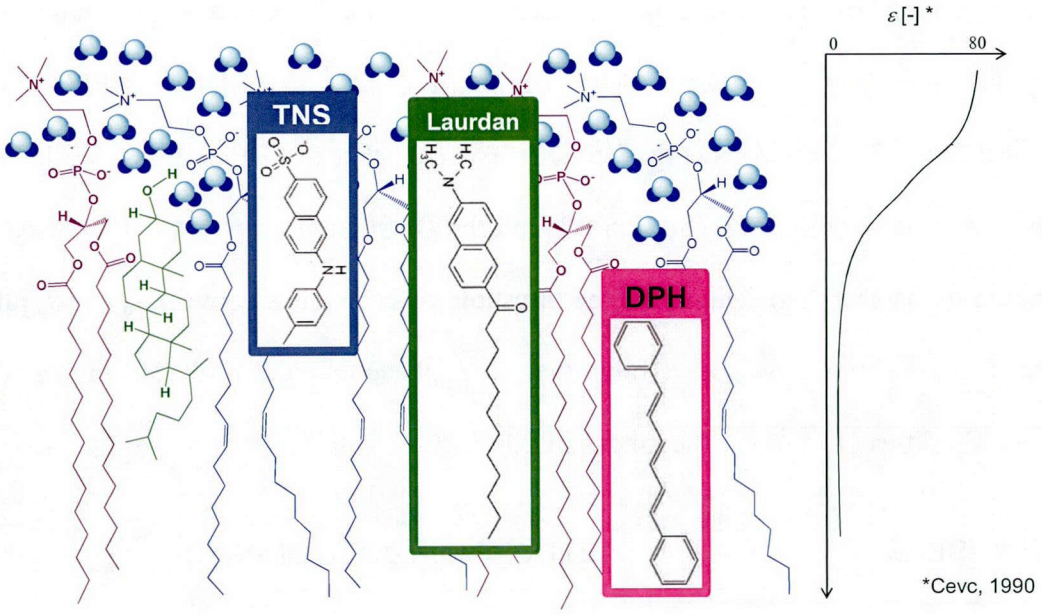

Fig. 2-3 Summary of the binding depth of fluorescent probes.

3.2 Evaluation of the Membrane Fluidity of Liposomes

DPH has been widely used to evaluate the membrane fluidity of various kinds of lipid membranes (Hayashi *et al.*, 2010). The temperature dependence of membrane fluidities, $1/P$ is shown in **Fig. 2-4(A)** (DOPC/DPPC binary lipid mixture) and **Fig. 2-4(B)** (DOPC/Ch binary lipid mixture and DOPC/DPPC/Ch ternary lipid mixture). The membrane fluidity of a l_d phase liposome was higher ($1/P$ >6) than that of a s_o phase liposome ($1/P$ <3). For the DOPC/Ch liposomes, the decrease in membrane fluidity depended on the molar fraction of Ch at the same temperature. At 30 °C, the $1/P$ value of DOPC/DPPC/Ch (40/40/20) liposome was higher than that of DPPC (s_o), but lower than that of DOPC/Ch (50/50) (l_o), indicating that there are two phases (s_o and l_o) in the DOPC/DPPC/Ch (40/40/20) liposome. It was found that the membrane fluidity was dependent on both the lipid composition and temperature. Because DPH is distributed evenly in both disordered and ordered domains (Lentz *et al.*, 1976; Ahmed *et al.*, 1997), the $1/P$ values reflect membrane fluidities originating from both ordered and disordered phases. Therefore, analysis of membrane fluidity provides us with "macroscopic"

information about lipid membrane phase states, such as fluid phase (l_d), gel phase (s_o), and mixed phase (l_d + l_o (s_o)) (Luckey, 2008). The phase transitions of DOPC/DPPC liposomes were revealed by DSC analysis (**Fig. 2-5**). It was found that the DPPC liposome indicated a phase transition temperature (T_c) at 42.6 °C, and the DPPC liposome at 45 °C showed higher membrane fluidity ($1/P$ >6). Therefore, the threshold of $1/P$ values between l_d and s_o phases is estimated to be $1/P$ = 6. It was also found that the l_o phase DOPC/Ch (50/50) indicated lower membrane fluidities ($1/P$ <6) in the ranges of 20-50 °C.

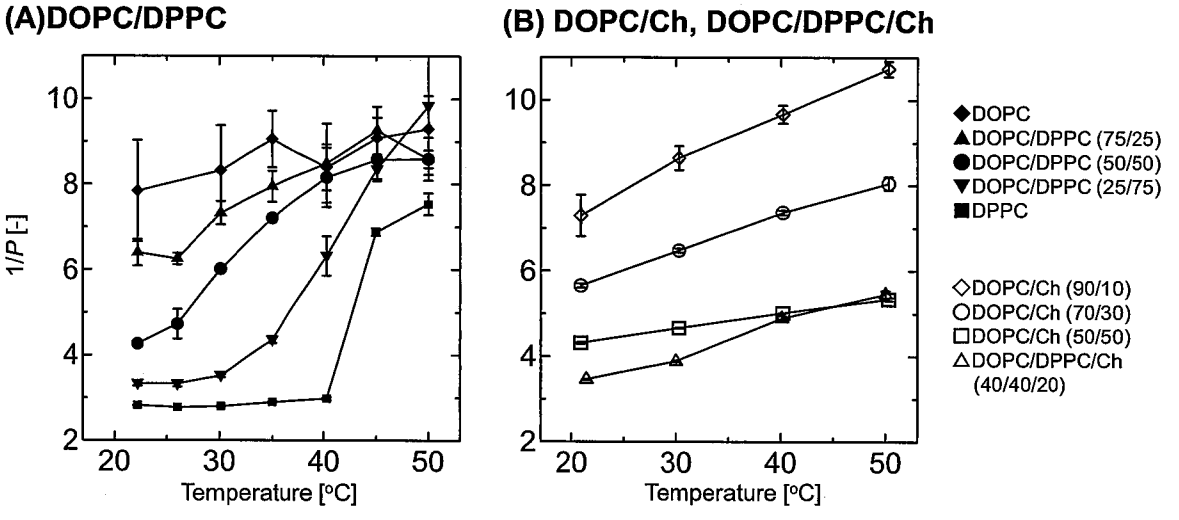

Fig. 2-4 Evaluation of membrane fluidity, $1/P$. (A) DOPC/DPPC liposomes, (B) DOPC/DPPC/Ch liposomes.

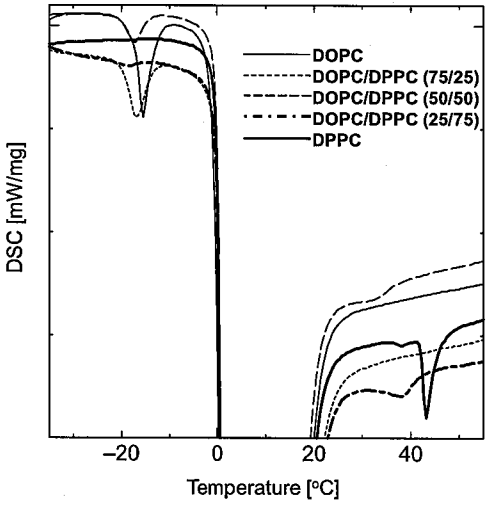

	ΔH_{DOPC}	ΔH_{DPPC}	$\Delta H_{boundary}$
DOCP	-1.95 J/g	-	0
DOPC/DPPC (75/25)	-1.31 J/g (74.1%)	-	-0.45 J/g (25.9%)
DOPC/DPPC (50/50)	-0.64 J/g (40.4%)	-0.16 J/g (10.1%)	-0.79 J/g (49.5%)
DOPC/DPPC (25/75)	-0.11 J/g (7.8%)	-0.51 J/g (36.4%)	-0.78 J/g (55.8%)
DPPC	-	-1.22 J/g	0

ΔH_{DOPC} : phase transition enthalpy of DOPC
ΔH_{DPPC} : phase transition enthalpy of DPPC
$\Delta H_{boundary}$ $= \sum(\Delta H_{DOPC} + \Delta H_{DPPC}) - (\Delta H_{DOPC} + \Delta H_{DPPC})$

Fig. 2-5 DSC analysis of DOPC/DPPC liposomes.

3.3 Membrane Polarity Determined by Using Laurdan

Laurdan has been used as a molecular probe to monitor the heterogeneity of liposomes. Laurdan shows specific emission peaks at 440 and 490 nm that originate from lipid membranes in an ordered phase (l_o, s_o) and disordered phase (l_d), respectively (Parasassi *et al.*, 1991; Parasassi *et al.*, 1995; Parasassi *et al.*, 1998). **Figure 2-6** shows fluorescent spectra of Laurdan at 30 °C and the GP_{340} values in the range of 20-50 °C. A single peak at 490 nm was observed in the case of DOPC (l_d), whereas a single peak at 440 nm was observed in the case of DPPC (s_o). These results indicate that DOPC and DPPC liposomes are in homogeneously disordered and homogeneously ordered phases, respectively. In contrast, DOPC/DPPC (50/50) and DOPC/Ch (70/30) systems exhibited emission peaks at both 440 and 490 nm. An isosbestic point was observed in the spectra of the DOPC/DPPC binary system, but not in those of the DOPC/Ch system. The GP_{340} values of the systems were measured as an indicator of the degree of hydration of the membrane surface (Parasassi *et al.*, 1998; Viard *et al.*, 2007). As the DOPC liposome was heated from 20 to 50 °C, the GP_{340} values decreased gradually in proportion to the increase in temperature. The GP_{340} values of DPPC from 20 to 40 °C were almost constant, while they decreased significantly at temperatures above the T_c. For the DOPC/Ch liposomes, the GP_{340} values decreased gradually as the temperature increased. The GP_{340} values of DOPC/DPPC/Ch (40/40/20) were higher than that of DOPC/Ch (50/50) below 30 °C. However, the GP_{340} values of the DOPC/DPPC/Ch (40/40/20) liposome were slightly lower at temperatures exceeding 40 °C. This result indicates a possible phase transition of the DOPC/DPPC/Ch (40/40/20) liposome between 30 and 40 °C. Laurdan spectra in the liposomes (*e.g.*, DOPC/DPPC (50/50) and DOPC/Ch (70/30)) showed two peaks, indicating that there are at least two kinds of phases with different hydrophobic environments in their membranes. The spectra of Laurdan in **Fig. 2-6(A)** show an isosbestic point, while those in **Fig. 2-6(B)** do not. It is suggested that the DOPC lipid and DPPC lipid are immiscible, while Ch is miscible with DOPC. These

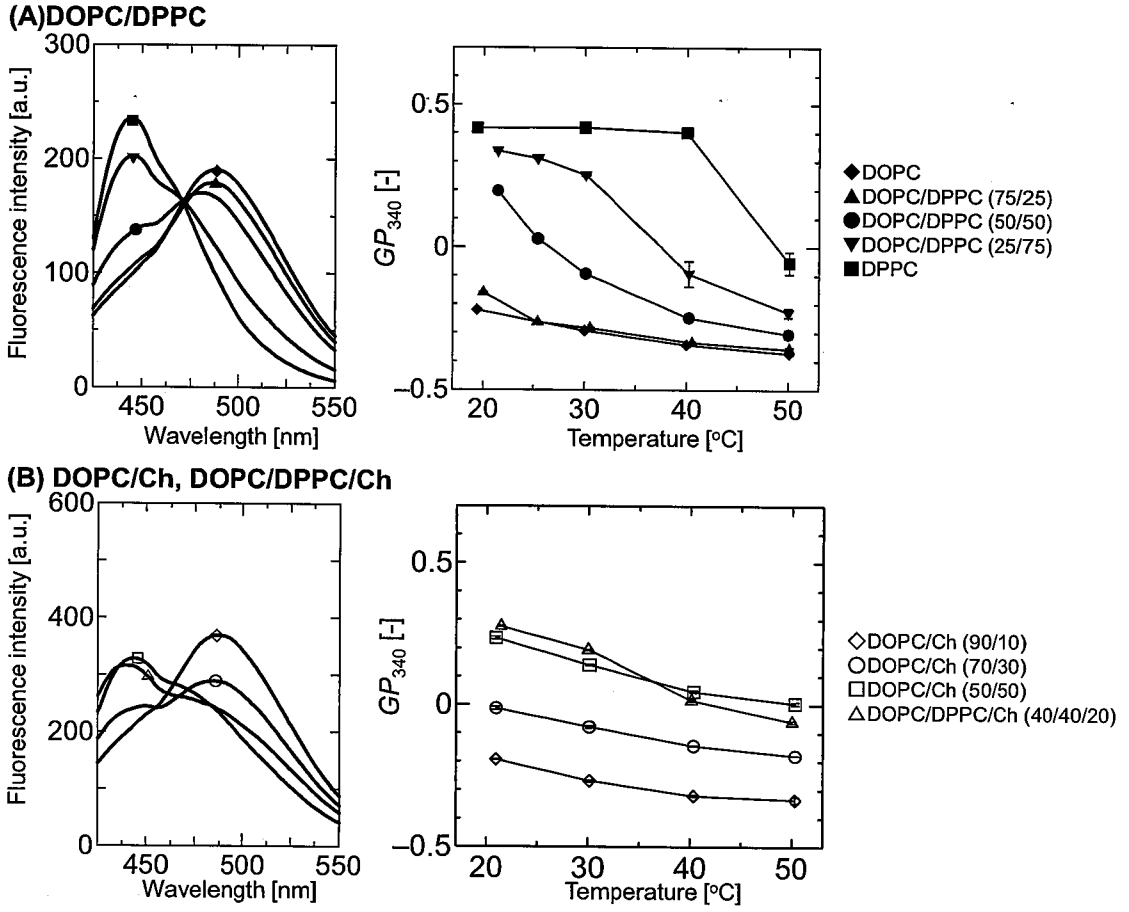

Fig. 2-6 Evaluation of membrane polarities using Laurdan. Fluorescent spectra of Laurdan excited at 340 nm (*left column*) and GP_{340} values (*right column*) are shown for (A) DOPC/DPPC liposomes and (B) DOPC/DPPC/Ch liposomes.

results also imply that the fluorescence of Laurdan can be used to monitor "microscopic" phase separation and the coexistence of ordered and disordered phases in liposome membranes. Because the GP_{340} values of DOPC liposomes were <-0.2 in the ranges of 20-50 °C, the threshold temperature between disordered and ordered phases is estimated to be GP_{340} = -0.2.

3.4 Heterogeneity of Membranes Evaluated by Pyrene

Pyrene shows a monomer emission peak at 398 nm and an excimer emission peak at

475 nm, when it is excited at 346 nm (Canpos *et al.*, 1995; Pillot *et al.*, 1996). **Figure 2-7** shows the E/M ratio of liposomes. It has been reported that POPC liposomes containing Ch molecules indicated higher E/M ratio values (Yoshimoto, 2005). Within zwitterionic liposomes, DOPC/Ch (70/30) indicated the highest value of E/M ratio, showing that DOPC/Ch (70/30) is in the most heterogeneous membrane. Although DOPC/DPPC/Ch (40/40/20) has possible membrane domain (Veatch *et al.*, 2003), the E/M ratio of DOPC/DPPC/Ch (40/40/20) was almost the same with that of DOPC. It is thus suggested that 1-pyrenedodecanoi acid, which has a negative charge at headgroup, is oriented to l_d phases. It was also found that s_o phase DPPC indicated a higher E/M ratio, while DOPC/DPPC binary liposomes showed similar values with DOPC. It is therefore shown that Pyrene can monitor the heterogeneity of disordered phases in the zwitterionic liposomes. Because "raft" is in ordered phases, other methods are needed to detect the domains formed in the membranes.

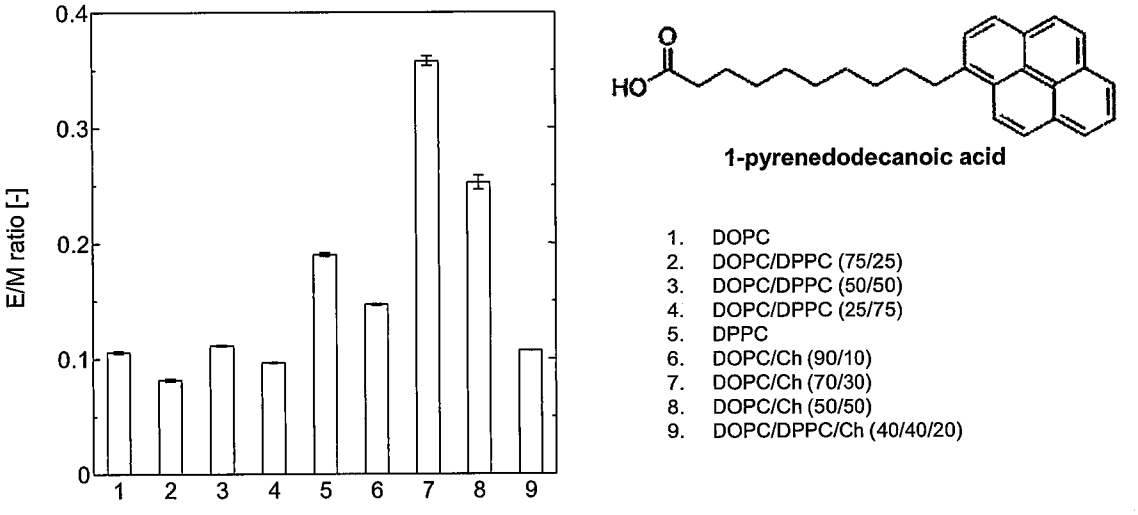

Fig. 2-7 E/M ratio of liposomes evaluated using 1-pyrenedodecanoi acid.

3.5 Raman Spectroscopic Analysis of Liposomes

Raman spectroscopy is a powerful tool to analyze materials *in site* without any labeling or staining. It has been reported that the packing densities of lipids can be monitored using Raman spectroscopy (Batenjany *et al.*, 1994). **Figure 2-8(A)** shows Raman spectra of the DMPC liposome at 20-40 °C, and corresponding peak assignments are summarized in **Table 2-3** (Batenjany *et al.*, 1994; de Lange *et al.*, 2007; Fox *et al.*, 2007). The intensity of the peak at 2882 cm^{-1} was strong at temperatures below 20 °C, while it decreased at temperatures above 30 °C. Because the T_c value of DMPC is 23 °C, the packing density of the DMPC liposome varied in the range of 20-30 °C. To evaluate the phase transition of the pure liposomes, the variation of R values (= I_{2882} / I_{2930}) that indicate the lipid packing density (Batenjany *et al.*, 1994) was investigated in relation to various liposomes (**Fig. 2-8(B)** and **(C)**). The T_c values of DOPC, DMPC, and DPPC are -18.3, 23.6, and 41.3 °C, respectively. The R values of DOPC were found to be lower (R <1.2) in the temperature range of 20-50 °C than those of DMPC and DPPC (R >1.7) under T_c. Therefore, a liposome with a lower R value is in the disordered phase state (l_d), while one with a higher R value is in the ordered phase state (s_o). **Figure 2-8(C)** shows the temperature dependence of R values for DOPC/DPPC liposomes. The T_c values of DOPC/DPPC (75/25), (50/50), and (25/75), were estimated to be <20, <25, and <35 °C, respectively. However, the R value of DOPC/DPPC/Ch (40/40/20) was lower (R <1.3, data not shown), and decreased slightly in proportion to the temperature increase. Therefore, Raman spectroscopic analysis can also reveal an information on a phase transition of s_o to l_d for the phospholipid liposomes (Fox *et al.*, 2007), although the liposomes containing Ch indicated a slight variation in R values. Because the Ch molecule itself has stable Raman intensities around 2800-3000 cm^{-1} (de Lange *et al.*, 2007), the packing density of the phospholipids, analyzed by the vibrations from hydrocarbons in the acyl chain regions (Orendorrf *et al.*, 2002), cannot be used in the presence of Ch without data deconvolution. Thus, studies based on membrane fluidity and polarity are necessary to estimate

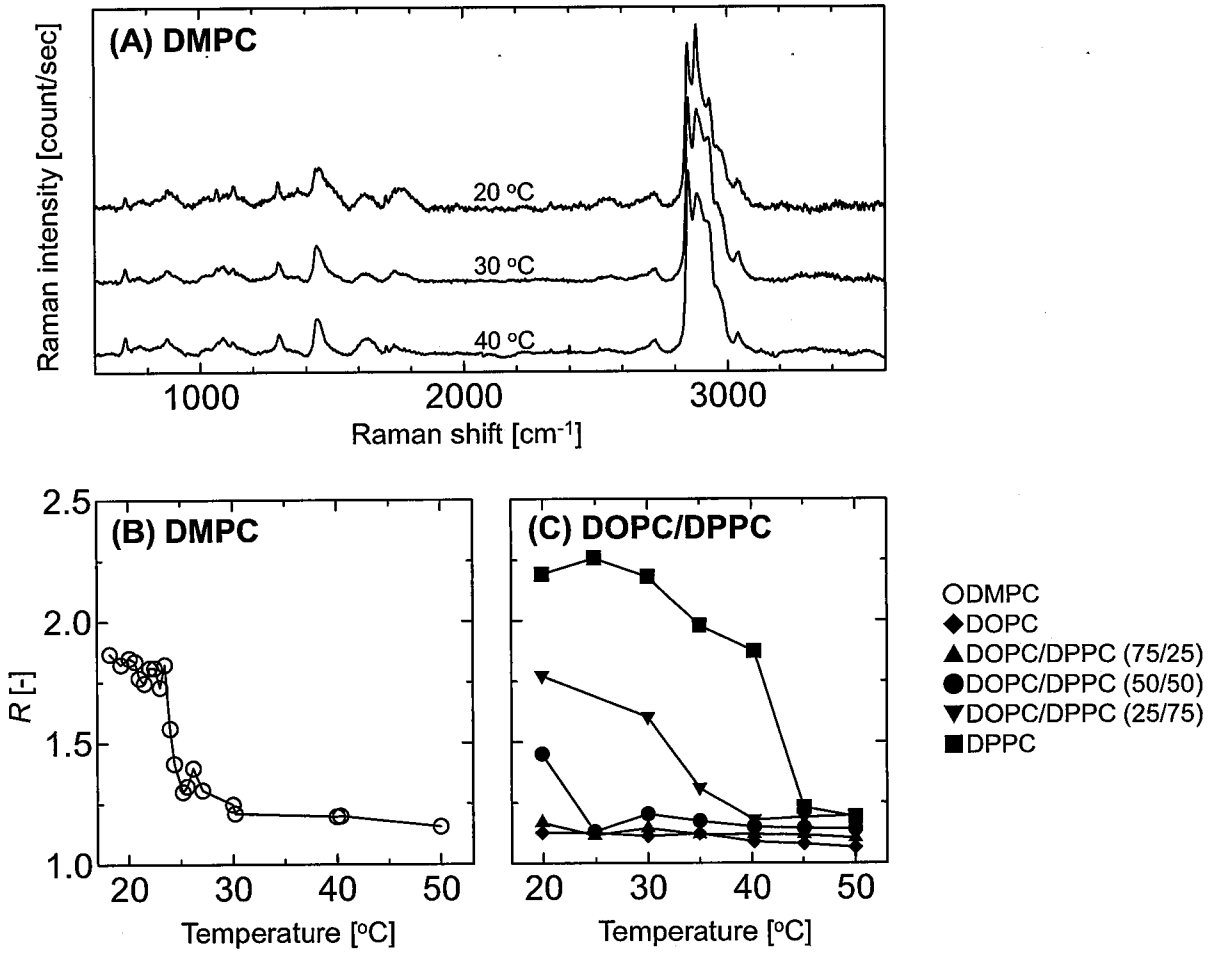

Fig. 2-8 Raman spectroscopic analysis of liposomes. (A) Raman spectra of DMPC, (B) *R* values of DMPC at the temperature range of 20-50 °C, (C) *R* values of DOPC/DPPC liposomes.

Table 2-3 Peak assignment of lipids

Peak [cm^{-1}]	Assignment	Intensity
714	$N^+(CH_3)_3$ symmetric str.	s
873	$N^+(CH_3)_3$ asymmetric str.	m
1062	C-C trans str.	w
1086-1090	C-C gauche str.	w
1126	C-C trans str.	w
1298	$-CH_2-$ twist	m
1438	$-CH_2-$ bend	m
1654	C=C str.	s
1740	C=O str.	w
2850	$-CH_2-$ symmetric str.	vs
2882	$-CH_2-$ asymmetric str.	vs
2930	$-CH_3$ symmetric str.	vs
3040	$-CH_3$ choline asymmetric str.	m

the physicochemical properties of DOPC/DPPC/Ch ternry systems containing LUVs. In order to determine the nano-sized domains, it is important to evaluate the distribution and orientation of lipid molecules or fluorescent probes.

3.6 Detection of Nano-Domains by TEMPO Quenching Method

It has previously been reported that micro- and nano-sized domains are formed on the vesicle membranes in binary and ternary lipid mixtures (Veatch *et al.*, 2005; De Almeida *et al.*, 2005; Heberle *et al.*, 2010; Pathak *et al.*, 2011). The size of these domains was calculated by using the TEMPO quenching method described in the Materials and Methods. TEMPO prefers to bind to l_d domains (Bakht *et al.*, 2007), whereas DPH is distributed evenly over both disordered and ordered domains (Lentz *et al.*, 1976; Ahmed *et al.*, 1997). In a membrane that is partially or totally in an ordered phase, TEMPO quenching is weak, while it is strong in a membrane that is completely in the l_d phase. **Figure 2-9(A)** and **(B)** show the $Q_{liposome}$ values in the presence of TEMPO. The Q_{DPPC} were higher than the Q_{DOPC}, indicating that TEMPO quenching is strong in the l_d phase. At 50 °C, the difference in both $Q_{liposome}$ values was quite small (**Fig. 2-10**), because the DPPC liposome (T_c = 42 °C) is in the l_d phase at 50 °C. The estimated domain size and related properties calculated by using Eq. (1)-(3) are summarized in **Fig. 2-9(C)** and **Table 2-1**. Because the head group diameter of both DPPC and Ch is ca. 4 Å (Marrink *et al.*, 2004; De Meyer *et al.*, 2007), it was able to show that liposomes could definitely form nano-sized ordered domains (>4 Å). Determining the size of nano-domains by FRET requires knowledge of the partitioning of donors and acceptors between nano-domains and the remaining l_d bilayer. Assuming realistic distribution coefficients of the fluorescent probes, previous studies have explored the theoretical limit of FRET to determine nanodomain size (Šachl *et al.*, 2011). In the present study, the TEMPO quenching method, where DPH was quenched by the TEMPO distributed in the disordered phase (Pathak *et al.*, 2011), was developed. Microscopic phase separation was found to occur

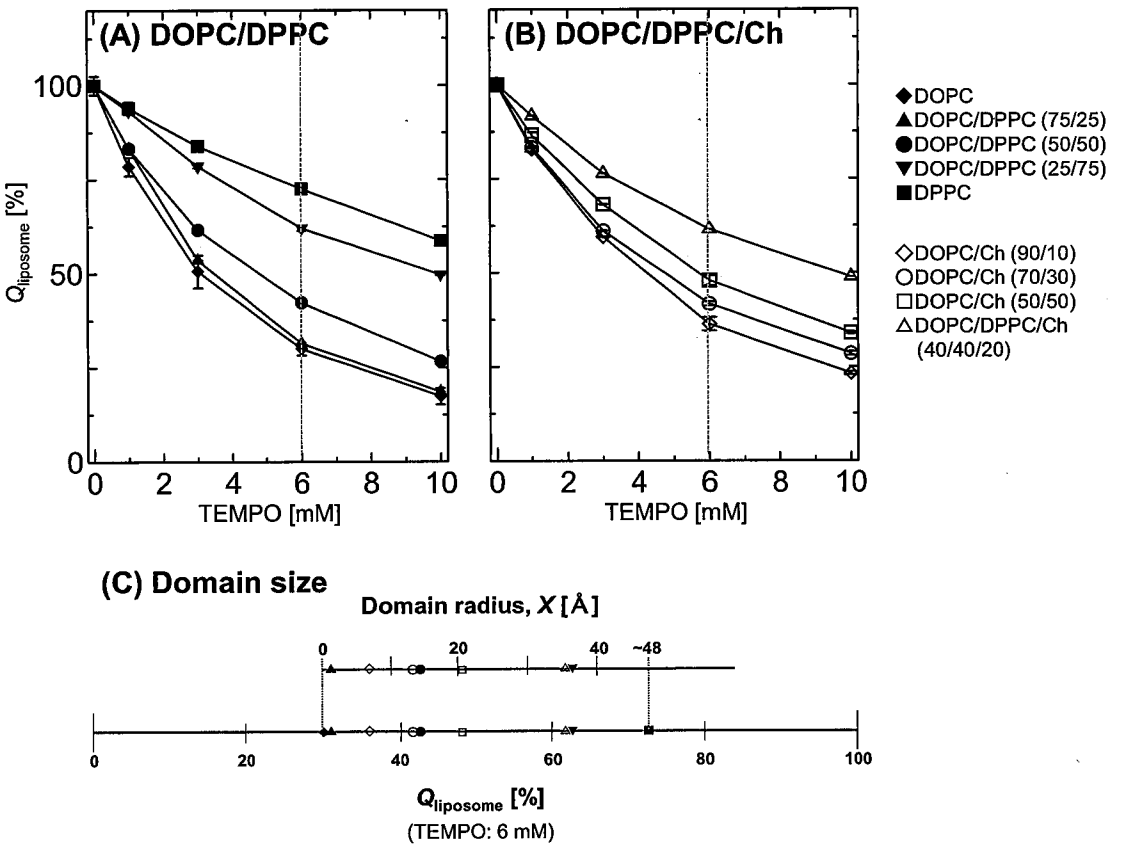

Fig. 2-9 Remaining DPH fluorescence ($Q_{liposome}$) of (A) DOPC/DPPC liposomes and (B) DOPC/DPPC/Ch liposomes. (C) Calculated domain sizes.

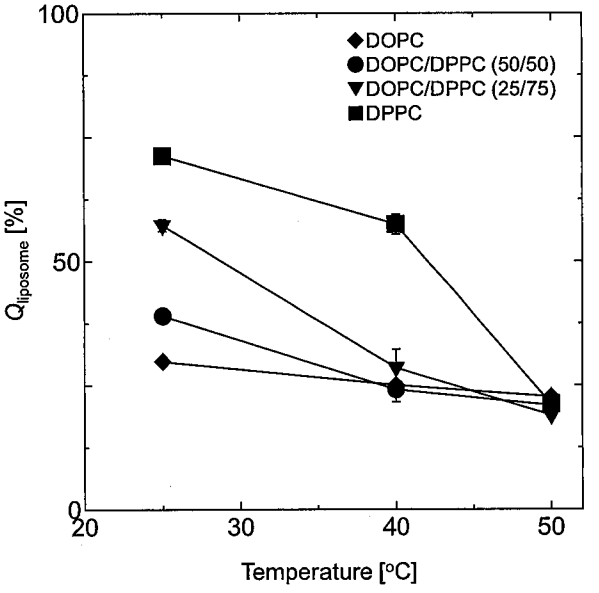

Fig. 2-10 Remaining DPH fluorescence at various temperatures.

at 30 °C in the DOPC/DPPC (50/50) liposome, which is an equimolar lipid mixture of DOPC (T_c <30 °C) and DPPC (T_c >30 °C).

There are ca. 40,000 phospholipids on the surface of an LUV with a diameter of 100 nm. Because the experiments were performed at a lipid/DPH molar ratio of 40000/1, one DPH molecule was distributed in each ordered phase of a liposome. TEMPO quenching strongly depends on the distance between TEMPO and DPH; the sum of their Förster radii is 48 Å. If a DOPC/DPPC (50/50) liposome is perfectly segregated, its $Q_{liposome}$ value should be the same with the Q_{DPPC}. However, the $Q_{DOPC/DPPC\ (50/50)}$ was lower than the Q_{DPPC}, indicating the formation of ordered domains with a size of 13.9 Å. Conversely, DOPC/DPPC (75/25) did not form domains ($Q_{DOPC/DPPC\ (75/25)} \approx Q_{DOPC}$). Furthermore, there was no difference in $Q_{liposome}$ values at 50 °C, indicating that the TEMPO quenching method can detect nano-sized ordered domains in LUVs. Because this TEMPO quenching method simply depends on the distance between DPH and TEMPO, it could be speculated that the nano-domains formed in DOPC/Ch binary lipid mixture (*i.e.*, nano-domains with a size of 13.2 Å in DOPC/Ch (70/30)) and DOPC/DPPC/Ch ternary lipid mixture (*i.e.*, nano-domains with a size of 35.5 Å in DOPC/DPPC/Ch (40/40/20)).

3.7 Phase Diagram of DOPC/DPPC/Ch Ternary Liposomes

Cartesian diagram, that shows membrane fluidity ($1/P$, x-axis) and polarity (GP_{340}, y-axis), were shown in **Fig. 2-11**. The cross point of x- and y-axes is the threshold points of the phase transition in DPPC liposomes ($1/P$ = 6.0 and GP_{340} = -0.2). Based on Cartesian diagram analysis, the liposomes in the 4th quadrant are in disordered phases, while those existing in the 2nd quadrant are in ordered phases. The liposomes in the 1st quadrant, *i.e.*, DOPC/DPPC (50/50) and DOPC/Ch (70/30), are thus in heterogeneous phases at 30 °C. Because the $1/P$ values depend on the lipid/DPH molar ratio and DPH is oriented to ordered phases, the $1/P$ values decreased in proportion to the molar ratio of DPPC; DOPC/DPPC

(25/75) were also estimated to be heterogeneous, but the $1/P$ value were lower due to rich DPPC. Laurdan analysis also revealed that DOPC/DPPC (50/50) and DOPC/Ch (70/30), were thus in heterogeneous phases, as shown in **Fig. 2-6**. These analyses can be useful to sketch the membrane domains and heterogeneity. Span 80 and linoleic acid vesicles are also plotted in **Fig. 2-11** at 30 °C. Span 80 vesicles are reported to consist of nonionic bilayer structure with a higher fluidity (Hayashi *et al.*, 2011), which fits comfortably into Cartesian diagram. In contrast, linoleic acid vesicles were found to be fluid and heterogeneous, possibly due to the dynamic behaviors of fatty acid vesicles (Chen *et al.*, 2004). It was also found that Cartesian diagram analysis could be effective for the monitoring of the possible phase transitions.

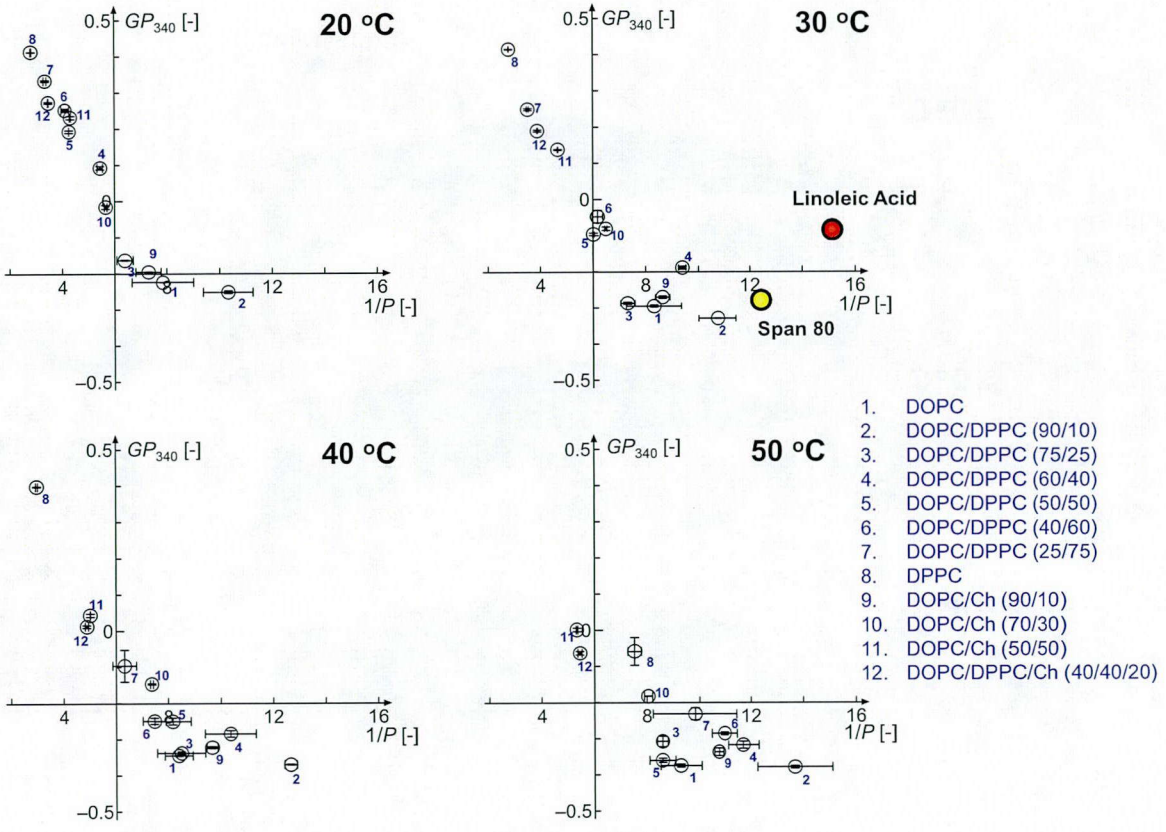

Fig. 2-11 Cartesian diagram of DOPC/DPPC/Ch liposomes

Based on the present results and previous reports, the phase diagrams of DOPC/DPPC/Ch ternary system of LUV liposomes were shown in **Figure 2-12**. Conventional techniques depend on hardware (*e.g.*, a high-quality microscope) and have not yet reported the phase diagram and not detected nano-sized domains in LUVs. In contrast, the assays of DPH, Laurdan, and the TEMPO quenching method can provide new insight into lipid nano-domain formation. Lipid domains play important roles in biological systems. Our previous studies have shown that the heterogeneous liposomes containing Ch exhibited significantly enhanced biological reactions (Bui *et al.*, 2008; Umakoshi *et al.*, 2012), and the lipid membranes are therefore shown to be a functional platform in biological systems (Brown *et al.*, 1998).

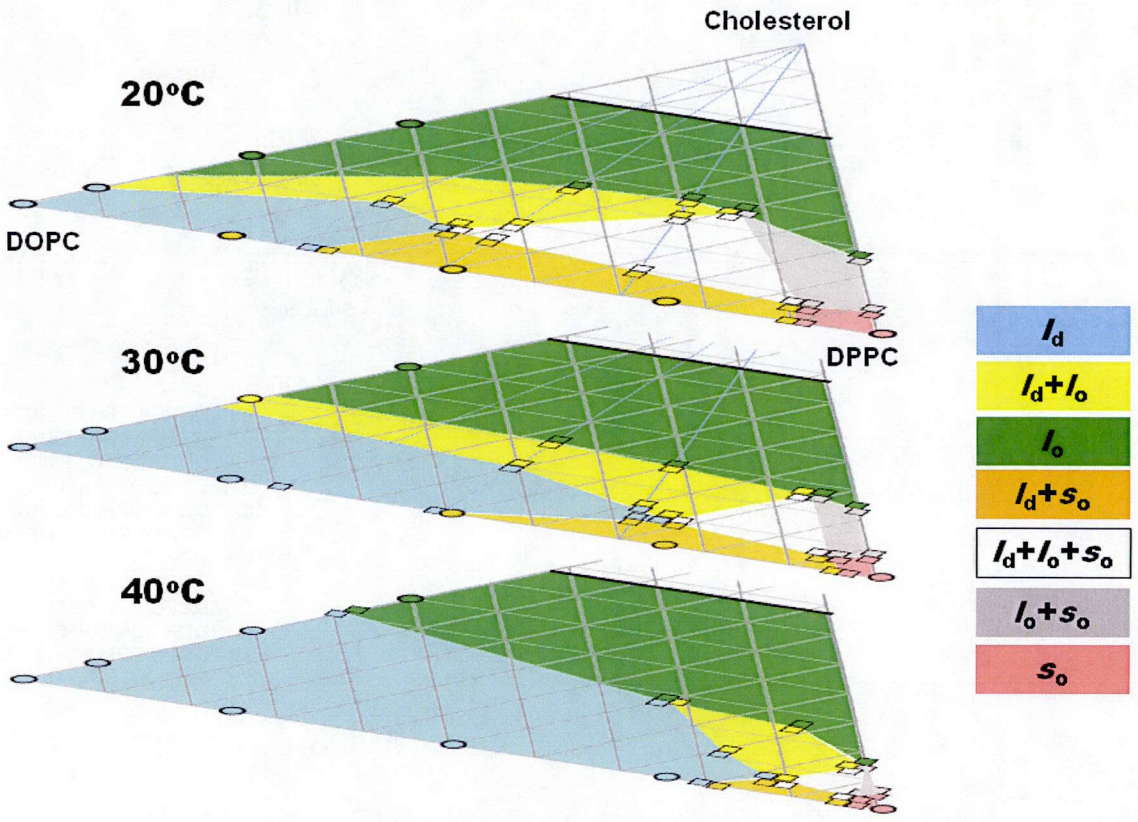

Fig. 2-12 Estimated phase diagram of DOPC/DPPC/Ch ternary system of LUV liposomes.

4. Summary

The physicochemical properties of DOPC/DPPC and DOPC/Ch binary lipid mixtures of LUVs were determined, and nano-sized ordered domains were detected using a newly-developed TEMPO quenching method (**Fig. 2-13**). Analysis of membrane fluidity and polarity revealed that the DOPC/DPPC binary system with LUVs formed immiscible "microscopic" segregated regions. These nano-sized ordered domains were detected by using the TEMPO quenching method, and average domain sizes of 13.9, 36.2, ~13.2 and 35.5 Å were determined for DOPC/DPPC (50/50), DOPC/DPPC (25/75), DOPC/Ch (70/30) and DOPC/DPPC/Ch (40/40/20), respectively. Based on the obtained results in **Chapter 2**, the scheme for membrane characterization is thus established (**Fig. 2-14**). The design of nano-domains on lipid bilayer membranes is very important to regulate the interactions of nucleic acids and other biomacromolecules with lipid membranes. It has been reported that the heterogeneous liposomes can interact with nucleic acids, depending on the surface state of the membrane (Janas *et al.*, 2006; Michanek *et al.*, 2010). This suggests that not only Ch, but also the nano-domains on membrane, could be important factors that regulate the interaction and function of nucleic acids. Therefore, it might be possible to design a liposome surface that can recognize a target biomacromolecule with a structure that fits with the shape (*i.e.*, concavity and convexity with domains) of membrane surface. The detection of nano-domains formed on lipid membranes can also aid the deeper understanding for the function of biomembranes. It is therefore important to understand the structure and function of lipid membranes in biological systems, and to develop artificial biomembrane systems to regulate biomacromolecules. Present findings may be a key to understanding self-assembled systems, and to designing the "*Bio-Inspired*" membranes.

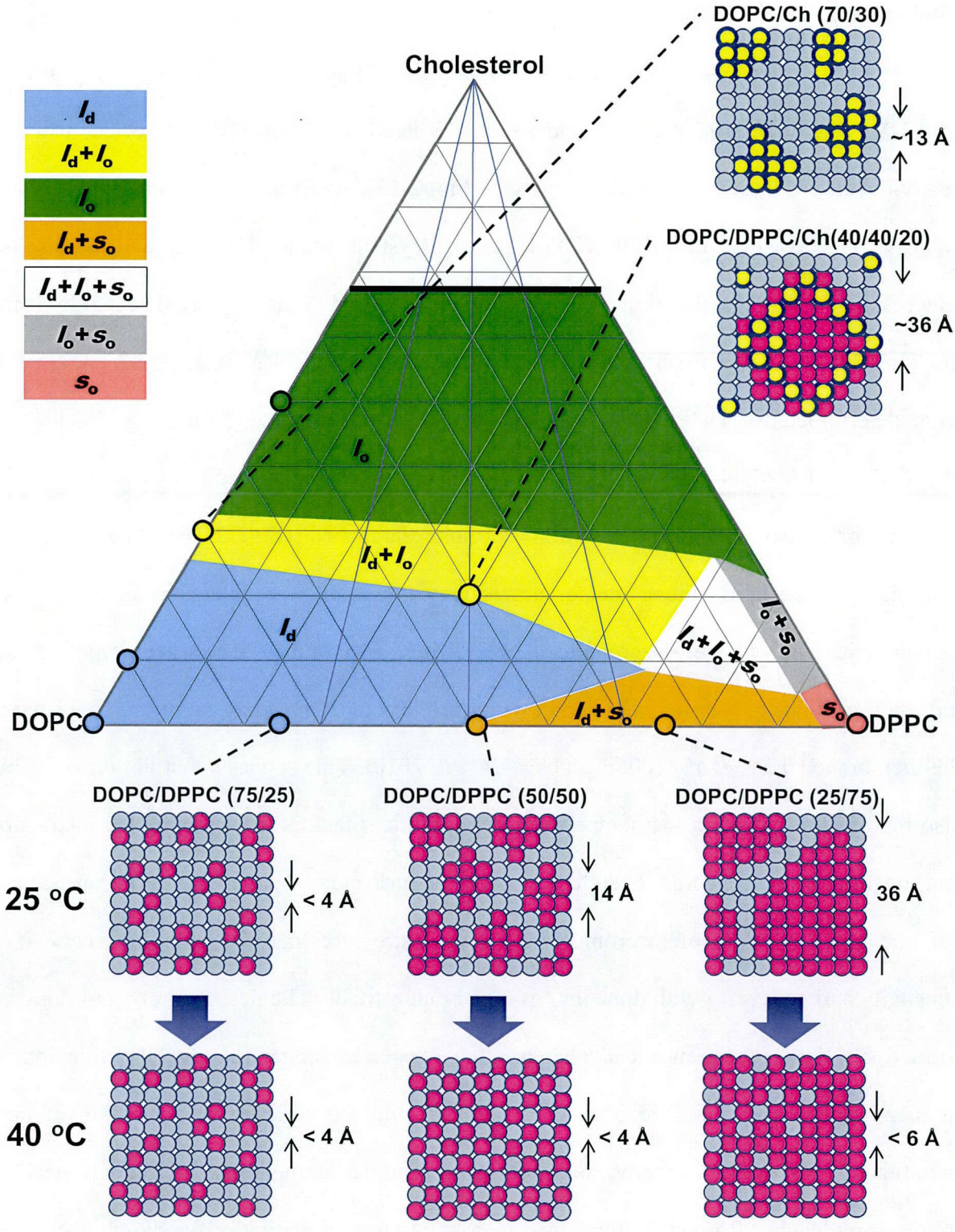

Fig. 2-13 Summary of Chapter 2.

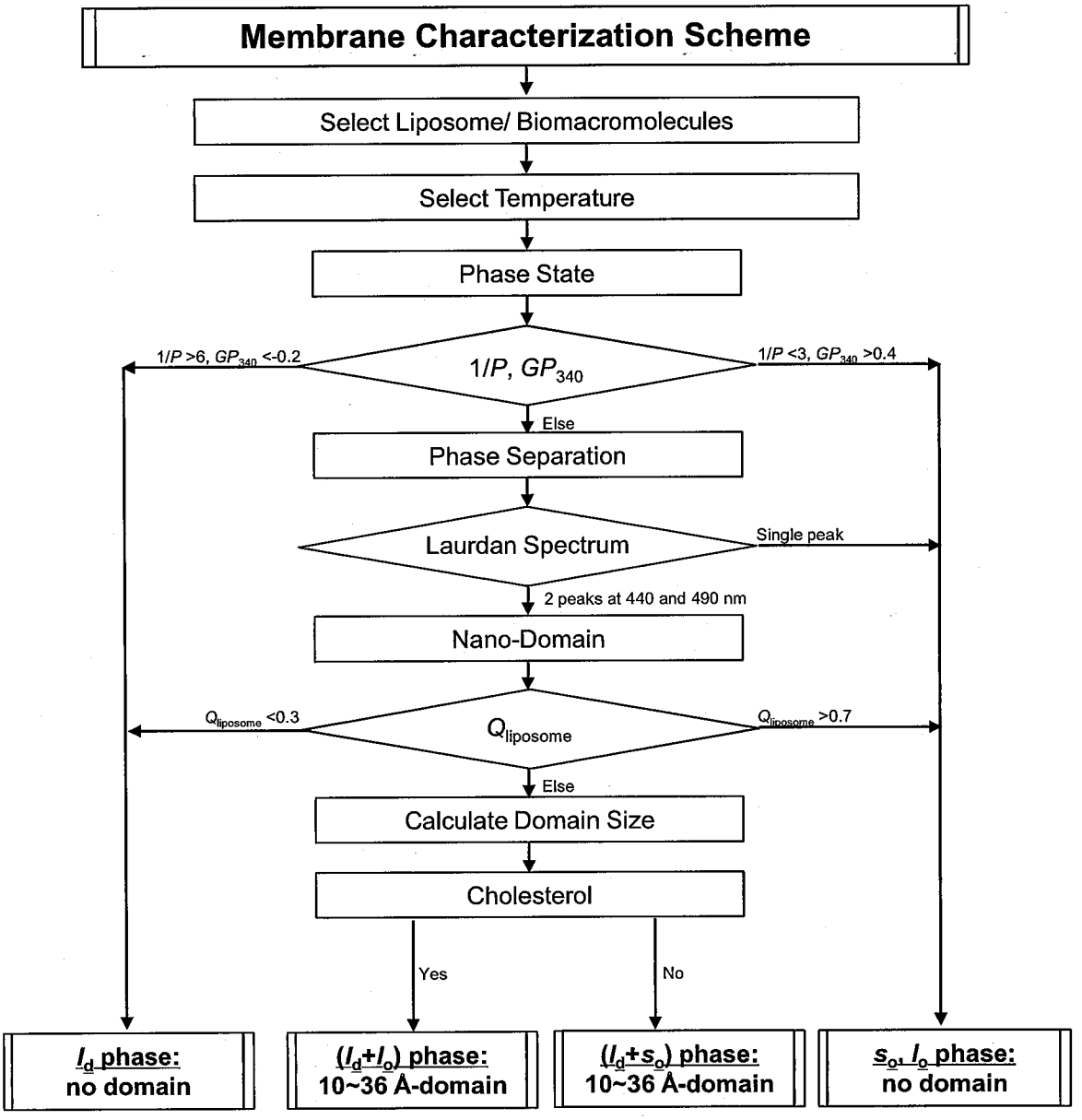

Fig. 2-14 Scheme for characterization of the liposome membranes.

Chapter 3

Mechanism of Liposome Interaction with Biomacromolecules ~Design for Recognition of Single-Stranded RNAs and Polypeptides together with Their Folding and Functionalization~

1. Introduction

In recent years, attempts have been made to use various kinds of self-assemblies for gene delivery techniques in medical and industrial applications (*e.g.*, RNA interference) (Hannon, 2002). Liposomes, which are assemblies of various kinds of lipids, have been studied as carriers for nucleic acids and drugs, whereby liposome-nucleic acid complexes (lipoplexes) are delivered to target cells through endocytotic or direct membrane fusion pathways (Xu *et al.*, 1996; Zohra *et al.*, 2007; Koynova *et al.*, 2009). Modification of liposome surfaces improves the efficiency of gene delivery (Macdonald *et al.*, 1999; Chabaud *et al.*, 2006; Zohra *et al.*, 2007; Xu *et al.*, 2008; Klein *et al.*, 2010). Cationic liposomes (CLs), that are modified with cationic lipids such as 1,2-dioleoyl-3-trimethylammonium propane (DOTAP) and 3β-[N-(N',N'-dimethyl-aminoethane)-carbamoyl]cholesterol (DC-Ch), are quite useful for forming lipoplexes (Muñoz-Úbeda *et al.*, 2010; Giatrellis *et al.*, 2011), although there is little information about the surface properties of CLs and their relation in interaction with nucleic acids. From the viewpoint of gene therapy strategy, there are many advantages in the delivery of RNA molecules by using the liposomes as carriers: siRNA delivery for RNA interference that can knock down target genes, while mRNA can be delivered directly to the cytosol and target organelles (Zou *et al.*, 2010). With regard to synthetic cells, the polynucleotide-lipid membrane interaction has recently attracted significant attention (Luisi,

2007; Ricardo *et al.*, 2009; Walde, 2010; Kurihara *et al.*, 2011; Stano *et al.*, 2011). It is therefore important to clarify the liposome-polynucleotide interaction and control the RNA functions. In order to develop high-affinity liposomes for RNA molecules, the design based on not only electrostatic forces, but also hydrogen bonding, hydrophobic forces, van der Waals forces, is necessary to obtain an appropriate interaction between the liposome surface and polynucleotides. Co-induction of multiple attracting forces on an accumulating surface can be able to produce higher affinity, similar to the molecular recognition in the biological systems (Tezareva *et al.*, 1994; Onda *et al.*, 1996; Patel *et al.*, 2000).

One of the essential roles of lipid membranes is to localize functions on the membranes through the binding of biomacromolecules (Walde, 2010). It has been reported that lipid membranes affect the conformation and function of enzymes (Umakoshi *et al.*, 2009; Ngo *et al.*, 2010; Umakoshi *et al.*, 2012). In most cases, a protein folding process is irreversible, while a folding of polynucleotide is reversible. In both cases, the conformational stability of biomacromolecules is absolutely-required factors to induce and regulate their functions. Polynucleotides, such as DNA or RNA, can be functionalized on biomembranes and their mimics, liposomes (Kato *et al.*, 2009; Kato *et al.*, 2010; Tsuji *et al.*, 2010). Indeed, lipid membranes can (i) recognize biomacromolecules, (ii) induce minor conformational changes, and thus (iii) regulate their functions. According to Janas *et al.*, specific RNAs can bind to ordered phospholipid bilayers, where it has been shown that the DOPC/SM/Ch (60/30/10) liposome effectively interacts with RNA 10 (~15% binding), while DOPC/SM (70/30) and DOPC/SM/Ch (40/30/30) do not (<5% binding). These reports suggest that the design of the physicochemical properties of lipid membranes, such as surface charge density, membrane fluidity, membrane polarity, and nano-domain structure, are extremely important for the recognition of RNAs or other biomacromolecules, and controlling their conformation.

In this chapter, the interaction mechanism of liposomes with biomacromolecules was investigated, focusing on the recognition, folding, and functionalization by selecting

single-stranded RNAs as target (**Fig. 3-1**). Liposome surfaces were modified with cholesterol (Ch), DOTAP, and DC-Ch, and the physicochemical properties of liposomes were analyzed by using fluorescent probes, 1,6-diphenyl-1,3,5-hexatriene (DPH) and 6-lauroyl-2-dimethylaminonaphthalene (Laurdan), as described in **Chapter 2**. Laurdan spectra indicated both an ordered phase (Em: 440 nm) and a disordered phase (Em: 490nm) in the DOPC/DC-Ch (70/30) liposome, which suggests that a microscopic phase separation occurs. In the presence of mRNA, the dehydration of membrane surfaces was evaluated by the variation of general polarity of the Laurdan spectra (general polarization, GP_{340}). The binding sites of mRNA were identified by Raman and Fourier transform infrared (FTIR) spectroscopies. The dissociation constant, K_d, was calculated in order to discuss the effect of membrane designs for RNA recognition. In addition, the conformational change of RNAs was evaluated by using circular dichroism (CD) spectroscopy. It was found that the liposomes

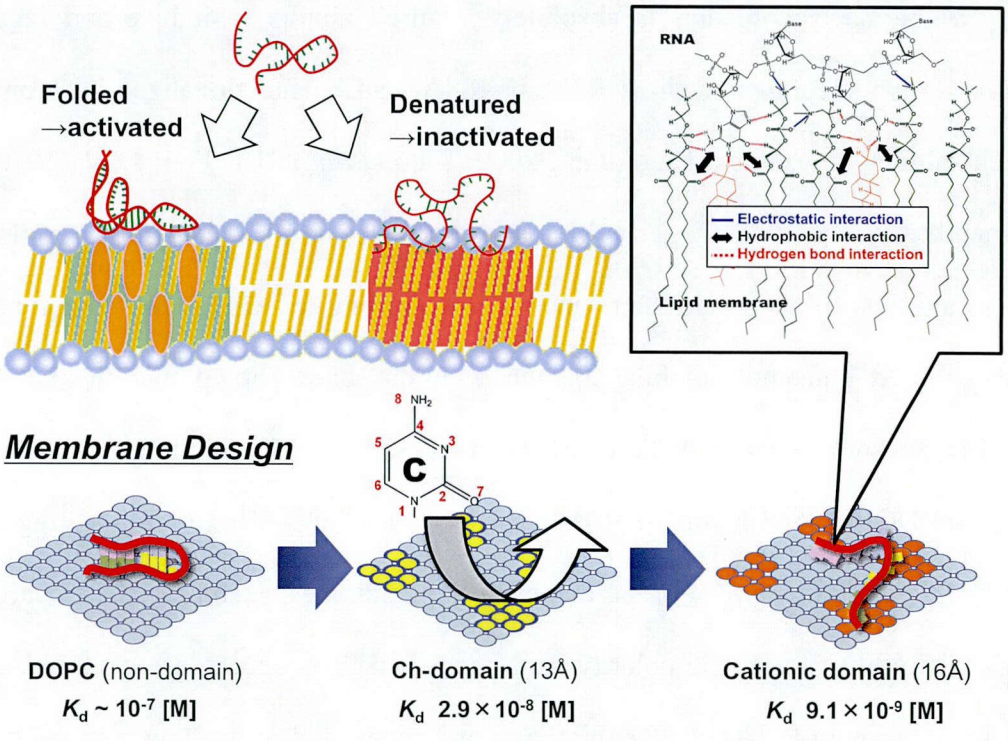

Fig. 3-1 Conceptual illustration of Chapter 3.

affected the conformation of single-stranded RNAs, which is a key parameter affecting their functions (Laso *et al.*, 1993; Lilley, 2005; Marsden *et al.*, 2006). The dependence of liposome-RNA interaction on the phase state of CLs is also discussed. Based on the above findings, the key factors for liposome design for the recognition, folding, and functionalizing of biomacromolecules (*i.e.*, polynucleotide and polypeptide) were investigated, especially focusing on their interaction mechanism.

2. Materials and Methods

2.1 Materials

1-Palmitoyl-2-oleoyl-*sn*-glycero-3-phosphocholine (POPC), 1,2-dipalmitoyl-*sn*-glycero-3-phosphocholine (DPPC), 1,2-dioleoyl-*sn*-glycero-3-phosphocholine (DOPC), 1,2-dioleoyl-3-trimethylammonium propane (DOTAP), 1,2-dipalmitoyl-3-trimethylammonium propane (DPTAP), and 3β-[N-(N',N'-dimethylaminoethane)-carbamoyl]cholesterol (DC-Ch) were purchased from Avanti Polar Lipids, Inc. (Alabaster, AL, USA). Cholesterol (Ch), transfer RNA (tRNA) originating from *E. coli*, nucleotide triphosphate (NTP; ATP, UTP, CTP, and GTP) were purchased from Sigma-Aldrich (St. Louis, MO, USA). A Rapid Translation System RTS 100 *E. coli* HY Kit (RTS-Kit) was purchased from Roche Diagnostics (Indianapolis, IN, USA). T7 RiboMAX™ Expression Large-scale RNA Production System and SV Total RNA Isolation System were purchased from Promega (Madison, WI, USA). Other chemicals were purchased from Wako Pure Chemical (Osaka, Japan) and were used without further purification.

2.2 Liposome Preparation

A solution of phospholipids in chloroform was dried in a round-bottom flask by rotary evaporation under vacuum. The obtained lipid films were dissolved in chloroform and the solvent evaporated. The lipid thin film was kept under high vacuum for at least 3 h, and then hydrated with distilled water at room temperature. The vesicle suspension was frozen at -80 °C and then thawed at 50 °C to enhance the transformation of small vesicles into larger multilamellar vesicles (MLVs). This freeze-thaw cycle was repeated five times. MLVs were used to prepare large unilamellar vesicles (LUVs) by extruding the MLV suspension 11 times through two layers of polycarbonate membrane with a mean pore diameter of 100 nm using an extruding device (Liposofast; Avestin Inc., Ottawa, Canada). Liposomes with different compositions were also prepared by using the same method.

2.3 Transcription and Purification of mRNA

pIVEX control vector GFP (Roche) was used as the plasmid DNA. The plasmid DNA was treated once with the restriction enzyme *ApaL* I for one hour incubation at 37 °C in order to cleave the *Amp*R gene and to obtain line DNA fragments harboring the GFP gene before its transcription. The transcription of the mRNA encoding the GFP gene (861 bp) was carried out using T7 RiboMAX^{TM} Expression Large Scale RNA Production System (Promega, Madison, WI, USA), which includes T7 RNA polymerase as a transcriptional enzyme. Transcription was performed for 30 min at 37 °C. The obtained mRNA was recovered and purified with the SV total RNA Isolation Kit (Promega, Madison, WI, USA). The mRNA products were quantified from the absorbance at 258 nm and the electrophoresis on 1 % of agarose gel.

2.4 Evaluation of GFP Expression Using *E.coli* Cell-Free Translation System

GFP expression was performed by using *E. coli* CF, RTS-Kit. GFP was expressed in the presence of liposomes, where gene vectors were pIVEX control vector GFP (plasmid DNA) or the transcribed mRNA. In the case of evaluation at translation step, liposomes and mRNA were pre-incubated at 30 °C for 15 min, and then added to the RTS-Kit. GFP expression was performed for 6 h at 30 °C, and the obtained GFP was kept at 4 °C for 24 h. The amount of GFP synthesized by using the RTS-Kit was evaluated by SDS-PAGE analysis and the fluorescence of GFP (Ex = 395 nm, Em = 509 nm), based on the previously-published methods (Bui *et al.*, 2008).

2.5 Evaluation of Membrane Fluidity and Polarity of Liposomes

The inner membrane fluidity of the liposomes was evaluated in a similar manner to previous reports (Lentz *et al.*, 1976). Fluorescent probe DPH was added to a liposome suspension with a molar ratio of lipid/DPH = 250/1; the final concentrations of lipid and DPH were 100 and 0.4 μM, respectively. The fluorescence polarization of DPH (Ex = 360 nm, Em

= 430 nm) was measured using a fluorescence spectrophotometer (FP-6500 and FP-8500; JASCO, Tokyo, Japan) after incubation at 30 °C for 30 min. The sample was excited with vertically polarized light (360 nm), and emission intensities both perpendicular ($I_{\perp}$) and parallel ($I_{\parallel}$) to the excited light were recorded at 430 nm. The polarization (P) of DPH was then calculated by using the following equations:

$$P = (I_{\parallel} - GI_{\perp}) / (I_{\parallel} + GI_{\perp})$$

$$G = i_{\perp} / i_{\parallel},$$

where $i_{\perp}$ and $i_{\parallel}$ are emission intensity perpendicular and parallel to the horizontally polarized light, respectively, and G is the correction factor. The membrane fluidity was evaluated based on the reciprocal of polarization, $1/P$.

The fluorescent probe Laurdan is sensitive to the polarity around itself, which allows the surface polarity of lipid membranes to be determined (Parasassi *et al.*, 1991). Laurdan emission spectra exhibit a red shift caused by dielectric relaxation. Thus, emission spectra were calculated by measuring the general polarization (GP_{340}) for each emission wavelength as follows:

$$GP_{340} = (I_{440} - I_{490}) / (I_{440} + I_{490}),$$

where I_{440} and I_{490} are the emission intensity of Laurdan excited with 340 nm light. No fluorescence was observed from an mRNA solution (without liposomes). The final concentrations of lipid and Laurdan in the test solution were 100 and 2 μM, respectively. The final concentration of lipid and Laurdan was 10 μM and 0.2 μM, respectively.

2.6 Agarose Gel Electrophoresis for Evaluation of mRNA Binding onto Cationic Liposomes

mRNA samples were prepared in the presence of DOPC/DOTAP liposomes or DOPC/DC-Ch liposomes, containing ×1 loading buffer (0.1 % SDS, 5 % glycerol, 0.005 % of bromophenol blue). The final concentration of mRNA and lipid was 1 μM and 1 mM,

respectively. After 30 min of sample incubation at 30 °C, electrophoresis was performed in a 1 % agarose gel with a voltage of 150 mV for 20 min, the running buffer is a ×1 TBE buffer (89 mM Tris, 89 mM boric acid, 2 mM EDTA). The gel was stained with SYBR Green II, which is a RNA-specific fluorescence probe that enables quantitative analysis of RNA (Morozkin *et al.*, 2003), and the density of mRNA bands was analyzed by using the SCION image software obtained at http://www.scion.com/. The densitometer analysis was carried out at least three times at different points along the lane.

2.7 Evaluation of UV Spectra

The turbidity of liposome suspension in the presence or absence of tRNA was evaluated by using a UV-1800 Spectrophotometer (SHIMAZU, Kyoto) and an Ultramark microplate reader (Bio-Rad Japan, Tokyo). The turbidity at 405 nm (OD_{405}) was measured using a quartz cell (1 cm path length) for a spectrophotometer and with 96-well plate for the microplate reader at 30 °C. The increase of OD_{405} was defined as ΔOD_{405} ;

$$\Delta OD_{405} = OD_{405,\,(+)\,RNA} - OD_{405,\,(-)\,RNA}.$$

It was confirmed that no absorbance (at 405 nm) was observed in the case of tRNA only. The final concentration of tRNA was 2.2 μM, where the lipid concentration was 1 mM for the zwitterionic (POPC/Ch) liposomes and 1.17 mM for the cationic (POPC/DOTAP) liposomes. Dissociation constant, K_d, was calculated based on the previous reports (Stephanos *et al.*, 1996; Marty *et al.*, 2009).

2.8 Fluorescence Measurement of TNS

TNS was directly added to a liposome suspension and was then incubated for one hour at room temperature in order to complete TNS insertion into lipid membrane. After the addition of tRNA, samples were incubated in the dark for 30 min at 30 °C. The fluorescence spectra of TNS (Ex = 340 nm) were measured from 380 nm to 500 nm using a fluorescence

spectrophotometer (FP-6500; JASCO, Tokyo, Japan) with 5 nm light path. The final concentrations of TNS and lipid were 20 μM and 0.5 mM, respectively. TNS fluorescence was not observed with tRNA only.

2.9 Infrared Spectroscopy of tRNA

A 30-μl tRNA sample was applied in 50-μm-thick cell with a CaF_2 window. The infrared spectra were measured by using an FTIR 4100 spectrometer (JASCO, Japan) equipped with an Hg–Cd–Te detector. The resolution was set up at 2 cm^{-1}; the frequency range from 1750 to 1150 cm^{-1} was collected for each sample. The infrared spectrum of water was subtracted from those of the samples. The accuracy of the frequency reading was better than ±0.1 cm^{-1}. One hundred scans excluding buffer and liposome background signals were accumulated. The spectra were smoothed with the Savitzky-Golay procedure (Conn *et al.*, 1998; Madore *et al.*, 1999). The concentration of tRNA and the lipid was adjusted at 3.94 mM and 0-98.5 μM, respectively, and the lipid/tRNA molar ratios were 0/100, 1/100, and 1/40.

2.10 Raman Spectroscopic Analysis

Raman spectra of mRNA and nucleotide triphosphates (NTPs) were measured using a confocal Raman microscope (LabRAM HR-800; HORIBA, Ltd., Kyoto, Japan) at a wavelength of 266 and 532 nm, with laser power of 50 and 100 mW, respectively. A total data accumulation time was 30 s. For each sample, the background signal of the solution was removed, and then the baseline was corrected. Peak intensities were normalized by the peak at 878 cm^{-1} (I_{878}) for excitation laser of 266 nm, and at 1090 cm^{-1} (I_{1090}) for that of 532 nm, as inner references. The final concentration of mRNA and lipid in Raman samples was 0.77 μM and 50 or 500 μM, respectively.

2.11 Evaluation of the Conformation of mRNA Using Circular Dichroism (CD) Spectra

The conformation of RNA was evaluated by using a JASCO J-820 SFU spectropolarimeter (JASCO, Tokyo) (Suga *et al.*, 2011). The CD spectrum from 300 nm to 200 nm was measured with a quartz cell (0.1 cm path length) at a scan speed of 50 nm per min and a width of 2 nm. Five scans excluding buffer and liposome background signals were obtained at 30 °C, and the data was calculated as molar ellipticity. Each sample was prepared with 0.77 μM of mRNA and 10 mM Tris-HCl at pH 7.8 in the presence or absence of CLs.

2.12 Statistical Analysis

Results are expressed as mean ± standard deviation. All experiments were performed at least three times. The distribution of data was analyzed, and statistical differences were evaluated using the Student's t-test. A P-value of <5% was considered significant.

3. Results and Discussion

3. 1 Inhibitory Effect of CLs on the Translation Step of the *in vitro* GFP Expression

The inhibitory effect of cationic liposomes on the "translation" step was investigated by initiating the *in vitro* GFP expression from the mRNA. The attractive electrostatic interactions between negatively-charged nucleic acids and positively-charged CLs containing DOTAP or DC-Ch are very strong. Thus, although CLs can offer higher transfection efficiency in a variety of host cells, these strong electrostatic interactions inhibit the release of the gene, preventing gene expression (Xu *et al.*, 1996; Barreau *et al.*, 2006). In order to determine the inhibitory effect of CLs on the translation step, DOPC liposomes were modified with 10–50 mol% of cationic molecules (DOTAP or DC-Ch), focusing on the lipid structure (**Fig. 3-2**), and the amount of GFP expressed from the mRNA was evaluated as a function of cationic lipid concentration (**Figs. 3-3** and **3-4**). Both DOPC/DOTAP and DOPC/DC-Ch liposomes inhibited the *in vitro* GFP expression with an increase in total lipid concentration.

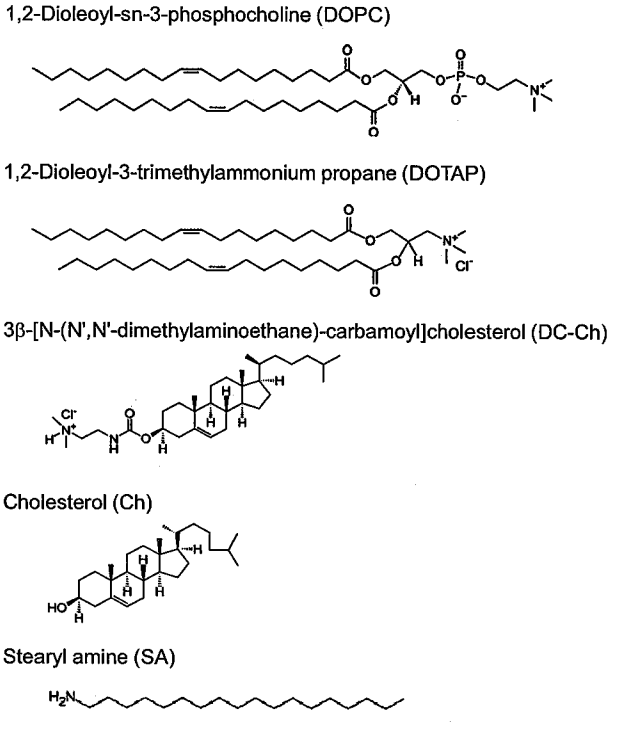

Fig. 3-2 Structure of lipids.

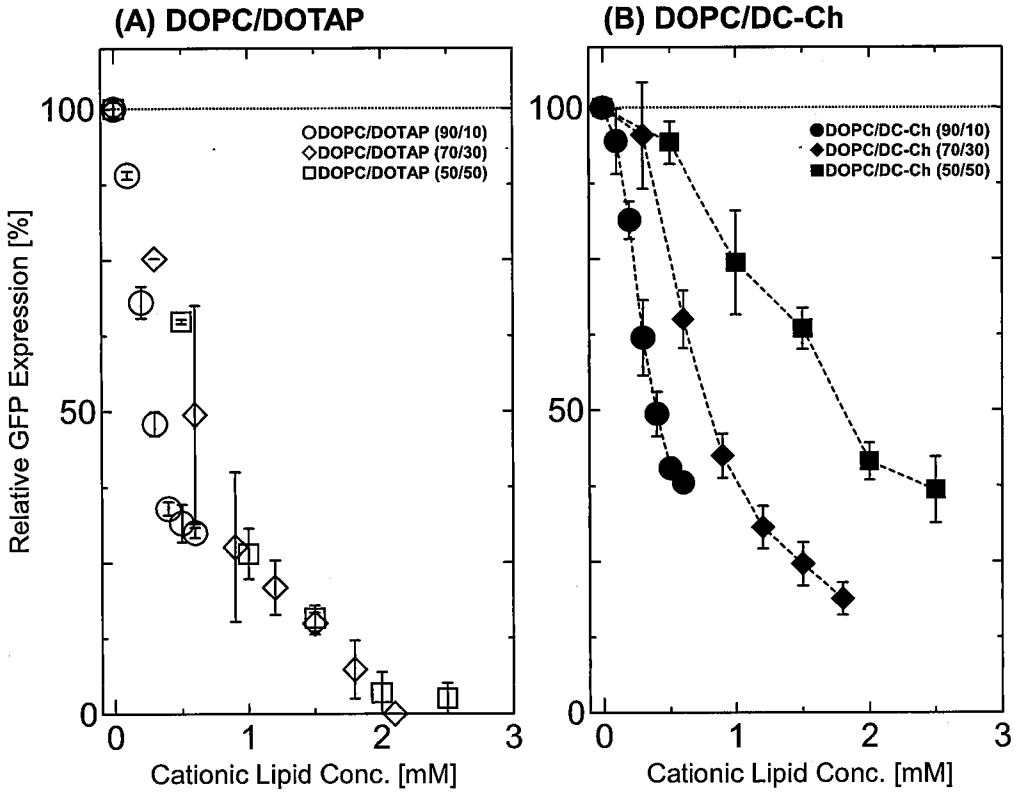

Fig. 3-3 Relative GFP expression in the presence of (A) DOPC/DOTAP liposomes and (B) DOPC/DC-Ch liposomes.

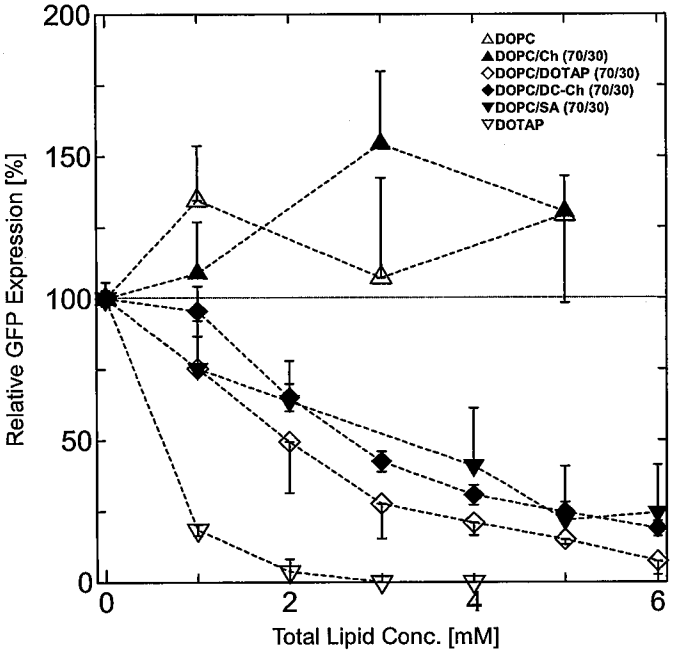

Fig. 3-4 Relative GFP expression in the presence of various liposomes.

There was similar inhibition efficiency between DOPC/DOTAP (90/10), DOPC/DOTAP (70/30), and DOPC/DOTAP (50/50) formulations (**Fig. 3-3(A)**), while that of DOPC/DC-Ch liposomes was different (**Fig. 3-3(B)**). Because Ch causes rigidity in a lipid membrane (De Almeida *et al.*, 2003), DOPC/DC-Ch liposome membranes can also be rigid, depending on the mole fraction of DC-Ch molecules. It is expected that a difference in the phase state of DOPC/DC-Ch can affect the inhibition efficiency of CLs. To estimate the effect of cationic lipid type, GFP expression was performed in the presence of DOTAP-, DC-Ch-, and SA-modified DOPC liposomes (**Fig. 3-4**). The zwitterionic liposomes (DOPC and DOPC/Ch (70/30)) enhanced GFP expression, while CLs, containing DOPC/DOTAP (70/30), DOPC/DC-Ch (70/30), DOPC/SA (7030), and DOTAP, inhibited expression. The inhibition efficiency was lower (~5%) in the case of DOPC/DC-Ch (70/30) at 1 mM, while that of DOPC/DOTAP (70/30) or DOPC/SA (70/30) was higher (~25%), and that of DOTAP was markedly higher (~80%). The interaction between CLs and single-stranded RNAs depends both on the surface charge density of membranes and on the amount of cationic lipids in the experimental systems (Thomas *et al.*, 2005), indicating that the inhibition of mRNA translation is due to the interaction between CLs and the mRNA (Tachibana *et al.*, 2002). These results suggest that the inhibitory effect of CLs on mRNA translation, although their interaction is likely to be related to the physicochemical properties (*i.e.*, fluidity, polarity, and heterogeneity) of CLs.

3.2 Characterization of Physicochemical Properties of CLs

DPH and Laurdan are micro-environment-sensitive fluorescent probes that are used to characterize liposome membrane surfaces (Lentz, 1993; Parasassi *et al.*, 1998). **Figure 3-5(A)** shows a Cartesian diagram of CLs (at 30 °C), where the *x*- and *y*-axes indicate membrane fluidity ($1/P$) and membrane polarity (GP_{340}), respectively. DOPC, DOPC/DOTAPs and DOPC/SA (70/30) are located at similar positions in the diagram,

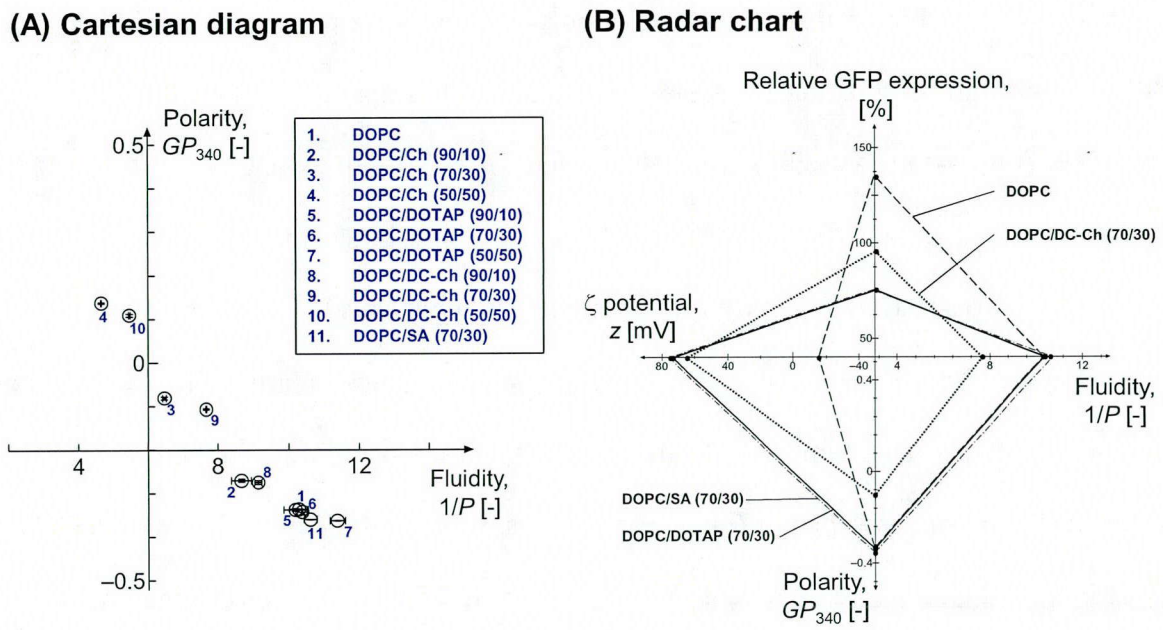

Fig. 3-5 (A) Cartesian diagram of CLs and (B) Radar chart of CLs on GFP expression.

indicating that these liposomes are in liquid-disordered (l_d) phases. Although a strong interaction between the phosphate groups [$-PO_2^-$-] of DOPC and trimethyl-ammonium groups [$-N^+(CH_3)_3$] of DOTAP is expected to be induced (Troutier *et al.*, 2005), the membrane fluidities of DOPC and of DOPC/DOTAPs are similar, suggesting that DOTAP molecules are distributed homogeneously on the membrane surface. On the other hand, l_o phase DOPC/Ch (50/50) (Veatch *et al.*, 2003) and DOPC/DC-Ch (50/50) indicated similar physicochemical properties and appeared in the 2nd quadrant. It has previously been reported that DPH anisotropy of the DC-Ch/1,2-dioleoyl-*sn*-glycero-3-phopshoethanolamine liposome increased with an increase in the DC-Ch content (Muñoz-Úbeda *et al.*, 2010), indicating that the membrane fluidity decreased in the presence of DC-Ch molecules, as well as Ch molecules. It is therefore shown that liposomes located in the 2nd quadrant in the diagram are in ordered phases. DOPC/Ch (70/30) and DOPC/DC-Ch (70/30) appeared in the 1st quadrant, indicating that they are in heterogeneous (l_d + l_o) phases. Laurdan is sensitive to the polarity of

surrounding media which differs in dielectric constant, and shows the specific emission peaks at 440 and 490 nm, originating from the lipid membrane in disordered and ordered phases, respectively (**Fig. 3-6**) (Parasassi *et al.*, 1998). DOPC/Ch (70/30) and DOPC/DC-Ch (70/30) indicated peaks at both 440 and 490 nm. It is therefore shown that the phase states of DOPC/Ch (70/30) and DOPC/DC-Ch (70/30) are in heterogeneous ($l_d + l_o$) phases.

Figure 3-5(B) shows a radar chart, which compares relative GFP expression, membrane fluidity ($1/P$), membrane polarity (GP_{340}), and ζ potential (z) in the presence of 1 mM liposomes. In the presence of l_d phase liposomes, DOPC/DOTAP (70/30) and DOPC/SA (70/30) inhibited GFP expression, demonstrating that the CLs in disordered membranes have an inhibitory effect on mRNA translation. Although DOPC/DC-Ch (70/30) has a positively-charged membrane, similar to DOPC/DOTAP (70/30) and DOPC/SA (70/30), it slightly inhibited GFP expression. This indicates that heterogeneity of the liposome surface is key to regulating RNA functions. In the following sections, the liposome-RNA interactions are determined, focusing on the RNA binding affinity and its mechanism together with the conformation of RNA molecules (shown in **Fig. 3-7**).

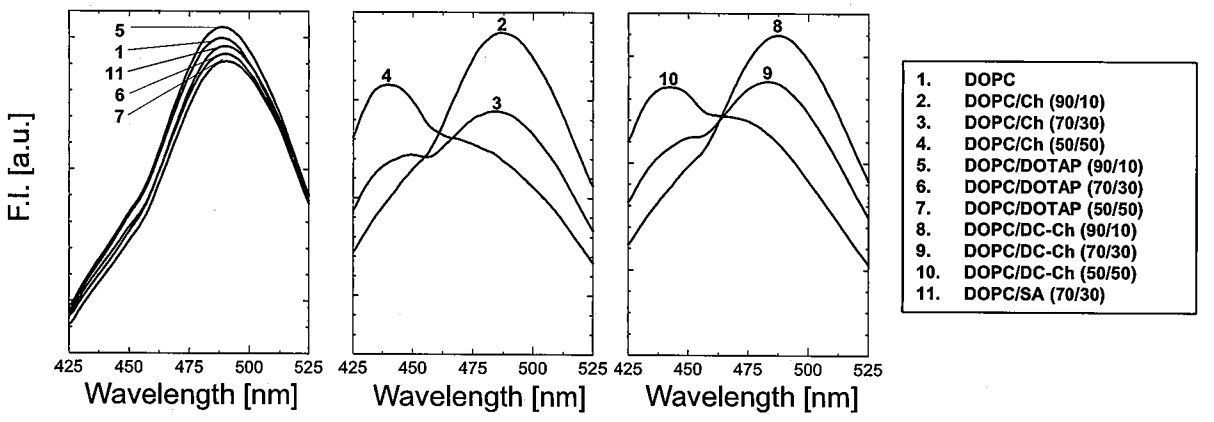

Fig. 3-6 Laurdan spectra of liposomes at 30 °C.

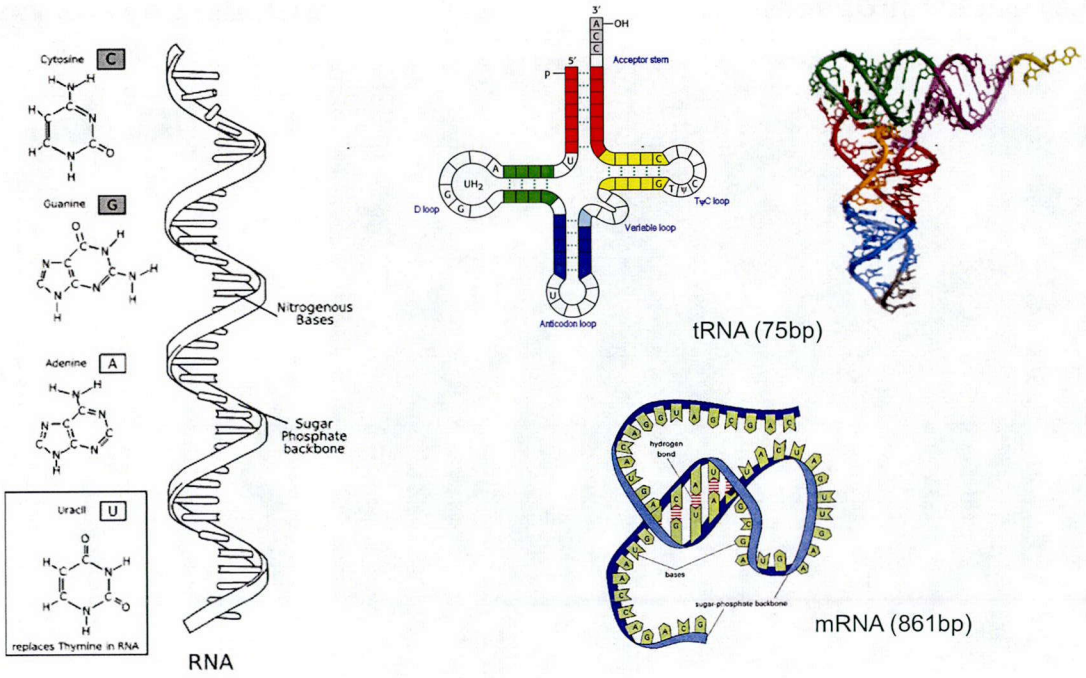

Fig. 3-7 Schematic illustration of RNA structures.

3.3 mRNA Binding to CL Membranes

3.3.1 Evaluation of mRNA Binding Using Agarose Gel Electrophoresis

Electrophoresis of mRNA using a 1% agarose gel was performed to elucidate the difference in mRNA adsorption of 1 mM of CLs (**Fig. 3-8**). The amount of mRNA adsorption onto DOPC/DOTAP liposomes and the inhibition efficiency increased in proportion to the mole fraction of DOTAP molecules, suggesting that DOPC/DOTAP liposomes inhibited mRNA translation by strong electrostatic interactions with mRNA. However, mRNA adsorption onto DOPC/DC-Ch liposomes reached a plateau at 30 mol% DC-Ch. Although the amount of mRNA binding was almost the same (~44%) at the total lipid concentration of 1 mM, the heterogeneous DOPC/DC-Ch (70/30) slightly inhibited mRNA translation. This result implies that the mRNA bound onto DOPC/DC-Ch liposomes exists in an "active" form for translation, while that binding onto DOPC/DOTAP liposomes is "inactive".

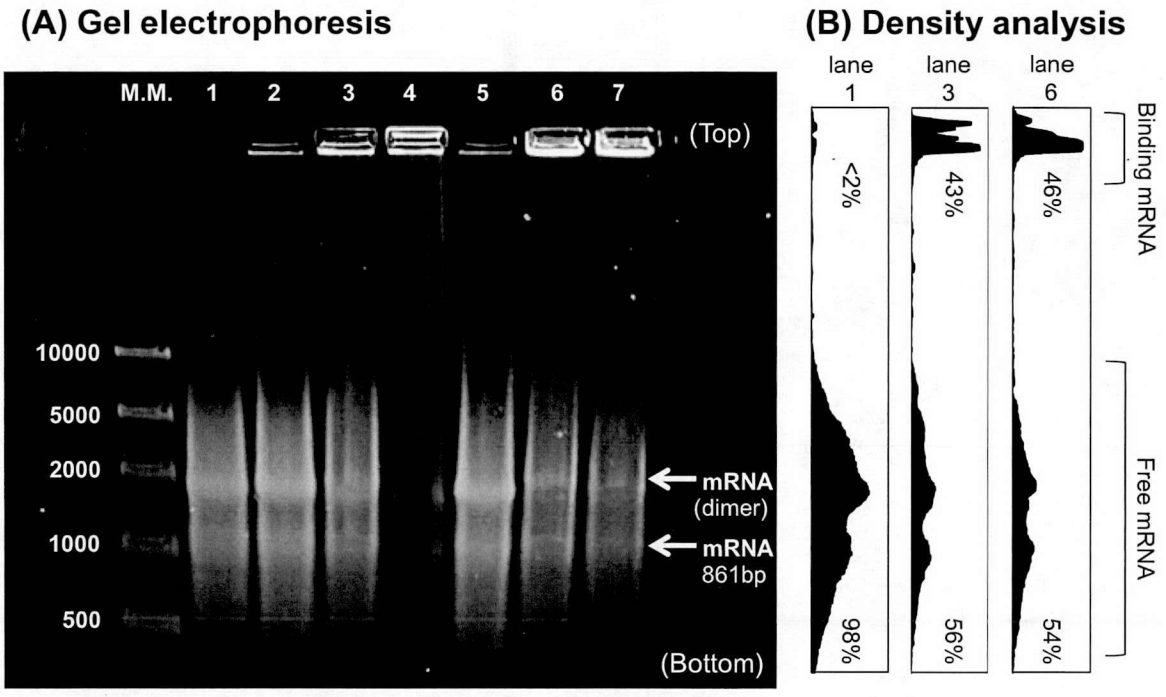

Fig. 3-8 (A) Agarose gel electrophoresis of mRNA. 1, mRNA; 2, +DOPC/DOTAP (90/10); 3, +DOPC/DOTAP (70/30); 4, +DOPC/DOTAP (50/50); 5, +DOPC/DC-Ch (90/10); 6, +DOPC/DC-Ch (70/30); 7, +DOPC/DC-Ch (50/50). (B) Densitometer analysis.

3.3.2 Evaluation of mRNA Binding Using Agarose Gel Electrophoresis and Laurdan

The polarity of the membrane was investigated by using the fluorescent probe, Laurdan (Viard *et al.*, 1997; Hirsch-Lerner *et al.*, 1999), and the general polarization (GP_{340}) was measured as an indicator of the hydration degree at the membrane surface. In the presence of mRNA, the spectrum of Laurdan for the CLs was shifted to that at hydrophobic environment, while that of DOPC was not (**Fig. 3-9(A)**). The hydrophobic-hydrophilic interface of the lipid membrane, which can be monitored by Laurdan, is one of the possible binding sites for nucleic acids (Kikuchi *et al.*, 1999; Michanek *et al.*, 2010), suggesting that mRNA binds at the interface region of CL membranes. The variations of GP_{340} values of CLs were examined in the presence of mRNA (**Fig. 3-9(B)**). An increase in the GP_{340} value was observed in the presence of CLs, while it was not observed in the presence of DOPC. Because Laurdan does not possess fluorescence in aqueous solution or in a mRNA solution (data not

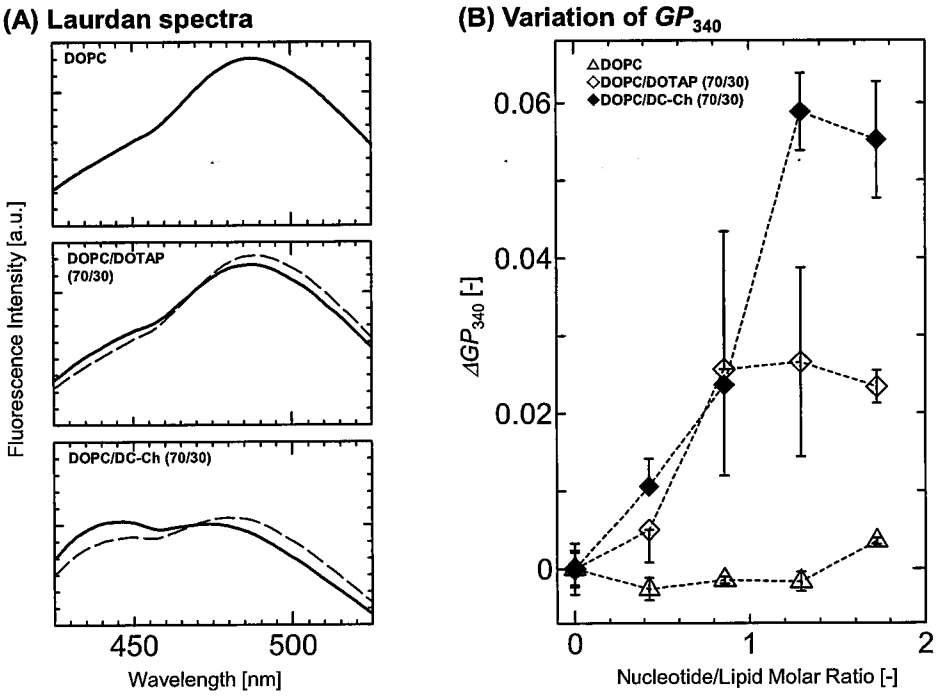

Fig. 3-9 (A) Laurdan spectra of liposomes in the presence (*bold line*) or absence (*dotted line*) of mRNA. (B) Variations of GP_{340} values. $\Delta GP_{340} = GP_{340,\,(+)\mathrm{mRNA}} - GP_{340,\,(-)\mathrm{mRNA}}$.

shown), the increase of GP_{340} value is due to dehydration of the membrane surface caused by mRNA binding. The surfaces of liposome membranes and nucleic acids are well hydrated (Auffinger *et al.*, 1997; Shih *et al.*, 1998; Shimanouchi *et al.*, 2011). Studies also show that the localization of nucleic acids onto lipid membrane induces dehydration (Hirsch-Lerner *et al.*, 1999), and subsequent conformational transitions in nucleic acids by entropic driven forces (Clark *et al.*, 1997; Kato *et al.*, 2010). It is therefore possible that the mRNA-CL interaction is governed in an entropy-driven manner through water of hydration. The degree of dehydration of DOPC/DOTAP (70/30) and DOPC/DC-Ch (70/30) reached a plateau at nucleotide/lipid molar ratios of 0.9 and 1.3, respectively. If negatively-charged nucleotides interact only with cationic molecules in CLs, the nucleotide/lipid molar ratio will reach a plateau at 0.15–0.3. The results also suggest that the nucleotides in mRNA interact not only with cationic molecules but also with zwitterionic DOPC molecules. The calculated

dissociation constant, K_d of DOPC/DOTAP (70/30) and DOPC/DC-Ch (70/30) was 5.0×10^{-9} and 9.1×10^{-9} M, respectively, while that of DOPC was $>10^{-8}$ M. Laurdan is located at the hydrophilic-hydrophobic interface of the lipid membrane, where the hydrocarbon moiety in Laurdan is aligned parallel to lipid acyl regions, and the fluorescent naphthalene residue is located at the level of the glycerol backbones (Parasassi *et al.*, 1995). Therefore, mRNA was found to bind CLs at the level of glycerol backbones of lipids, where the interaction moiety of mRNA was assumed to be the phosphate backbone and the nucleobases.

3.3.3 UV resonance Raman Spectroscopic Analysis for Liposome-RNA Interaction Mechanism

UV resonance Raman spectroscopic analysis is useful for the direct observation of biomacromolecules (Benevides *et al.*, 2005; Nagatomo *et al.*, 2011). **Figure 3-10** shows UV resonance Raman spectra of mRNA. The peaks at 878, 1245, 1338, 1485, and 1578 cm^{-1} are assigned as D-ribose (inner reference), cytosine (C), adenine (A), A/guanine (G), and G/A, respectively (**Table 3-1**) (Lanir *et al.*, 1979; Mathlouthi *et al.*, 1986; Zhelyaskov *et al.*, 1992; Florián *et al.*, 1996; Billinghurst *et al.*, 2009; Singh, 2012). The relative peak intensities of A, G, and C increased in the presence of CLs. Increases in Raman intensity are caused by a decrease in base stacking (Carmona *et al.*, 1999), while decreases in Raman intensity are caused by a hydrogen bonding or hydrophobic surrounding (Nagatomo *et al.*, 2011). Raman spectra of NTPs and their mixture indicated that Raman peak intensities varied due to the hydrogen bonding interaction (**Fig. 3-11(A)**). Because nucleobases are more hydrophobic than phosphate backbones (Sasaki *et al.*, 1987), nucleobases can interact with the hydrophobic regions in lipid membranes. In order to estimate the liposome-nucleobase interaction, Raman spectroscopic analysis of NTP was performed in the presence of CLs (**Fig. 3-11(B)**). In the presence of a higher concentration of NTPs (30 mM), NTP can form non-Watson-Crick base pairs each other (Leontis *et al.*, 2002). It is therefore suggested that the increases in Raman

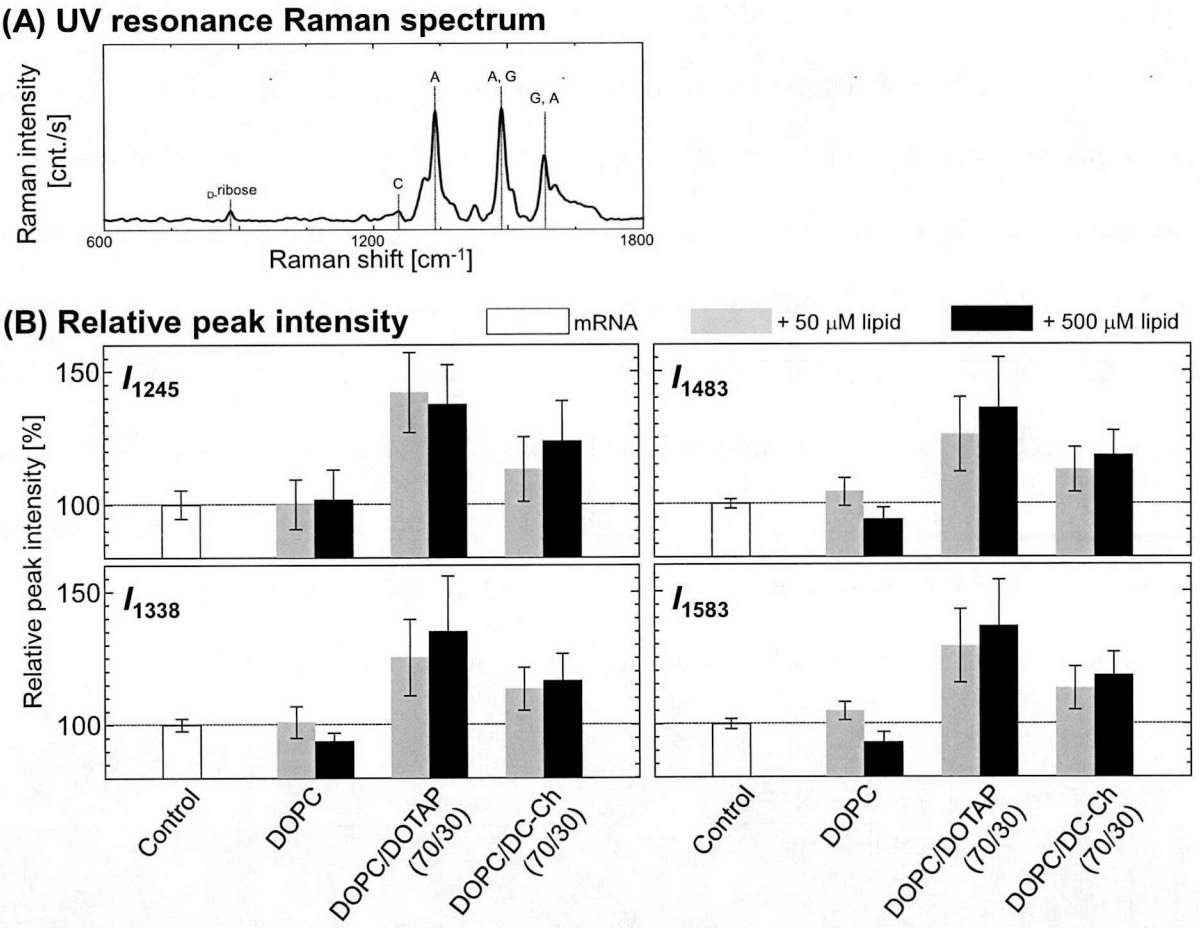

Fig. 3-10 (A) UV resonance Raman spectrum of mRNA. (B) Relative peak intensities of mRNA in the presence of liposomes.

Table 3-1 Peak assignment of Raman spectra

ATP		UTP		GTP		CTP	
I [cm^{-1}]	Assignment	I [cm^{-1}]	Assignment	I [cm^{-1}]	Assignment	I [cm^{-1}]	Assignment
730	νN_3C_4	570	beC_2O_7	669	δring	600	δC_6N_1
878	D-ribose	785	νC_4C_5	878	D-ribose	785	νN_1C_2
1117	νPO_2	878	D-ribose	1118	νPO_2	878	D-ribose
1223	δC_8H	1117	νPO_2	1179	δC_8H	994	δC_6H
1253	νC_8N_7	1233	νring	1327	νC_5N_7	1117	νPO_2
1310	νN_9C_8	1398	νC_2N_3	1369	νC_8N_7	1245	δN_1C_2
1339	νN_7C_5	1683	νC_4O_8	1417	νC_8N_7	1295	νC_2N_3
1378	νN_7C_5			1489	νC_8N_7	1532	νC_4N_8
1428	νN_1C_6			1579	νC_2N_3	1600	νC_2O_7
1484	νC_4N_9			1683	νC_6O_{11}		
1509	νN_7C_8						
1583	νC_4C_5						

peaks of NTPs can be also an evidence of hydrogen bonding interaction with liposomes. FTIR analysis implied that tRNA could bind to the liposome membranes via electrostatic, hydrophobic, and hydrogen bond interactions (See following sections). It is therefore revealed that nucleobases, A, C, and G in mRNA can bind to the CL membranes by electrostatic, hydrophobic, and hydrogen bond interactions. The effects of CLs on mRNA are summarized in **Table 3-2**. The CLs inhibited mRNA translation due to their strong electrostatic interactions. Not only phosphate backbones but also nucleobase moieties in mRNA or NTPs interacted with liposomes via hydrophobic and hydrogen bonding interactions. Based on the case study of cationic liposomes, it was found that heterogeneity of membranes was key factors to control the interaction and function of mRNA molecules. In the next section, a smaller single-stranded RNA, tRNA, and its interaction mechanism were estimated.

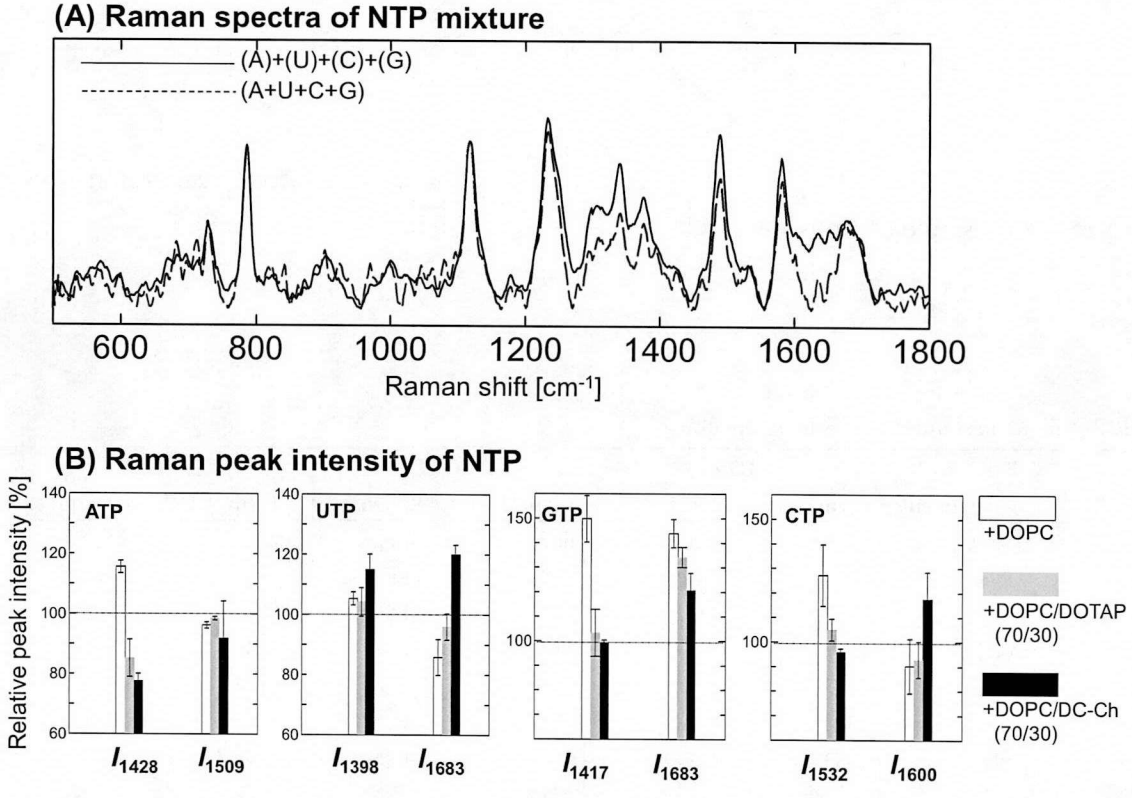

Fig. 3-11 (A) Raman spectra of NTPs. *Bold line* and *dotted line* show the Raman spectrum of the sum of NTP and that of the NTP mixture, respectively. (B) Relative peak intensities of NTPs in the presence of liposomes.

Table 3-2 Effect of liposomes on mRNA interaction

	DOPC	DOPC/DOTAP (70/30)	DOPC/DC-Ch (70/30)
Phase state (Cartesian diagram)	l_d	l_d	$l_d + l_o$
mRNA adsorption*1 (Electrophoresis)	-	43.0 %	46.4 %
mRNA translation*1 (RTS-Kit)	137 %	75.2 %	95.4 %
Dissociation constant, K_d (Laurdan)	$>>10^{-8}$ M	5.0×10^{-9} M	9.1×10^{-9} M
Nucleobase interaction*2 (UV resonance Raman)	G, A	G, C, A	G, C, A
NTP interaction*1, *3 (Raman at 532 nm)	A/ N_1 U/ O_8 G/ N_7, O_{11} C/ N_8	A/ N_1 G/ O_{11}	A/ N_1 U/ O_8, N_3 G/ O_{11} C/ O_7

*1 Lipid concentration at 1 mM.
*2 Lipid concentration at 500 mM
*3 NTP concentration at 30 mM

3.4 Interaction Mechanism of Liposomes with tRNA

3.4.1 Binding Mechanism of tRNA with Liposomes

The interaction between liposomes and tRNA (the structure of tRNA was shown in **Fig. 3-7**), which is a model single-stranded RNA, was investigated by using a fluorescent probe TNS. Although TNS fluorescence in bulk water solution was very weak, TNS inserted into the vesicle membrane was found to emit strong fluorescence (**Fig. 2-2**), indicating the micro-polarity of the lipid vesicles or liposomes (Eisenberg *et al.*, 1979; Guo *et al.*, 2009). The variations of relative fluorescence intensity of TNS are shown as a function of tRNA concentration (**Fig 3-12**). The emission peaks of TNS embedded in the membrane of various liposomes were 441-446 nm, indicating that TNS was embedded approximately 1 nm below the liposome surface (Cevc, 1990). Because no peak shift was observed at higher tRNA concentrations, the decrease of fluorescence intensity was possibly due to the replacement of TNS by tRNA. The values of relative fluorescence intensity of TNS became lower as the tRNA concentration increased: 85 % for POPC, 96 % for POPC/Ch (70/30), and 49 % for

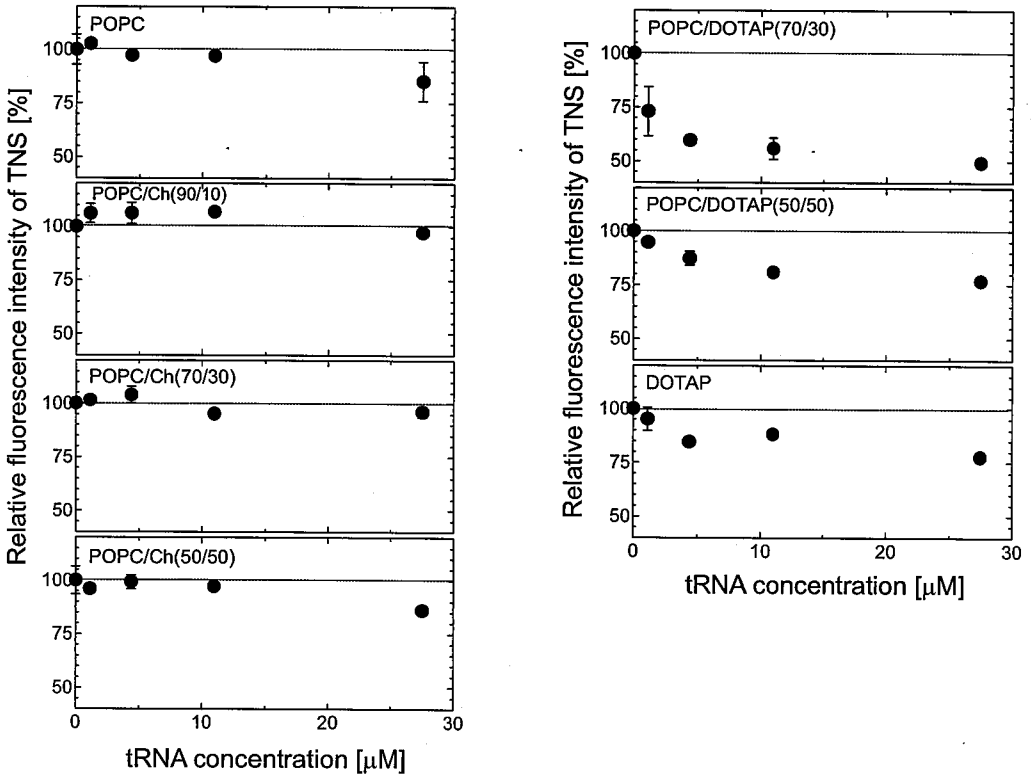

Fig. 3-12 Relative fluorescence intensity of TNS in the presence of tRNA.

POPC/DOTAP (70/30), where the fluorescence intensity of TNS without tRNA was defined as 100 %. These results can be regarded as an evidence for the binding of tRNA to liposome surfaces. POPC/Ch (90/10) and POPC/Ch (70/30) indicated the slight decrease of TNS fluorescence, showing that tRNA binding was so weak and bound tRNA was not inserted into the liposome (TNS was not altered). To confirm this point, the turbidity of liposome suspension (OD_{405}) in the presence or absence of tRNA was measured (**Fig. 3-13**). The turbidity of POPC/Ch (70/30) was markedly increased in the presence of tRNA although no increase was observed with POPC/Ch (90/10), suggesting that the liposome-RNA interaction was dependent on the phase state of liposome membrane. This turbidity increase suggests the formation of a liposome-RNA complex (Janas *et al.*, 2006). These results indicate that the binding mechanism of tRNA can also vary, depending on the physicochemical properties of liposome.

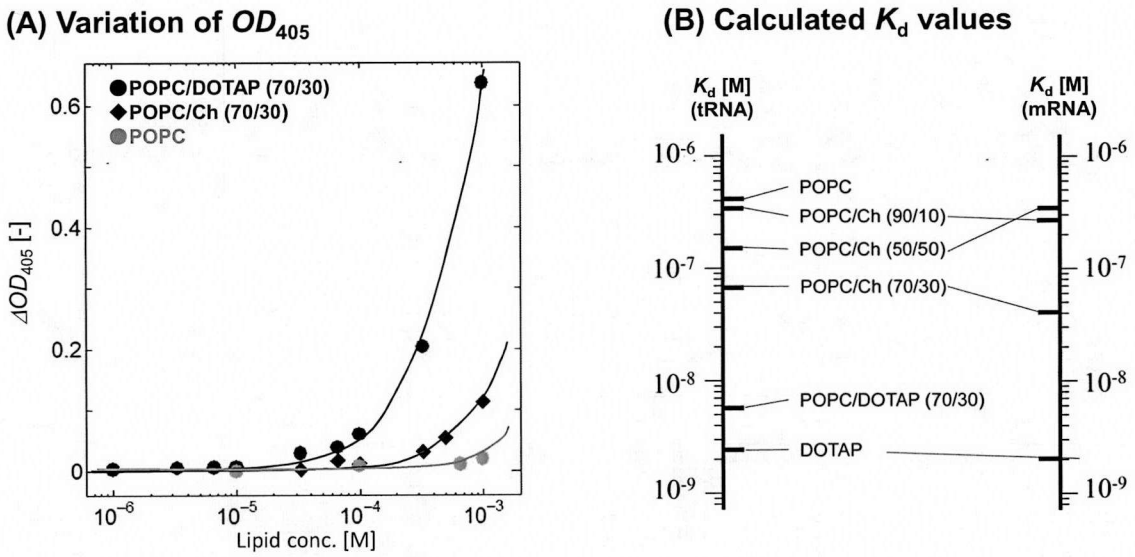

Fig. 3-13 (A) Variation of OD_{405} values in the presence of tRNA. $\Delta OD_{405} = OD_{405,\,(+)\text{tRNA}} - OD_{405,\,(-)\text{tRNA}}$. (B) Calculated K_d values based on the normalized ΔOD_{405}.

3.4.2 Binding of Nucleobases of tRNA onto Liposomes

The liposome-tRNA interaction mechanism was investigated in details by using FTIR spectroscopy (**Fig. 3-14**). It has been reported that the hydrophobic interaction between the lipid acyl-chain and the hydrophobic parts of tRNA was estimated by FTIR studies (Marty *et al.*, 2009). In the presence of liposomes, increases in the peak intensity derived from nucleobases were observed (data not shown): 1706 cm^{-1} (guanine C=O stretching), 1656 cm^{-1} (uracil C=O stretching), 1603 cm^{-1} (adenine C=N stretching), and 1492 cm^{-1} (cytosine plane ring vibration). The observed peak shifts were summarized in **Fig. 3-14** (Table). In common with all kinds of liposomes, the peak of [-PO_2^--] asymmetric stretching at 1236 cm^{-1} was shifted to a higher frequency (1240-1242 cm^{-1}). The phosphate backbone of tRNA has a negative charge and lipid head groups of POPC, DOTAP, and DC-Ch have a positive charge, clearly indicating the electrostatic interactions. Giel-Pietraszuk and Barciszewski have previously reported that the blue shift of IR peak is due to an increase of bond energy as a result of the shortening of the hydrogen bonds followed by dehydration of tRNA. It is therefore found that the higher frequency-peak shift was caused by liposome

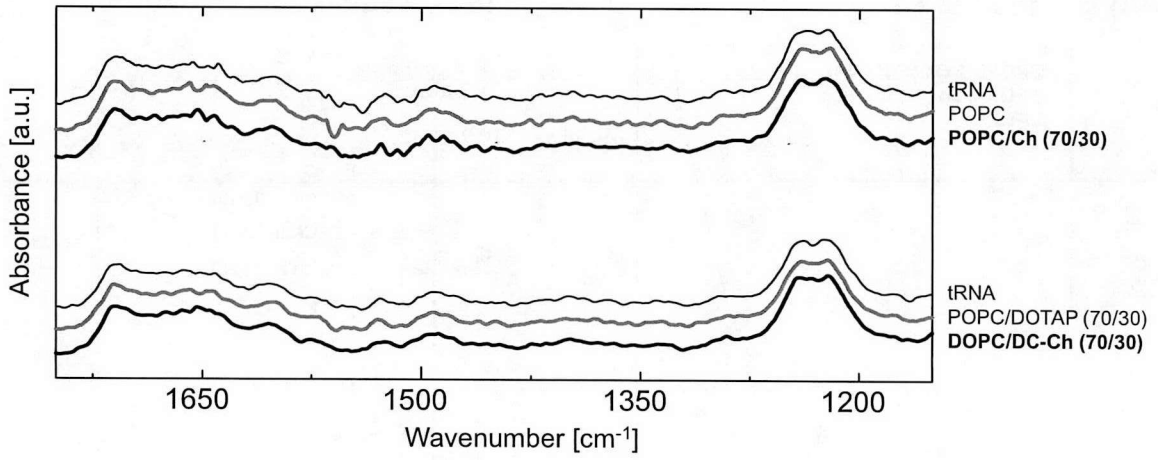

Wavenumber [cm^{-1}]	$\Delta\nu$ [cm^{-1}]				Assignment
	POPC	POPC/Ch (70/30)	DOPC/DOTAP (70/30)	DOPC/DC-Ch (70/30)	
1706	+2.16	+0.96	+2.84	-0.48	Guanine (C=O stretching)
1656	+1.45	+0.96	-	+0.96	Uracil (C=O stretching)
1603	+1.45	0	+1.45	-0.48	Adenine (C=N stretching)
1492	0	+3.38	+0.96	+3.86	Cytosine (plane ring vibration)
1236	+4.34	+4.82	+2.89	+4.34	PO_2^- (asymmetric stretching)

Fig. 3-14 FTIR spectra of tRNA in the presence of liposomes. Table shows the peak shift and the peak assignment (Marty *et al.*, 2009).

binding, and that phosphate backbones and nucleobases of tRNA were dehydrated. A hydrophobic interaction between the lipid aliphatic tail and tRNA has been reported to occur in a specific nucleobases, such as guanine, adenine and uracil (Marty *et al.*, 2009). In the case of POPC/Ch (70/30) liposome, a specific peak shift at cytosine (1495 cm^{-1}) was observed, while other Ch-modified POPC liposomes did not show such peak shifts at cytosine. DOPC/DC-Ch (70/30) also indicated the peak shift at 1495 cm^{-1}, showing that the micro-domain liposomes can specifically interact with cytosine of tRNA. Raman spectroscopic analysis also revealed that heterogeneous liposomes (DOPC/Ch (70/30), domain size ~13.3 Å; DOPC/DC-Ch (70/30), domain size ~ 16 Å) interacted with CTP at O_7 moieties.

Such a specific interaction of the nucleobases with lipid membranes would be important from the viewpoint of functionalization of biomolecules on the membrane surface (Guo *et al.*, 2009). The peak shifts of all four nucleobases were observed in DOTAP, indicating the strong hydrophobic interaction with nucleobases.

3.5 Conformational Change of Single-Stranded RNAs

3.5.1 Evaluation of Single-Stranded RNA Conformation by CD Spectra

Single-stranded RNAs, *e.g.*, mRNA and tRNA (**Fig. 3-7**), have A-form conformation (Gregoire *et al.*, 1997; Bailor *et al.*, 2007), and their biological functions are closely related to conformation (Laso *et al.*, 1993; Lilley, 2005; Marsden *et al.*, 2006). It has been reported that tRNA in A-form double helix conformation shows a negative CD peak at 208 nm and a positive peak at 265 nm (Gregoire *et al.*, 1997; Carmona *et al.*, 1999). The positive peak at 265 nm in the tRNA and mRNA CD spectrum is an indicator of base stacking (formation of intra-molecular base pairs), where the negative peak at 208 nm is the A-form marker (Clark *et al.*, 1997; Gregoire *et al.*, 1997). **Figure 3-15** shows CD spectra of tRNA and mRNA. Although it is difficult to predict the conformation of mRNA due to its large molecular weight, the CD data indicated that the mRNA was also in an A-form double helix conformation, similar to the case of tRNA (**Fig. 3-15(A)**). The decreases in CD peaks of tRNA were observed in water/methanol solutions (**Fig. 3-15(B)**), suggesting the tRNA denaturation in hydrophobic environments. Furthermore, the decreases of CD peak intensities were also observed in both cases of tRNA and mRNA in heat stress conditions (**Fig. 3-15(C)** and **(D)**). It was therefore found that the decrease of peaks at 208 and 265 nm indicated the denaturation of single-stranded RNAs. Because liposomes have hydrophobic regions in their membranes, the conformational change of RNA molecules is expected to be induced when RNA molecules bind to liposome membranes at deeper regions.

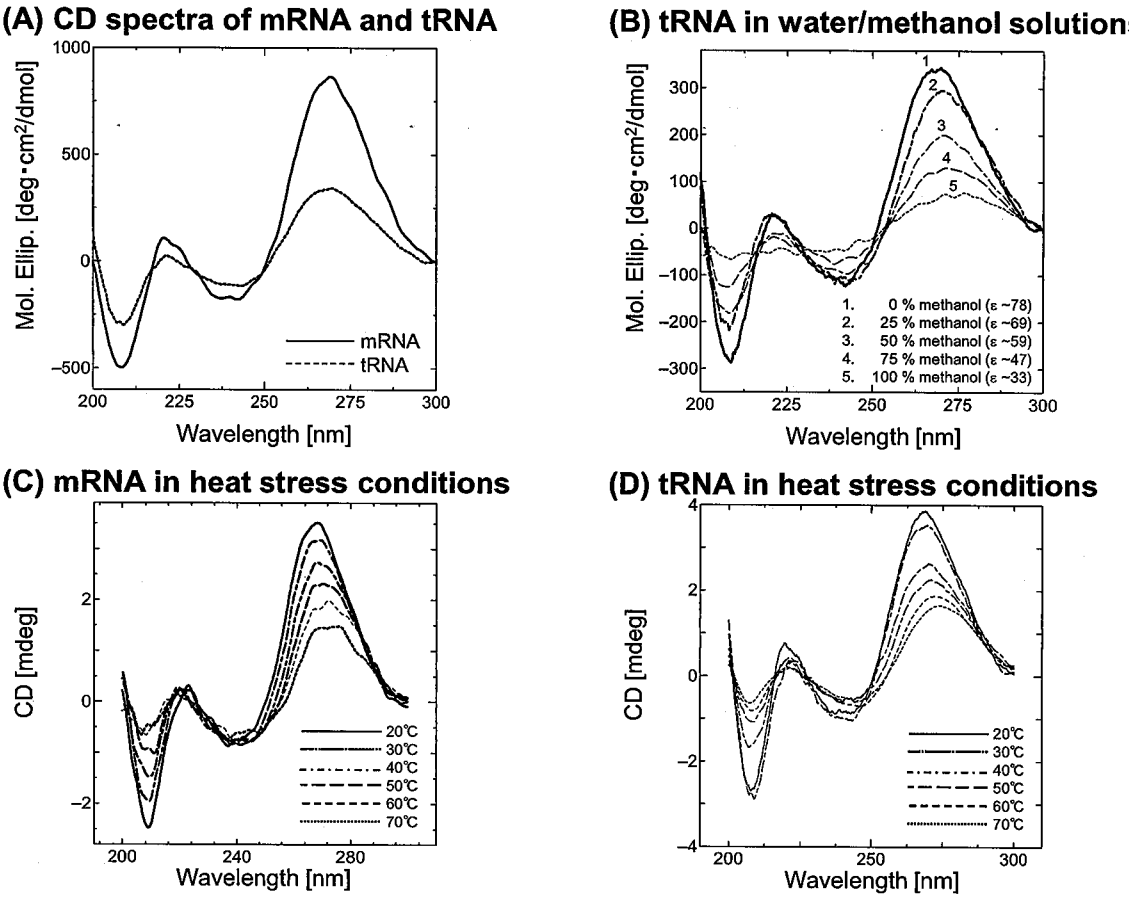

Fig. 3-15 (A) CD spectra of mRNA (*bold line*) and tRNA (*dotted line*). (B) CD spectra of tRNA in water/methanol solutions. The graphs (C) and (D) show CD spectra of mRNA and tRNA in heat stress conditions, respectively.

3.5.2 Conformational Change of tRNA Induced by Liposome Binding

CD spectra of tRNA were measured in the presence of liposomes (**Fig. 3-16**). Under the experimental condition at 30 °C, tRNA conformations in the presence of POPC and POPC/Ch (70/30) were maintained, wherein CD peak intensities slightly decreased. In contrast, tRNA significantly denatured in the presence of CLs (POPC/DOTAP (70/30) and POPC/DOTAP (50/50)). CD peak intensities decreased in proportion to the surface charge density of liposomes. Because the anionic liposome, POPC/POPG (70/30), had little effect on the tRNA conformation, it was therefore indicated that the CLs denatured tRNA conformation

due to the strong electrostatic interaction. In order to discuss the conformation of tRNA on the liposomes, the melting temperature (T_m) of tRNA was calculated under heat stress conditions (**Fig. 3-17**), wherein the T_m value is defined as a parameter to describe the stability of RNA. The coexistence of Mg^{2+}, that stabilizes the RNA conformation (Conn *et al.*, 1998; Madore *et al.*, 1999), resulted in the increase of the T_m value (48 °C to 60 °C), whereas POPC/Ch (70/30) destabilized the tRNA together with the decrease of T_m (48 °C to 38 °C). Because lipid membranes in l_o phases are tightly packed, tRNA insertion would be difficult. It is therefore speculated that the binding sites of tRNA would be limited to the membrane surfaces (Michanek *et al.*, 2012). In contrast, the T_m values increased in proportion to the surface charge density of CLs, indicating that CLs denatured tRNA and then the denatured tRNA was stabilized on the CL membranes. In other words, CLs induced tRNA denaturation, and the denatured tRNA conformation was preserved on the CL membranes. It is therefore found that conformational changes of tRNA were induced by liposome binding. Similar conformational changes are expected to be induced in the case of mRNA.

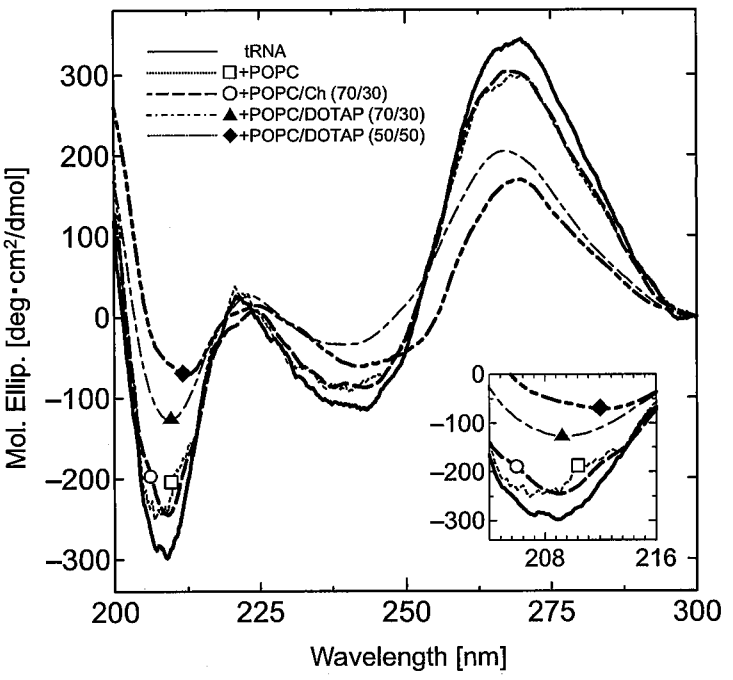

Fig. 3-16 CD spectra of tRNA in the presence of liposomes at 30 °C.

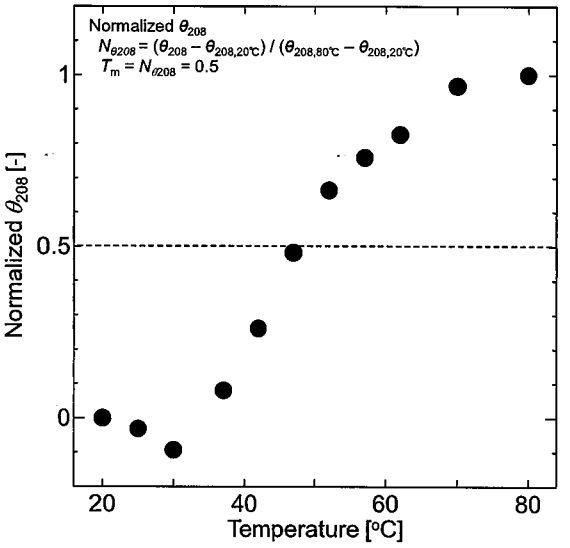

	T_m [°C]
tRNA	48
+ Mg2+ (1 mM)	60
+POPC	46
+POPC/Ch (90/10)	50
+POPC/Ch (70/30)	38
+POPC/Ch (50/50)	44
+POPC/DOTAP (70/30)	53
+POPC/DOTAP (50/50)	N.D.
+DOTAP	62

Fig. 3-17 T_m values of tRNA in the presence liposomes. Lipid concentration was 1 mM.

3.5.3 Conformational Change of mRNA and Its Relation with mRNA Translation

The conformational change of "mRNA" in the presence of liposomes was also investigated (**Fig. 3-18**), based on the above results on tRNA. mRNA in A-form also has a positive peak and a negative peak at 265 and 208 nm, respectively. The CD spectra of mRNA in the presence of DOPC/DOTAP (70/30) and DOPC/DC-Ch (70/30) are shown in **Fig. 3-18(A)**. Both peaks decreased in proportion to the increase in lipid concentration, while the tendencies of CD spectrum variations were different (**Fig. 3-18(B)**). The addition of the homogeneous DOPC/DOTAP (70/30) gradually decreased the peak intensities at 208 and 265 nm with increasing lipid concentration. Because a decrease in CD peaks is due to conformational change in RNAs (Johnson *et al.*, 2005), it is therefore found that DOPC/DOTAP (70/30) denatures mRNA. In contrast, heterogeneous DOPC/DC-Ch (70/30) indicated different tendencies which can be regarded as mRNA denaturation, resulting in partial conformational changes of mRNA. The peak at 265 nm gradually decreased, while the degree of decrease was not so large as compared with that of DOPC/DOTAP (70/30). The peak at 208 nm decreased despite the variations of the lipid concentration. These differences

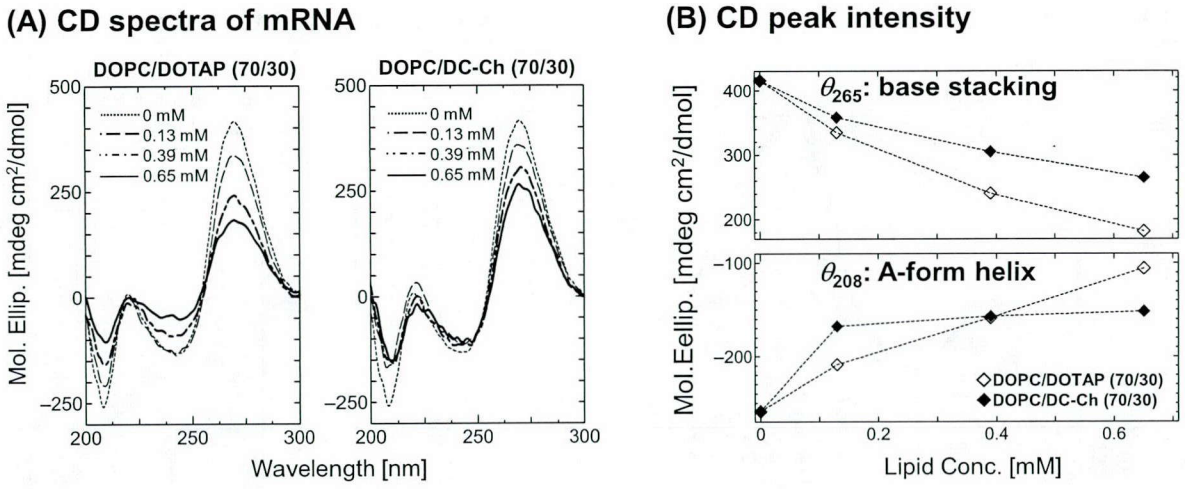

Fig. 3-18 (A) CD spectra of mRNA in the presence of CLs at 30 °C. (B) Variations of CD peaks.

in the mRNA denaturation are due to the phase state and the lipid mobility of CLs. The DOPC/DC-Ch (70/30) membrane, which is in the (l_d + l_o) phase, is a partially ordered (*i.e.*, micro-domain) structure, with limited lipid mobility. Therefore, nucleobases cannot freely attack the hydrophobic region of the membrane. Based on the results shown in **Figs. 3-10** and **3-11**, heterogeneous DOPC/DC-Ch (70/30) could interact with cytosine residues in mRNA. These finding suggest that the difference in mRNA interaction can affect its translation.

The conformation of RNAs is strongly related to their functions (Laso *et al.*, 1993; Marsden *et al.*, 2006). The conformation and translational activity of mRNA are shown in **Fig. 3-19**. POPC/Ch (70/30) liposome maintained mRNA conformation and enhanced GFP expression to 116 % as compared with the control (without liposomes). Because the T_m value of mRNA decreased in the presence of POPC/Ch (70/30), a suitable destabilization of mRNA was found to enhance mRNA translational activity. In addition, liposomes recognized not only mRNA but also other single-stranded RNAs (*e.g.*, tRNAs), and the condensation effect is likely to be a reason for the enhanced effect at translation step (Yu *et al.*, 2001; Stano *et al.*, 2011). On the other hand, CLs inhibited mRNA translation, depending on the degree of

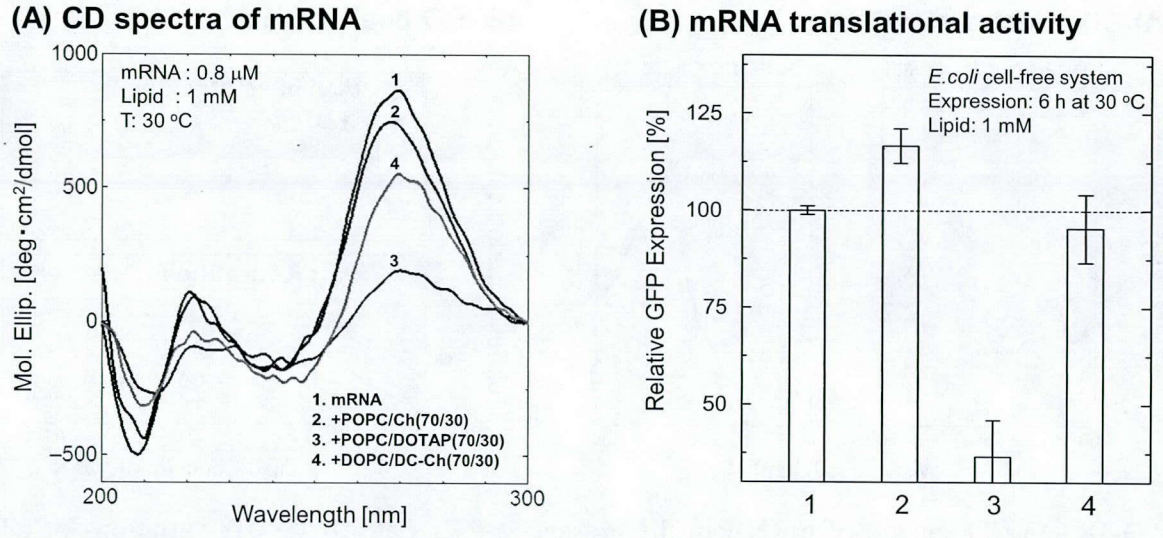

Fig. 3-19 (A) CD spectra of mRNA in the presence of liposomes. (B) Relative GFP expression in the presence of liposomes.

mRNA denaturation. The addition of the homogeneous POPC/DOTAP (70/30) significantly denatured mRNA and inhibited mRNA translation, while heterogeneous DOPC/DC-Ch (70/30) partially denatured mRNA and slightly inhibited mRNA translation. Taken together, these results imply that liposomes can functionalize biomacromolecules, including mRNA and tRNA, at the membrane surfaces.

3.6 Liposome Affinity to tRNA during Heat Stress Condition

The physicochemical properties of both liposome membranes and biomacromolecules are known to vary, depending on the surrounding temperatures. At a higher temperature, the surfaces of RNA and polypeptide turned to be hydrophobic (**Chapter 1**) (Kuboi *et al.*, 2004). The values of the dissociation constant of tRNA with liposomes under heat stress condition were summarized in **Table 3-3**. It was also found that POPC/Ch (70/30) showed 14-fold higher affinity with denatured tRNA, in comparison with POPC liposome. Lipid or Ch molecules also show an affinity with tRNA, although there is little difference

Table 3-3 Conformation of tRNA conformation and dissociation constant, k_d

	Folded (30 °C)	**Unfolded (50°C)**
tRNA conformation		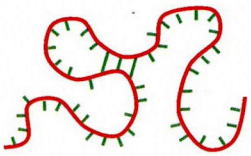
***HFS* [kJ/mol]**	-180 [kJ/mol]	-100 [kJ/mol]
+POPC	$K_d = 4.0 \times 10^{-7}$ [M] (control, 1-fold)	$K_d = 3.1 \times 10^{-7}$[M] (1.3-fold affinity)
+POPC/Ch (70/30) (Ch domain)	$K_d = 6.5 \times 10^{-8}$[M] (6-fold affinity)	$K_d = 2.9 \times 10^{-8}$[M] (14-fold affinity)

(Marty *et al.*, 2009). The reversibility of tRNA conformation was determined in the presence of POPC, DPPC, DOTAP, and DSTAP (**Fig. 3-20**). The irreversible conformational transition was observed in the presence of DSTAP, which is a cationic liposome with saturated acyl chains ($T_{c,\,DSTAP}$ =60 °C), while the conformational transition in the presence of DOTAP was found to be reversible. Phase states of DSTAP at 30 and 70 °C has been reported to be in s_o and l_d, respectively (Lobo *et al.*, 2002). It is therefore suggested that tRNA cannot interact with hydrophobic regions in DSTAP membranes at 30 °C, while it turns to be accessible at 70 °C due to the phase transition. The DSTAP affinity for tRNA at 30 and 70 °C was estimated to be 40-fold and 182 fold, in comparison with that of POPC. It has been reported that the proteins and enzymes can also show such higher affinities to the surface-modified liposomes under oxidative or heat stress conditions (Yoshimoto *et al.*, 1998; Tuan *et al.*, 2008, Ngo *et al.*, 2010). It is therefore shown that the design of liposome membranes can be important factors for recognition and functionalization of biomacromolecules.

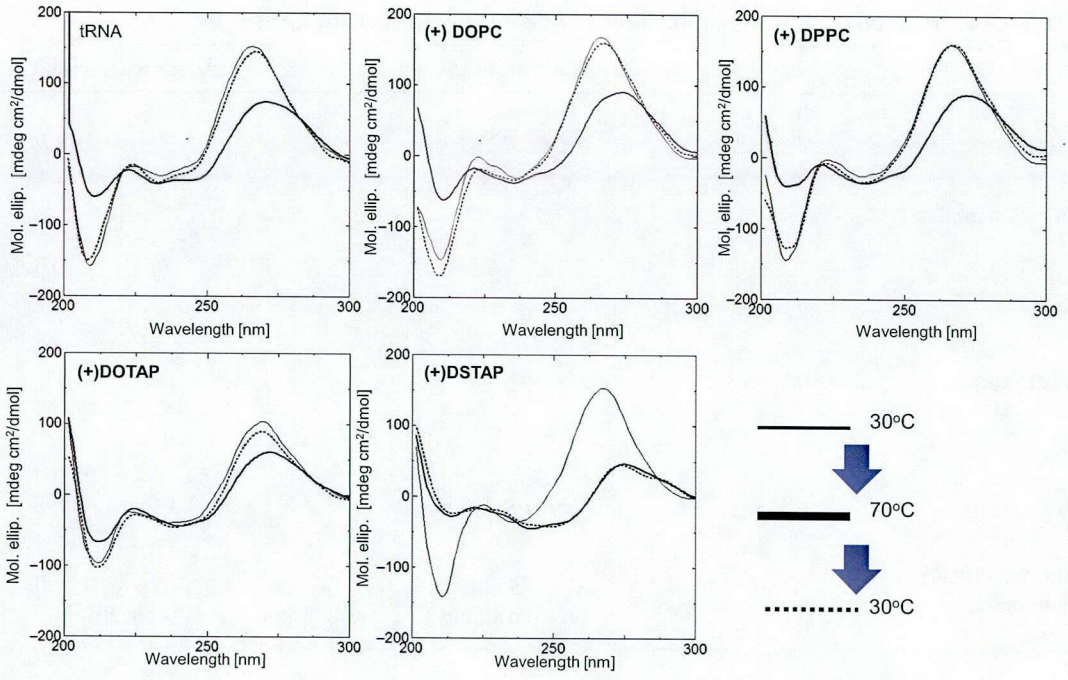

Fig. 3-20 Reversibility of tRNA conformation during heating and cooling processes.

4. Summary

The mechanism of the liposome interaction with single-stranded RNAs was investigated, focusing on their conformation and functions. An inhibitory effect on mRNA translation in the presence of CLs was explored by using an *E. coli* CFT system by employing its mRNA as an initial template of GFP gene. The membrane fluidity and polarity analyzed to identify the phase state of CLs; DOPC/DOTAP (70/30) for homogeneous (l_d), DOPC/DC-Ch (70/30) for heterogeneous (l_d + l_o) phases. The CLs in l_d phases markedly inhibited the translation of mRNA bound to membranes in an "inactive" state, while heterogeneous DOPC/DC-Ch (70/30) slightly inhibited the translation of mRNA, which was bound to membranes in an "active" state. Using Laurdan, which locates at glycerol backbones, it was found that membrane surfaces were dehydrated via mRNA binding, indicating that mRNA binds to CL membranes at the level of phosphate [-PO_2^--] to carbonyl [-C=O-] moieties.

Raman and FTIR assays indicated that nucleobases (A, G, C) in mRNA interacted with lipids in CLs, while those in DOPC did not. Cytosine residues interacted with the heterogeneous liposomes; DOPC/Ch (70/30) with 13.3 Å-domain and DOPC/DC-Ch with 16 Å-domain. POPC/Ch (70/30) maintained mRNA conformation, resulting in an enhancement of mRNA translation. In contrast, DOPC/DOTAP (70/30) denatured the conformations of both the A-form (208 nm) and that of base stacking (265 nm) in mRNA. DOPC/DC-Ch (70/30) denatured the A-form structure, despite the variation of lipid concentration. It is therefore concluded that heterogeneity of liposome membrane plays an important role in the regulation of the mRNA conformation and its function. Characterization and design of lipid membranes (De Almeida *et al.*, 2003; Veatch *et al.*, 2003) is also important in the research fields of synthetic cell biology, liposome-based drug delivery systems, and biomacromolecular engineering (Lonez *et al.*, 2008; Luisi, 2009; Walde, 2010; Stano *et al.*, 2011). Using the behavior of lipid membranes, further improvements can be achieved in the regulation of liposome-RNA interactions and the RNA functions.

Based on the obtained results in **Chapter 3**, the key important factors of liposome membrane design for biomacromolecular recognition can be shown as follows (**Fig. 3-21**); (i) surface charge density of liposome: electrostatic interaction; (ii) membrane fluidity: hydrophobic interaction; (iii) membrane polarity: interactions driven by entropic forces; (iv) the proton donor and acceptors in lipid molecules: hydrogen bonding interaction, especially for cytosine residues; (v) the micro-domain formation: van der Waals force caused by the matching of contact surfaces. Temperature setting is also important because of the increase of hydrophobic interaction between membranes and denatured biomacromolecules in unstable conformations. In this section, it is shown that heterogeneous membranes containing the micro-domains can play important role on recognition of biomacromolecules. It is therefore possible to design the liposome membrane that can recognize biomacromolecules and control their conformations, which are deeply relating to functions of biomacromolecules.

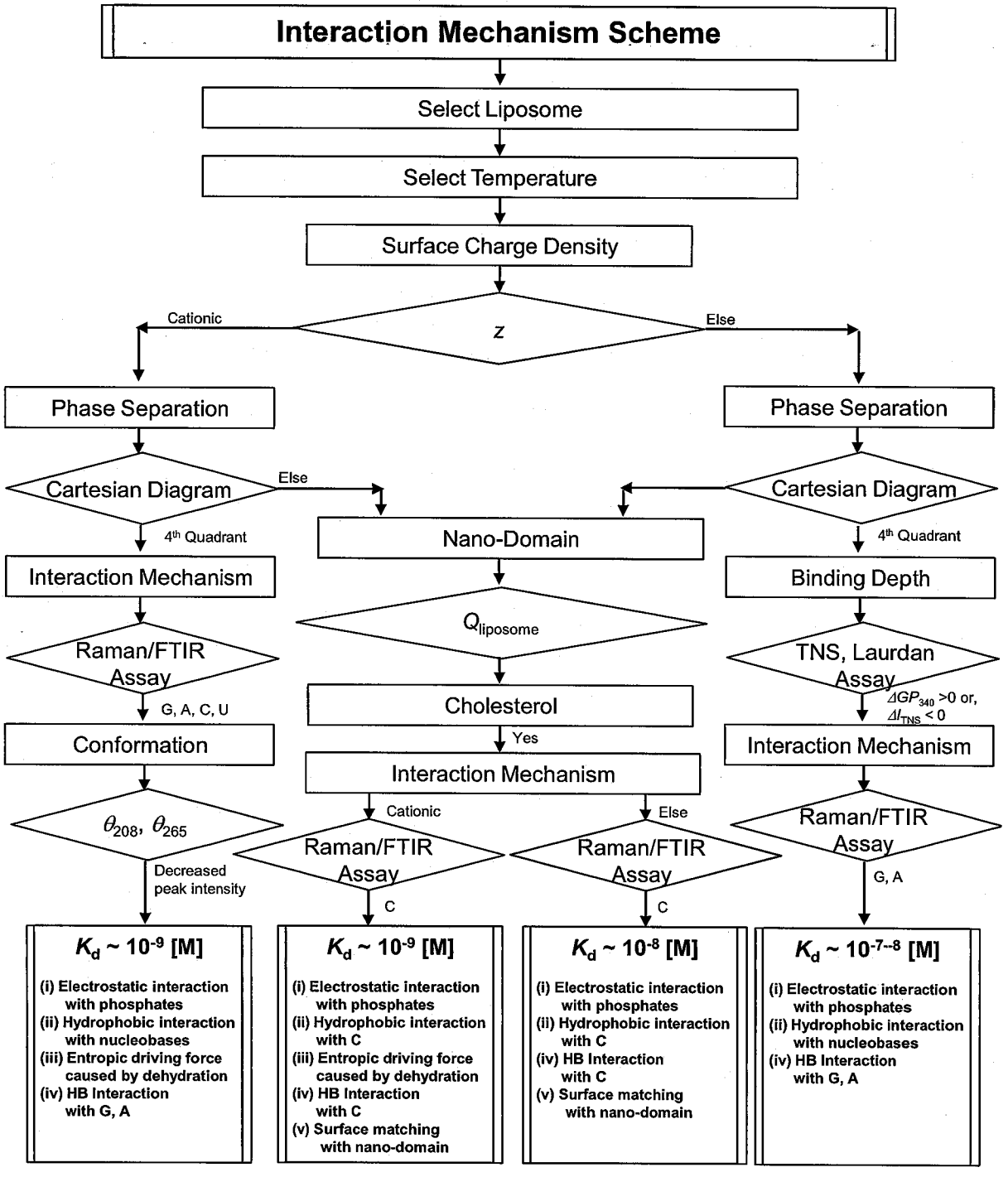

Fig. 3-21 Scheme for the interaction mechanism between the liposome and biomacromolecules.

Chapter 4

Liposome Membrane Design for Recognition of Biomacromolecules and Control of Their Conformation ~Recognition of RNA molecules~

1. Introduction

A general design for novel biofunctional materials is definitely required in order to develop innovative bio-/chemical processes. A key of the biofunctional design is a molecular recognition, which can act as a "glue" of different molecules and can induce an "emergence" on the self-assembly. A variety of specific recognition of biomacromolecules and chiral materials are known to be achieved in biological cellular systems to maintain the cellular homeostasis through nano-machineries relating to metabolism and also gene expression (Tzareva *et al.*, 1994; Korostelev *et al.*, 2006). For example, RNA aptamers were developed as molecular recognition tools, which recognize various kinds of biomolecules (*e.g.*, flavin mononucleotide (FMN), adenosine monophosphate (AMP), arginine, Tobramysin, and so on) (Patel *et al.*, 2000). In order to achieve the recognition and functionalizing of target molecules to be employed as building-block of the novel biofunctional materials, it is important to design a flexible surface of the "platform" that can freely match with the three-dimensional structure of target molecules. However, there are some difficulties to perform the selective separation or molecular recognition in designing of the above-mentioned artificial systems owing to their limited properties in physicochemical potentials. It is therefore necessary to develop "*Bio-Inspired*" systems (Yoo *et al.*, 2011) by using "self-assemblies" as effective platforms for recognition.

There are various kinds of self-assemblies, which play fundamental roles in living cell systems. Lipid membranes, one of essential components of a cell, have also been utilized as the "*Bio-Inspired*" materials for drug carrier, biosensor, and platform of biochemical events (Yoshimoto *et al.*, 1998; Peetla *et al.*, 2009; Shimanouchi *et al.*, 2010; Yoo *et al.*, 2011). Focusing on the molecular recognition, self-assembly systems play an important role on their interaction with target molecules (Borocci *et al.*, 2003; Banchelli *et al.*, 2007). Based on the previous reports, liposomes have been shown to recognize biomacromolecules by co-induction of multiple interactions, such as electrostatic, hydrophobic, and hydrogen bonding forces; (i) the liposomes interacted with damaged proteins and fragmented enzymes (Yoshimoto *et al.*, 2000; Tuan *et al.*, 2008); (ii) the anionic liposomes induced spherulitic aggregation of amyloid β peptides (Shimanouchi *et al.*, 2012); (iii) the liposomes regulated the *in vitro* gene expression (Bui *et al.*, 2008; Bui *et al.*, 2009); (iv) the liposomes induced the conformational change of single-stranded RNAs (Suga *et al.*, 2011). In **Chapter 3**, heterogeneous liposomes were shown to induce the specific interactions with cytosine residues in mRNA and tRNA, indicating that the nano-domain structure can also be a key factor for recognition of biomacromolecules. It is therefore suggested that liposomes can be utilize as functional platforms for recognition and functionalizing of target biomacromolecules.

Based on the results described in **Chapters 1, 2, and 3**, the design scheme of liposome membrane for biomacromolecular recognition was herewith proposed, especially focusing on the recognition, folding, and functionalization of single-stranded RNAs as case study (**Fig. 4-1**). Because the liposome-biomacromolecule interactions depended on the surface properties of biomacromolecules, decision of the surface charge density of liposomes are important. In the case of mRNA, the cationic liposomes strongly interacted with negatively-charged mRNA, while its translational activity decreased due to the conformational change. Cartesian diagram analysis is useful to understand the phase state of

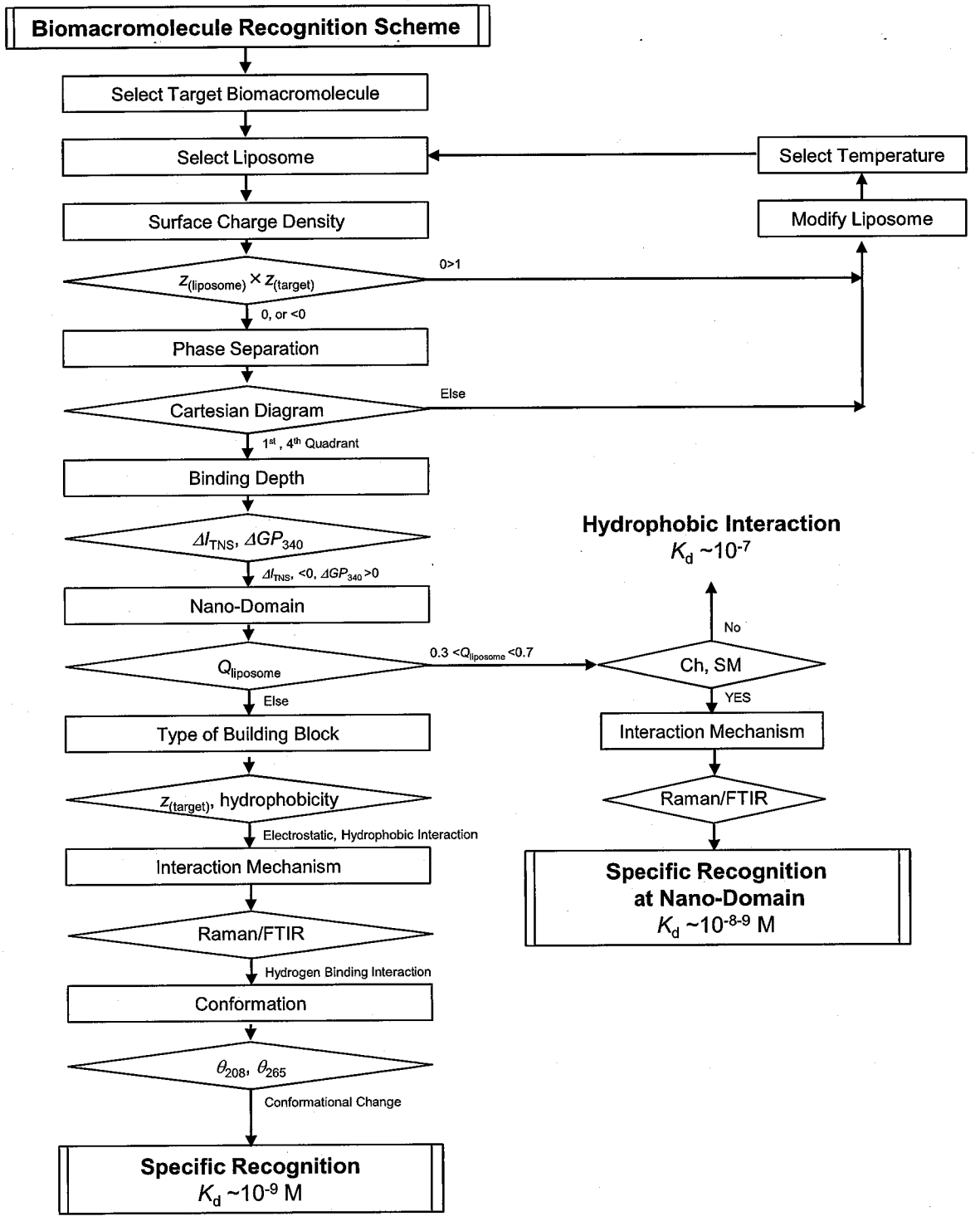

Fig. 4-1 Scheme for the recognition of a target biomacromolecule.

liposome at various temperatures. Using fluorescent probes, such as 1,6-diphenyl-1,3,5-hexatriene (DPH), 6-lauroyl-2-dimethylaminonaphthalene (Laurdan), and 6-(p-toluidino)naphthalene-2-sulfonate (TNS), the binding depth of RNAs can be evaluated. The interaction mechanism of liposomes and biomacromolecules should be then investigated, and, finally, the recognition of the target biomacromolecules and the relating functions of them can be controlled on the liposome membranes.

In the previous reports, the heterogeneous liposomes, including cholesterol (Ch), have been reported to induce the remarkable behaviors that can affect various biochemical reactions. The oxidation of cholesterol in the liposomes was found to modulate the catalytic functions of amyloid β-Cu complex (Yoshimoto *et al.*, 2005). From the viewpoint clarified in this thesis, because the amyloid β was found to be hydrophobic with higher values both in the surface net hydrophobicity (*HFS*) and local hydrophobicity (*LH*) (**Figs. 1-6** and **1-7**), it can be recognized by the Ch-modified liposomes that possess the heterogeneous surface with nano-domains. In addition, the refolding of carbonic anhydrase (CAB) was effectively enhanced in the presence the 1-palmitoyl-2-oleoyl-*sn*-glycero-3-phosphocholine/Ch (POPC/Ch) (2/1), while that was not so significant with POPC only (Yoshimoto, PhD thesis (1999)). These previous findings suggest that the Ch-modified liposome can recognize the unstable polypeptides, showing that the micro-domain can act as a platform of the recognition, folding, and functionalization of the biomacromolecules. The oxidation of liposome surface can also vary the physicochemical properties of liposomes, indicating that their functions, such as the recognition, folding, and, functionalization of biomacromolecules, can be affected by the oxidative stress. It is therefore important to design the liposome surface as a functional platform, focusing on the hydrophobicity and the nano-domain.

In this chapter, liposome membranes were designed based on the scheme, together with the schemes described in **Chapters 1**, **2**, and **3**, by selecting a Hammerhead ribozyme (HHR) and tRNA as a target biomacromolecule (**Fig. 4-2**). Focusing on the natural

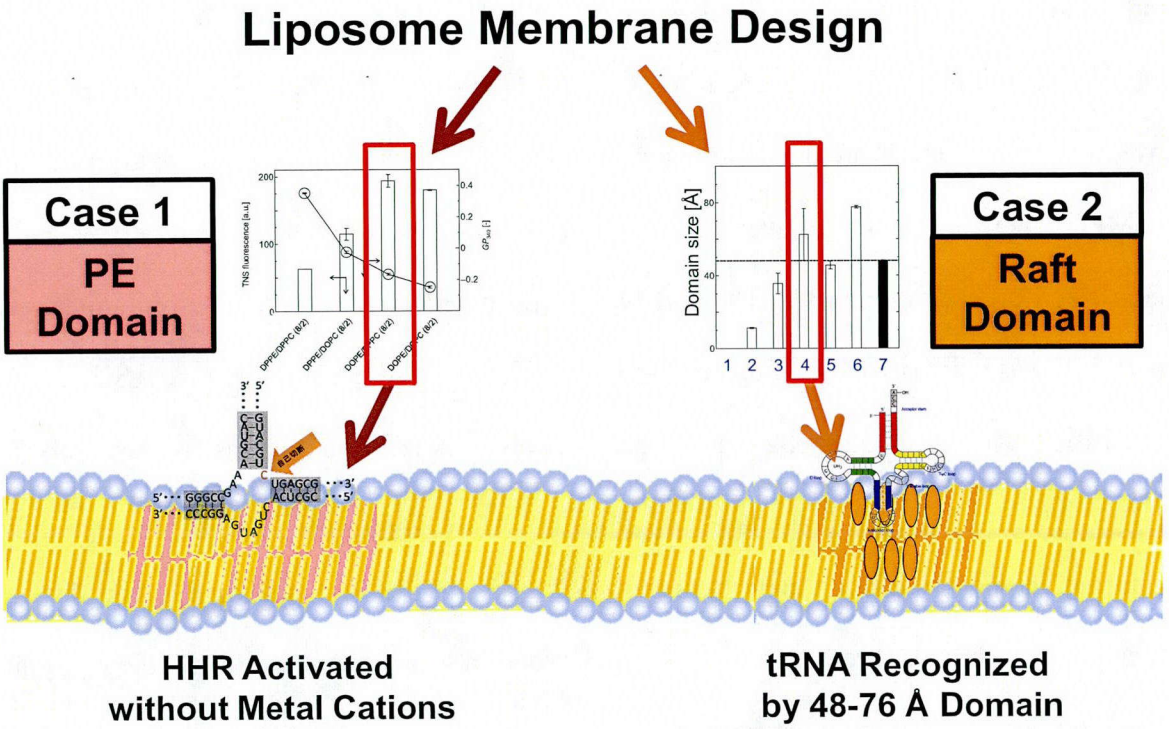

Fig. 4-2 Conceptual illustration of this chapter.

phospholipid bilayer membranes, including phosphoethanolamine (PE) and phosphocholine (PC), the recognition of HHR by utilizing the PE/PC liposomes were investigated in the case of HHR, where the artificially synthesized HHR (HHR-1, 5'-GUACGUCUGAGCG-3' (substrate); HHR-2, 5'-CGCUCACUGAUGAGGCCC-3'; HHR-3, 5'-GGGCCGAAA-CGUAC-3') were used. The PE/PC (8/2) liposomes were optimized by modifying acyl chain lengths, and their physicochemical properties were analyzed by fluorescent probes, DPH, TNS, and Laurdan, based on the scheme descried in **Chapter 2**. Because ribozymes are sensitive to both hydrophobic interiors (Chen *et al.*, 2005) and cations (Boots *et al.*, 2008), the liposome membranes are expected to act as optimal environments for the recognition of HHR: inner regions of bilayers for hydrophobic platform, and ethanolamine groups in PE molecules for quaternary ammonium cations. The UV resonance Raman spectroscopic analysis was

performed to evaluate the interaction mechanism of HHR. It was shown that the conformation and the self-cleavage reaction of HHR were regulated by the PE/PC liposomes.

Furthermore, the interaction between DOPC/SM/Ch liposomes and tRNA was investigated, focusing on the "raft" domain size. The Cartesian diagram analysis and the TEMPO quenching method were carried out for the physicochemical properties and the nano-sized ordered domains in DOPC/SM/Ch liposomes, respectively. The binding moieties of tRNA was evaluated by using SYBR Green I (SGI) and SYBR Green II (SGII), which binds to double-stranded stem regions and single-stranded loop regions, respectively. It is shown that the DOPC/SM/Ch (4/3/3) can selectively recognize both the stem and loop regions, resulting in the conformational change of tRNA. It is therefore shown that the design of liposome membranes through the schemes described in this thesis is useful for the recognition and fictionalization of biomacromolecules.

Materials and Methods

2.1 Materials

1,2-Dioleoyl-*sn*-glycero-3-phosphoethanolamine (DOPE), 1,2-dipalmitoyl-*sn*-glycero-3-phosphoethanolamine (DPPE), 1,2-dioleoyl-*sn*-glycero-3-phosphocholine (DOPC), 1,2-dipalmitoyl-*sn*-glycero-3-phosphocholine (DPPC), and sphingomyelin (SM) were purchased from Avanti Polar Lipids, Inc. (Alabaster, AL, USA). Cholesterol (Ch) and transfer RNA (tRNA) originating from *E. coli* were purchased from Sigma-Aldrich (St. Louis, MO, USA). Hammerhead ribozyme (HHR) were synthesized by Darmacon Inc. (Lafayette, CO, USA). Other chemicals were purchased from Wako Pure Chemical (Osaka, Japan) and were used without further purification.

2.2 Liposome Preparation

A solution of phospholipids in chloroform was dried in a round-bottom flask by rotary evaporation under vacuum. The obtained lipid films were dissolved in chloroform and the solvent evaporated. The lipid thin film was kept under high vacuum for at least 3 h, and then hydrated with distilled water at room temperature. The vesicle suspension was frozen at -80 °C and then thawed at 50 °C to enhance the transformation of small vesicles into larger multilamellar vesicles (MLVs). This freeze-thaw cycle was repeated five times. MLVs were used to prepare large unilamellar vesicles (LUVs) by extruding the MLV suspension 11 times through two layers of polycarbonate membrane with a mean pore diameter of 100 nm using an extruding device (Liposofast; Avestin Inc., Ottawa, Canada). Liposomes with different compositions were also prepared by using the same method.

2.3 Evaluation of Membrane Fluidity and Polarity of Liposomes

The inner membrane fluidity of the liposomes was evaluated in a similar manner to previous reports (Lentz *et al.*, 1976). Fluorescent probe DPH was added to a liposome

suspension with a molar ratio of lipid/DPH = 250/1; the final concentrations of lipid and DPH were 100 and 0.4 μM, respectively. The fluorescence polarization of DPH (Ex = 360 nm, Em = 430 nm) was measured using a fluorescence spectrophotometer (FP-6500 and FP-8500; JASCO, Tokyo, Japan) after incubation at 30 °C for 30 min. The sample was excited with vertically polarized light (360 nm), and emission intensities both perpendicular ($I_{\perp}$) and parallel ($I_{\parallel}$) to the excited light were recorded at 430 nm. The polarization (P) of DPH was then calculated by using the following equations:

$$P = (I_{\parallel} - GI_{\perp}) / (I_{\parallel} + GI_{\perp})$$

$$G = i_{\perp} / i_{\parallel},$$

where $i_{\perp}$ and $i_{\parallel}$ are emission intensity perpendicular and parallel to the horizontally polarized light, respectively, and G is the correction factor. The membrane fluidity was evaluated based on the reciprocal of polarization, $1/P$.

The fluorescent probe Laurdan is sensitive to the polarity around itself, which allows the surface polarity of lipid membranes to be determined (Parasassi *et al.*, 1991). Laurdan emission spectra exhibit a red shift caused by dielectric relaxation. Thus, emission spectra were calculated by measuring the general polarization (GP_{340}) for each emission wavelength as follows:

$$GP_{340} = (I_{440} - I_{490}) / (I_{440} + I_{490}),$$

where I_{440} and I_{490} are the emission intensity of Laurdan excited with 340 nm light. No fluorescence was observed from an HHR solution (without liposomes). The final concentrations of lipid and Laurdan in the test solution were 100 and 2 μM, respectively.

2.4 Fluorescence Measurement of TNS

TNS was directly added to a liposome suspension and was then incubated for one hour at room temperature in order to complete TNS insertion into lipid membrane. After the addition of HHR, samples were incubated in the dark for 30 min at 37 °C. The fluorescence

spectra of TNS (Ex = 340 nm) were measured from 380 nm to 550 nm by using a fluorescence spectrophotometer (FP-6500; JASCO, Tokyo, Japan) with 5 nm light path. The final concentrations of TNS and lipid were 20 μM and 0.5 mM, respectively. TNS fluorescence was not observed with HHR only.

2.5 Kinetic Analysis of HHR Reactions

HHR was stained with SGI for 30 min at 37 °C. Fluorescence of HHR was measured at the excitation of 494 nm. Kinetics of HHR reactions was calculated based on the previous reports (Ferrari *et al.*, 2002).

2.6. Raman Spectroscopic Analysis

Raman spectra of mRNA and nucleotide triphosphates (NTPs) were measured by using a confocal Raman microscope (LabRAM HR-800; HORIBA, Ltd., Kyoto, Japan) at a wavelength of 266 and 532 nm, with laser power of 50 and 100 mW, respectively. A total data accumulation time of 30 s. For each sample, the background signal of the solution was removed, and then the baseline was corrected. Peak intensities were normalized by the peak at 878 cm^{-1} (I_{878}) for excitation laser of 266 nm. The final concentration of HHR and lipid in Raman samples was 100 μM and 1 mM, respectively.

2.7 Evaluation of the Conformation of RNAs Using Circular Dichroism (CD) Spectra

The conformation of RNAs was evaluated by using a JASCO J-820 SFU spectropolarimeter (JASCO, Tokyo) (Suga *et al.*, 2011). The CD spectrum from 300 nm to 200 nm was measured with a quartz cell (0.1 cm path length) at a scan speed of 50 nm per min and a width of 2 nm. Five scans excluding buffer and liposome background signals were obtained at 37 °C, and the data was calculated as molar ellipticity. Each sample was prepared

with 1 μM of HHR or tRNA, and 10 mM Tris-HCl at pH 7.8 in the presence or absence of liposomes.

2.8 Evaluation of the Binding Site of tRNA by Using SGI and SGII Assay

tRNA was incubated with liposomes for 30 min at 30 °C. After incubation, tRNA was stained with SGI or SGII and incubated for 30 min at 30 °C. The fluorescence spectra of SGI and SGII (Ex = 494 nm) were measured from 500 nm to 550 nm by using a fluorescence spectrophotometer (FP-6500; JASCO, Tokyo, Japan) with 5 nm light path.

2.9 Statistical Analysis

Results are expressed as mean ± standard deviation. All experiments were performed at least three times. The distribution of data was analyzed, and statistical differences were evaluated using the Student's t-test. A P-value of <5% was considered significant.

3. Results and Discussion

3.1 Design of PE/PC Liposomes for HHR Recognition and Controlling Its Conformation

RNA catalysis (ribozyme) plays important roles inside a living cell in biological systems, and its behavior has been paid much attentions in the research fields of biology, gene therapy and life evolution in early Earth (Hammann *et al.*, 2002). It has been conventionally known that ribozymes, which show a self-cleavage reaction, molecular switch, self-splicing and so on, are functionalized in the presence of metal ions (*e.g.*, Mg^{2+}) (Curtis *et al.*, 2001). Hammerhead ribozymes (HHRs), which is originally discovered in plant virus satellite RNA, is a self-cleavage ribozyme, and its active center is comprised of three double-helical segments joined by single-stranded regions. The self-cleavage reaction of HHR has been reported to be sensitive to environmental conditions (Mg^{2+} concentration, and so on) (Curtis *et al.*, 2002; Boots *et al.*, 2008). HHR shows higher activity in the presence of 10 mM Mg^{2+}, while not in the physiological Mg^{2+} concentration (~1 mM). Therefore, there are other environmental factors that play important roles in regulating ribozyme activities in biological system. It has been reported that the accumulation of HHR within a limited compartment can

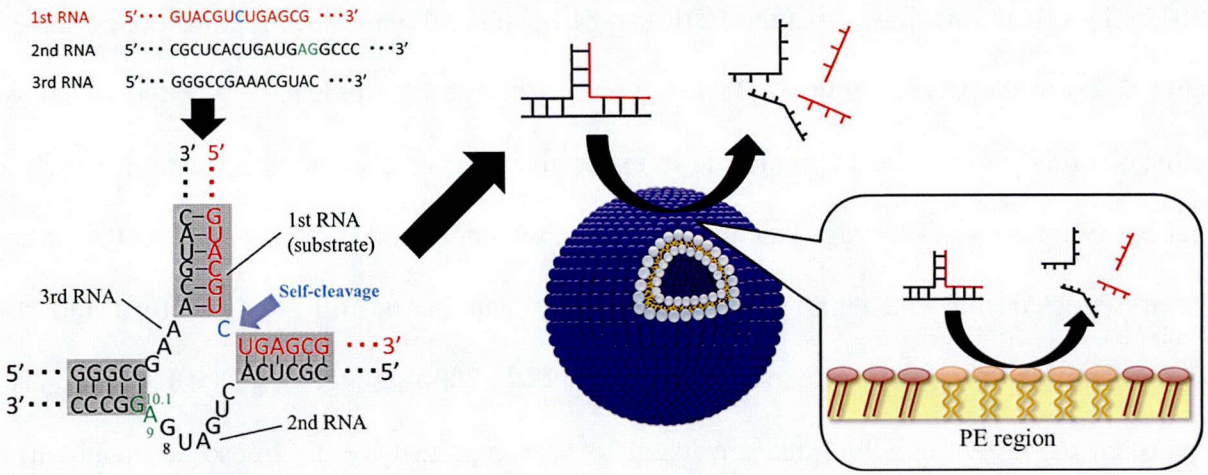

Fig. 4-3 Conceptual illustration of the recognition of HHR and the control of its activity.

enhance its self-cleavage reaction (Strulson *et al.*, 2012), suggesting that the accumulation of HHR on the liposome membrane might also enhance its activity. In this study, the artificially synthesized HHR, which are three core building-blocks of natural HHR, were used in this study (**Fig. 4-3**), and the PE/PC liposome membranes were designed in order to recognize HHR and to control the conformation and the relating function of HHR.

3.1.1 Design of Liposome with Optimal Physicochemical Properties for HHR Recognition

In order to determine key factors for the recognition of HHR, the physicochemical properties of PE/PC liposomes were evaluated by fluorescent probes, TNS and Laurdan, based on the strategy described in **Chapters 2** and **3**. **Figure 4-4** shows the relative fluorescence intensities of TNS and GP_{340} values at 37 °C. Membrane fluidities increased in proportion to the molar fraction of unsaturated lipids (DOPE and DOPC). GP_{340} values decreased in a similar manner, while TNS fluorescence showed the maximum value with DOPE/DPPC (8/2) liposome, indicating that DOPE/DPPC (8/2) liposome has the most hydrophobic surface. It has been previously reported that the adsorption of single-stranded RNA was significantly increased in membranes with lower packing density (Michanek *et al.*, 2012). It is therefore shown that the HHR can be bound at the interface regions (*i.e.*, ε: 25-35 (**Fig. 2-2**)) in the DOPE/DPPC (8/2) membranes. Because PE lipids have positively-charged ethanolamine groups, the PE molecule is expected to act as a monovalent cation, which is necessary for the self-cleavage reaction of HHR (Curtis *et al.*, 2001; Boots *et al.*, 2008). It has been reported that the smaller RNA molecules can be in rod-like structure and the hydrophobic nucleobases are exposed (Navarro *et al.*, 2000), suggesting that HHR are also expected to be hydrophobic, and are likely to be recognized by the liposome membranes. Because the DOPE/DPPC (8/2) liposome was found to be the most hydrophobic (the highest TNS fluorescence) (Yoshimoto, PhD thesis (1999)), it is shown that the DOPE/DPPC (8/2)

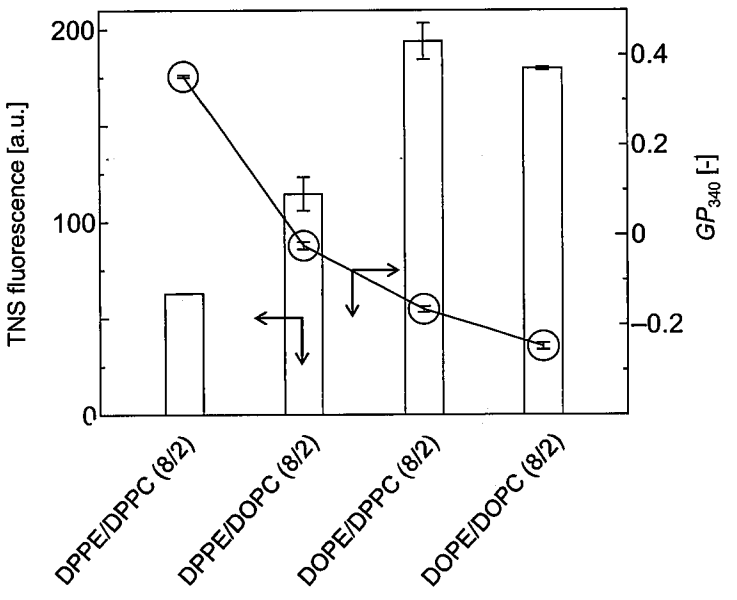

Fig. 4-4 Physicochemical properties of PE/PC liposomes at 37 °C.

can be a suitable liposome for the recognition of HHR. In the following section, the mechanism of HHR binding together with its conformational change was estimated, focusing on the DOPE/DPPC (8/2) liposomes.

3.1.2 Evaluation of the Binding Depth of HHR into the DOPE/DPPC (8/2) Liposome Membranes

Ribozyme activities are relating to the conformation of their active centers (Lilley, 2005; Strobel *et al.*, 2007), although the HHR deforms its structure due to self-cleavage just when the conformation of the active center is constructed. In order to prevent the HHR reactions and measure its conformation, a single-stranded DNA was used in replace of the HHR-1 (substrate). In the following, HHR-IC was studied focusing on the interaction mechanism and conformation. The binding depth of HHR-IC into DOPE/DPPC (8/2) membranes was determined by measuring TNS fluorescence and GP_{340} values (**Fig. 4-5**). After the addition of HHR-IC to the liposomes, the decreases of TNS fluorescence was

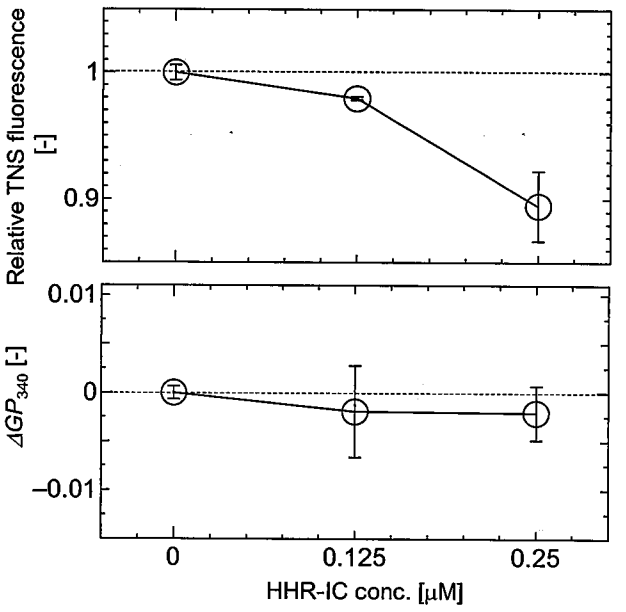

Fig. 4-5 Variations of TNS fluorescence and ΔGP_{340} values in the presence of HHR-IC.

observed, while GP_{340} values did not significantly vary. According to the findings in **Chapter 2**, TNS shows a strong fluorescence in hydrophobic environments, while it had little fluorescence in water solutions (**Fig. 2-2**). It is therefore revealed that the HHR-IC can bind to the interface regions (*i.e.*, ε: 25-35), where the binding depth is estimated to be ca. 1 nm from the bulk-water layer (Cevc, 1990). Because Laurdan monitors membrane polarities in the regions of phosphate to carbonyl groups, these regions can be excluded from the possible binding sites of HHR-IC in the DOPE/DPPC (8/2) liposome membrane.

3.1.3 Estimation of the Binding Moieties by UV Resonance Raman Spectroscopy

The binding moieties of HHR-IC were estimated by UV resonance Raman spectroscopic analysis. **Figure 4-6(A)** shows UV resonance Raman spectrum of HHR-IC and relative peak intensities. Peaks at 1250, 1367, and 1487 cm^{-1} are assigned as adenine (A), guanine (G), and G/A, respectively (**Table 3-1**) (Lanir *et al.*, 1979; Mathlouthi *et al.*, 1986;

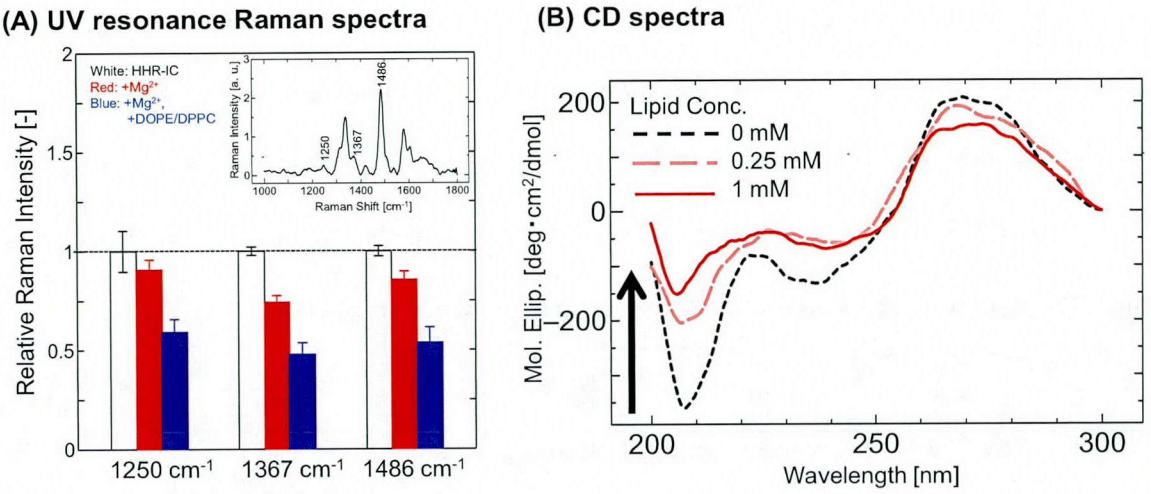

Fig. 4-6 (A) UV resonance Raman spectra and the relative peak intensities. (B) CD spectra of HHR-IC in the presence of DOPE/DPPC (8/2).

Zhelyaskov *et al.*, 1992; Florián *et al.*, 1996; Billinghurst *et al.*, 2009; Singh, 2012). The decreases in Raman intensity are caused by a hydrogen bond or hydrophobic environment (Nagatomo *et al.*, 2011). The relative peak intensities of A and G decreased in the presence of Mg^{2+}. It has been reported that Mg^{2+} binds to the $A_9G_{10.1}$ motif of HHR (Tanaka *et al.*, 2004), suggesting that the decreases in Raman peaks was due to Mg^{2+} binding. The larger decreases of Raman peaks were observed in the presence of DOPE/DPPC (8/2) liposome, indicating that DOPE/DPPC (8/2) could interact with HHR-IC at A and G moieties, including A_9G_{10}.

3.1.4 Evaluation of HHR-IC Conformation by Using CD Spectra

The conformation of HHR-IC was found to be in an A-form double helix structure (**Fig. 4-6(B)**). The decreases of CD peaks at 208 and 265 nm were observed in the presence of DOPE/DOPC (8/2). Based on the findings in **Chapter 3**, the decrease of CD peak indicated the conformational change of single-stranded RNAs. It has been reported that the conformational transition is required to form the active center of HHR (Hammann *et al.*, 2002). The present results indicated that A-form structure (θ_{208}) and base stacking (θ_{265}) of

HHR-IC decreased via liposome binding. Although the formation of the active center of HHR is very fast (Ferrari *et al.*, 2002), it was shown that the liposomes affected the conformation of HHR-IC. Because monovalent cations, *e.g.*, Na^+, K^+, and NH_4^+, also induce the self-cleavage reactions of HHR (Curtis *et al.*, 2001; Boots *et al.*, 2008), the direct interaction between PE molecules and HHR can also induce the self-cleavage reaction of HHR.

3.1.5 Effect of PE/PC Liposomes on HHR Kinetics

The recognition of HHR by the designed liposome was performed for the folding and functionalization of the HHR according to the scheme. The self-cleavage of HHR was determined in the presence of Mg^{2+} through the TOF/MS spectroscopy analysis. In the absence of Mg^{2+}, three notable peaks which indicate three RNAs constructing HHR were observed. In contrast, after adding 1 mM of Mg^{2+}, the peak of HHR-1 (4157.95) disappeared and two new peaks (1916.61 and 2245.70) appeared, indicating that HHR-1 was cleaved and resulted in the observation of these fragments. Because the molecular weights of two fragments agree well with theoretical values of those (GUACGUC and UGAGCG), it is suggested that the self-cleavage reaction of HHR can be performed with Mg^{2+}. In order to determine the effect of liposomes on HHR reactions, a kinetic assay was monitored by using a fluorescence probe, SYBR Green I (SGI) (**Fig. 4-7**). Because SGI is intercalated into various double-stranded DNA or RNA (Zipper *et al.*, 2004), similar to the ethidium bromide (Ferrari *et al.*, 2002), the self-cleavage of HHR causes the decrease of SGI fluorescence due to disruption of HHR conformation. The reaction rate of HHR, k_{obs}, was calculated by assuming a first-order kinetics based on the previous reports (Ferrari *et al.*, 2002). **Figure 4-7** (inert figure) shows the SGI fluorescence spectra of HHR. A strong peak at 524 nm was observed and it decreased after the substrate (HHR-1) addition, indicating that the self-cleavage reaction of HHR can be monitored by decreases of SGI. It was indicated that the HHR activity was effectively enhanced in the presence of the DOPE/DPPC (8/2) liposome, due to

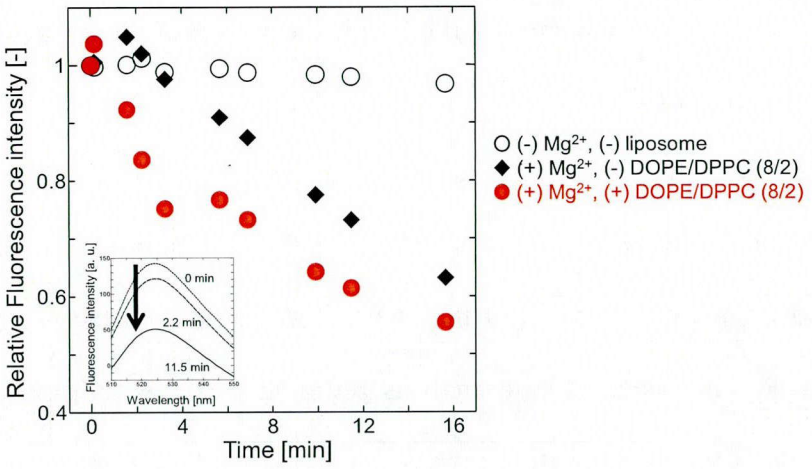

Liposome	k_{obs} [min^{-1}] (Rel. value)	Membrane fluidity, 1/*P* [-]	Phase state
Control	0.110	-	-
DPPE/DPPC	0.131 (1.12)	3.39 ± 0.04	ordered
DPPE/DOPC	0.127 (1.16)	3.83 ± 0.04	ordered
DOPE/DPPC	0.152 (1.39)	10.29 ± 0.05	heterogeneous
DOPE/DOPC	0.146 (1.33)	13.02 ± 0.88	disordered

Fig. 4-7 Kinetics of the self-cleavage reaction of HHR in the presence of liposomes.

the HHR binding to it (**Fig. 4-7** (Table)). The k_{obs} values in the presence of PE/PC liposomes with different acyl chain length also show that the liposomes, which have higher fluidities due to enough unsaturated acyl chains (DOPE/DOPC (8/2) and DOPE/DPPC (8/2)), indicated higher k_{obs} values, resulting in that the liposomes with higher membrane fluidity can efficiently activate the self-cleavage reaction of HHR. Although the enhanced degree of k_{obs} values in the presence of liposomes with lower fluidities were found to be not so high, resulting in 1.12-fold for DPPE/DPPC and 1.16-fold for DPPE/DOPC. These results suggest that the HHR reaction with various PE/PC liposomes depends on their phase states.

3.1.6. Self-Cleavage Reactions of HHR in the absence of Mg^{2+}

In the absence of Mg^{2+}, the self-cleavage reaction of HHR was not observed. In

contrast, HHR activities were observed with the DOPE/DPPC (8/2) liposomes (**Fig. 4-8(A)** and **(B)**), in spite of the "absence" of Mg^{2+}. Although the k_{obs} value was 0.23-fold lower in comparison with the values in the presence of Mg^{2+}, it is expected that that the DOPE liposome membranes can act as a platform of the recognition and folding of HHR without Mg^{2+}, and monovalent cations of the DOPE can act as a co-factor of its action center. UV resonance Raman spectroscopic analysis revealed that the addition of DOPE/DOPC (8/2) liposome itself reduced the Raman peaks of HHR-IC (**Fig. 4-8(C)**). It is therefore suggested that DOPE/DOPC (8/2) liposome directly interacted with A and G moieties. CD spectra analysis indicated that the addition of DOPE/DOPC (8/2) liposome significantly reduced the CD peak at 208 nm (A-form), showing that the liposomes can induce the conformational change of HHR and thus achieved the self-cleavage reaction of HHR because of the construction of "active-center" like conformation.

Based on the above results, it is concluded that the DOPE/DPPC (8/2) liposomes can (i) recognize the A and G residues in HHR, which containing $A_9G_{10.1}$ motif of Mg^{2+} binding sites; (ii) induce conformational change of HHR, especially at A-form structure, and (iii) enhance the self-cleavage reaction of HHR. The use of DOPE/DPPC (8/2) liposomes as a

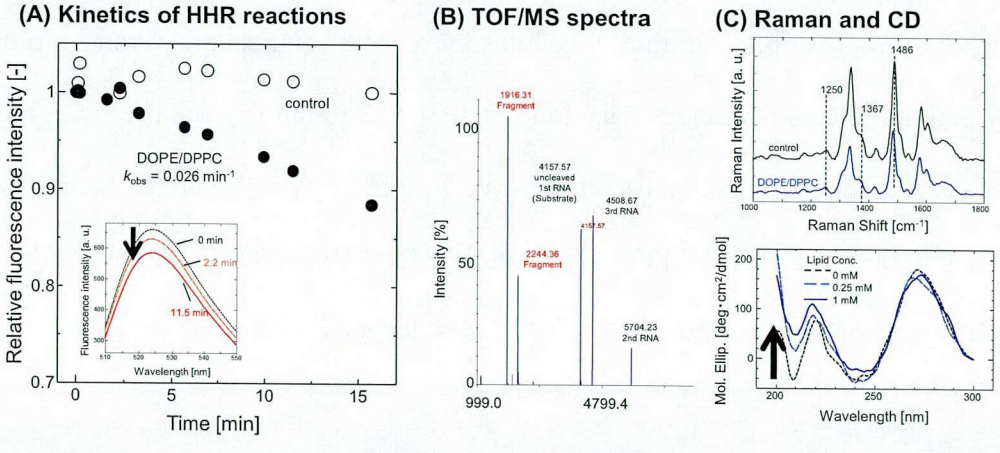

Fig. 4-8 (A) Kinetics of HHR reaction in the absence of Mg^{2+}. (B) TOF/MS spectra of HHR. (C) Raman and CD spectra of HHR-IC in the absence of Mg^{2+}.

platform of the nucleotide recognition was found to give the highest k_{obs} value of the self-cleavage reactions of HHR without Mg^{2+}, because the packing density of membranes were lower than others (TNS assay). Exposed inner hydrophobic regions are possible binding sites of biomacromolecules, together with the fact that Mg^{2+} bind to PE membranes (Gromelski *et al.*, 2006). It is therefore shown that the liposome membrane can be utilized as a functional platform for recognition and controlling of HHR.

3.2 Design of "Raft" Domain Liposomes for tRNA Recognition

The "raft" domain is one of the most functional membrane domains in biological systems (Brown *et al.*, 1998). It has been previously reported that the "raft" domain can play important role in recognition of RNA molecules (Janas *et al.*, 2006). In **Chapter 3**, it is shown that the micro-domain liposome (POPC/Ch (70/30)) can recognize tRNA molecules, although the role of micro-domains in the recognition has not been clarified yet. From the viewpoint of the lipoplex formation in drug delivery system (DDS), the mechanism of biomacromolecular recognition by the liposome membranes is required to be clarified in order to design the high-affinity liposomes with siRNAs. In this section, the effect of micro-domain size on the recognition of biomacromolecules was investigated by using tRNAs as model polynucleotides (**Fig. 4-9**).

3.2.1 Characterization of DOPC/SM/Ch Liposomes

The recognition of tRNA by designed liposome was performed by focusing on "nano-domain" of liposomes according to the scheme. Cholesterol (Ch) and sphingomyelin (SM) are main components of lipid "raft" in biological systems (De Almeida *et al.*, 2003; Veatch *et al.*, 2005). The physicochemical properties of DOPC/SM/Ch were analyzed by using fluorescent probes, DPH and Laurdan (**Fig. 4-10**), as described in above sections. The liposomes containing >30 mol% of Ch indicated the lower values of membrane fluidities

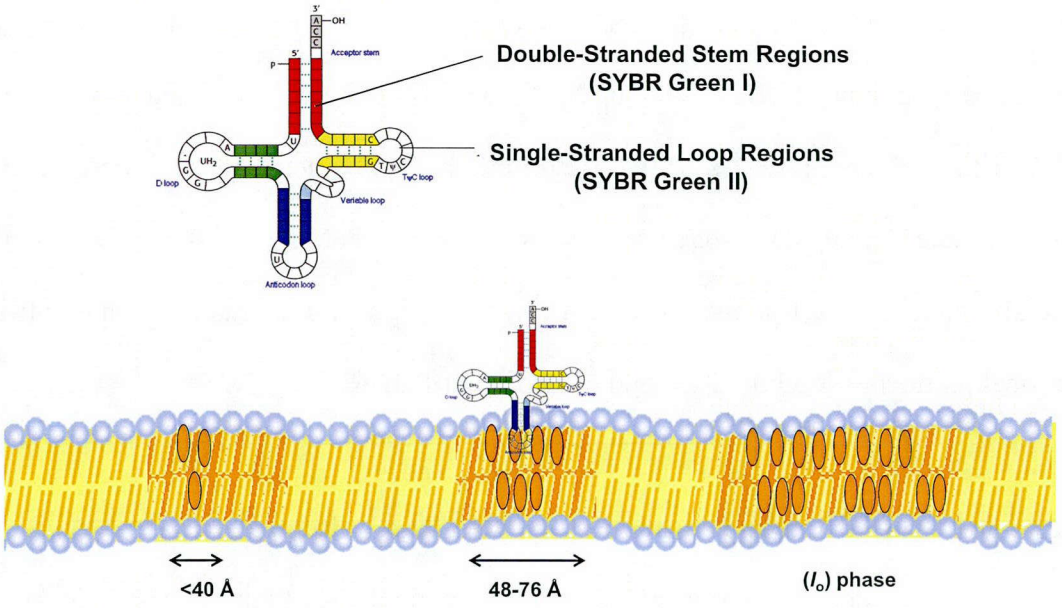

Fig. 4-9 Conceptual illustration of the recognition of tRNA.

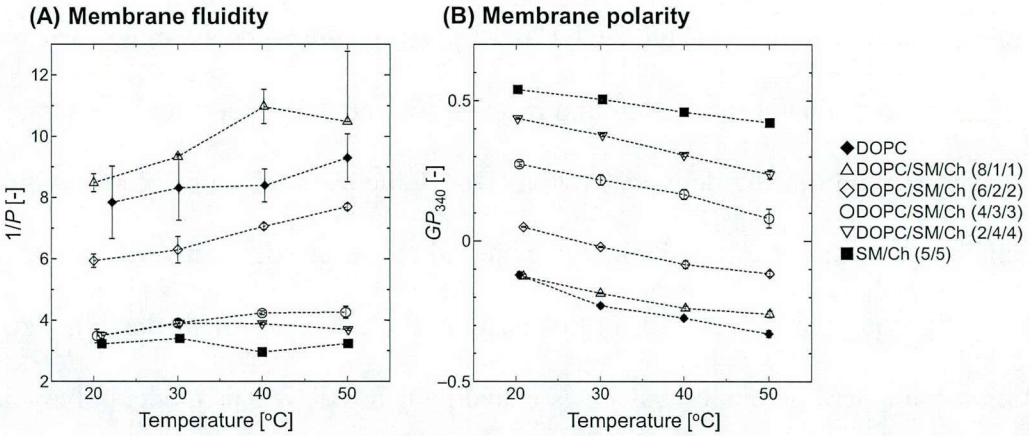

Fig. 4-10 (A) Membrane fluidity (1/*P*) and (B) membrane polarity (GP_{340}) of DOPC/SM/Ch liposomes.

(1/*P*) at the temperature range of 20-50 °C. Because DPH is likely to be distributed to ordered phases (Pathak *et al.*, 2011), it is suggested that large ordered domains can be formed in the DOPC/SM/Ch membranes. The GP_{340} values were proportional to the molar ratio of SM and Ch. It has been reported that SM can form hydrogen bonding with Ch due to its amide groups, while DPPC unlikely (Guo *et al.*, 2002). These results indicate that the liposomes containing

SM and Ch (>60 mol%) are in liquid-ordered (l_o) phases. These l_o phase domains were so-called "raft" domains.

3.2.2 Detection of Nano-Domains Formed on DOPC/SM/Ch Membranes

Figure 4-11(A) indicates the Cartesian diagram of DOPC/SM/Ch liposomes at 25 °C. Based on the scheme described in **Chapter 2**, it is shown that DOPC/SM/Ch (8/1/1) and DOPC/SM/Ch (6/2/2) can be in heterogeneous phases. Studies based the microscopy analysis has been reported that only one-liquid phases were formed within these liposomes (Veatch *et al.*, 2005), while the AFM studies has investigated the nano-sized domains (~1 nm) in DOPC/SM/Ch membranes (Yuan *et al.*, 2002). According to the obtained results in **Chapter 2**, the TEMPO quenching method can quantitatively detect the nano-sized ordered domains in the liposome membranes. Because this method depends on the distance between TEMPO and DPH, it can also be possible to quantify the "raft" domain sizes in DOPC/SM/Ch liposomes. According to the remaining DPH fluorescence, Q_{liposome} (data not shown), domain sized were calculated (**Fig. 4-11(B)**). It is notable that the $Q_{\text{SM/Ch (5/5)}}$ values were higher (~99 %) than that of DPPC (Q_{DPPC}, ~70 %), showing that the "raft" domains in the DOPC/SM/Ch liposomes are tightly packed, and are larger than 48 Å. In the present study, the variation of the domain size can be estimated to be 11-78 Å. Although Veatch *et al* reported the visible membrane domains (~μm) in DOPC/SM/Ch systems of giant unilamellar vesicles, the present study investigated that nano-sized l_o domains formed in DOPC/SM/Ch membranes (**Fig. 4-12**). The "raft" domain plays important roles in biological systems (*e.g.*, signal transduction, biogenesis and so on) (Brown *et al.*, 1998; Lingwood *et al.*, 2010). It has been reported the specific interaction between DOPC/SM/Ch (6/3/1) and RNA 10 (Janas *et al.*, 2006), suggesting the recognition of RNA molecules. Because SM and Ch molecules have donors and acceptors of hydrogen bonding (Boggs, 1987), possible hydrogen bonding interactions are expected between DOPC/SM/Ch liposomes and biomacromolecules.

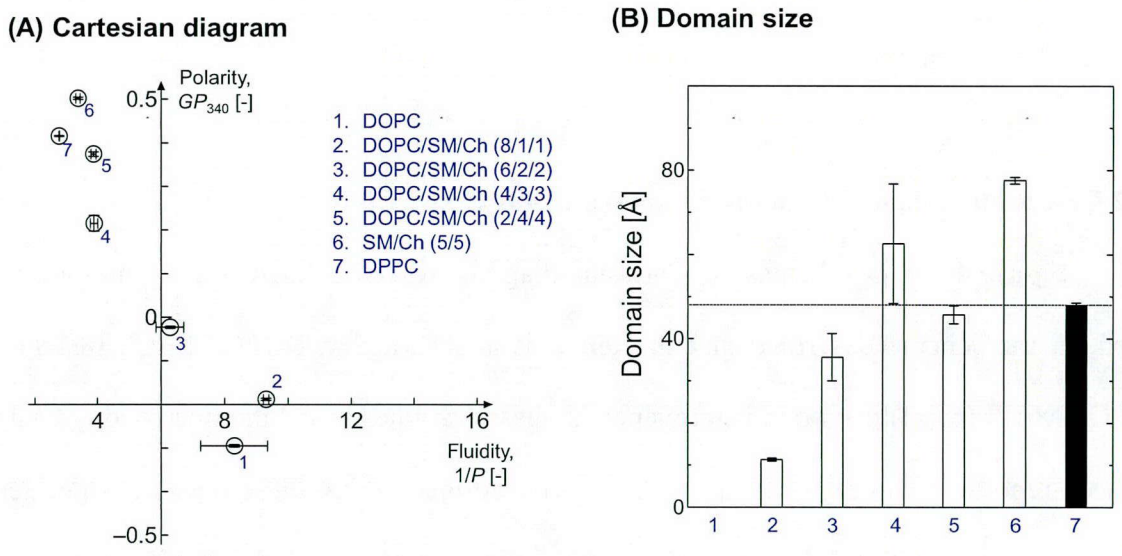

Fig. 4-11 (A) Cartesian diagram analysis and (B) calculated domain size at 25 °C.

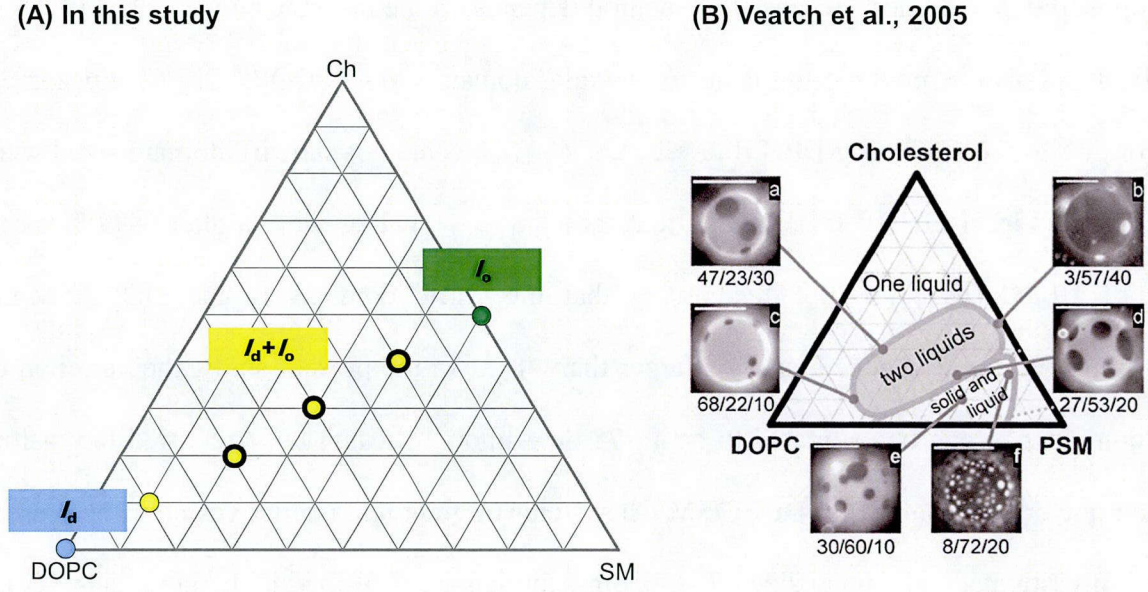

Fig. 4-12 Phase diagram of DOPC/SM/Ch liposomes described in this study (A) and in literature (Veatch *et al.*, 2005) (B).

3.2.3 Recognition of tRNA by Using DOPC/SM/Ch Liposomes

The binding sites of tRNA to liposomes were further studied by using fluorescent probes, SGI and SGII (**Fig. 4-13**). It has been reported that SGI binds to double-stranded stem

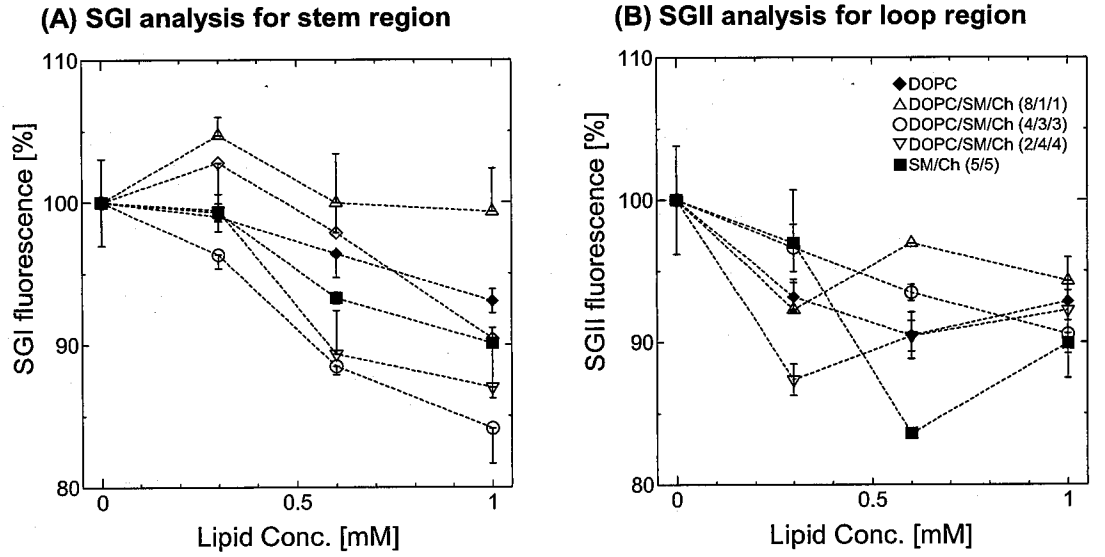

Fig. 4-13 (A) SGI binding assay for stem regions in tRNA. (B) SGII binding assay for loop regions in tRNA.

regions (Zipper *et al.*, 2004), while SGII binds to single-stranded loop regions (Morozkin *et al.*, 2003). SGI Fluorescence significantly decreased in the presence of DOPC/SM/Ch (4/3/3) (**Fig. 4-13(A)**), showing that DOPC//SM/Ch (4/3/3) can bind to stem regions in tRNA. Analysis of SGII fluorescence indicated that DOPC//SM/Ch (4/3/3) also bound to single-stranded loop regions (**Fig. 4-13(B)**). Together with these results, it is shown that DOPC/SM/Ch (4/3/3) can bind to tRNA, where DOPC//SM/Ch (4/3/3) recognized the stem and loop regions. The conformation of tRNA was changed in the presence of DOPC/SM/Ch and loop regions. The conformation of tRNA was changed in the presence of DOPC/SM/Ch (4/3/3), while that was not so much in the presence of DOPC (**Fig. 4-14**). It is therefore shown that the DOPC/SM/Ch liposomes can recognize tRNA molecules, depending on the domain size, and can induce the conformational change of tRNA.

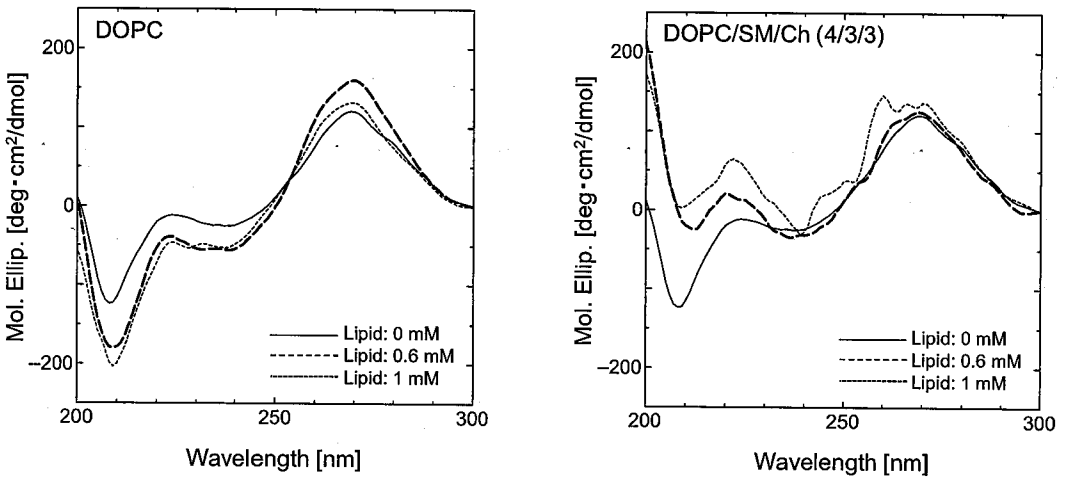

Fig. 4-14 CD spectra of tRNA.

4. Summary

A general design scheme for the recognition of biomacromolecules, accompanying with their folding and functionalizing, was proposed based on the results described in **Chapters 1**, **2**, and **3**. Liposome membranes were, in practice, designed for recognition of biomacromolecules, such as polypeptides, HHR, and tRNA.

In the case of HHR, DOPE/DPPC (8/2) effectively enhanced HHR activity in the presence of Mg^{2+}. TNS and UV resonance Raman spectroscopic assays indicated that HHR bound to the interface regions (ε: 25 -35), and the binding moieties of HHR were estimated to A and G. HHR interactions at A and G moieties were also observed in the "absence" of Mg^{2+}. The liposomes induced the conformational change of HHR-IC. DOPE/DPPC (8/2) liposomes fulfilled the conditions that are required for HHR activities, suggesting that DOPE molecules act as monovalent cations alternate to Mg^{2+}. In the case of tRNA, DOPC/SM/Ch (4/3/3) was found to bind the stem and loop regions in tRNA, because DOPC/SM/Ch (4/3/3) liposome has l_o phase domains with a radius of 48-76 Å, which can be fit to the stem regions in tRNA.

Above two cases indicate that not only physicochemical properties of membranes (fluidity, polarity, and heterogeneity) but also membrane structures with nano-sized domains are important to recognize biomacromolecules. Based on the present findings, liposome membranes can be utilized as a platform to control biomacromolecular functions. In early life on earth, lipid vesicles are likely to accumulate biomacromolecules on the membrane surface, and thus the life can be evolved (Ricardo *et al.*, 2009). Recent researchers try to understand the diversity of biomembranes, although the functions of biomembranes, especially recognition, have not been clarified yet. Liposome membranes are one of optical biomimetic membranes, because the surface design of membranes provides us a new insight into the biomacromolecular recognition. From the viewpoint of DDS, it is important to design the liposomes, which have higher affinity with small RNA molecules (*e.g.*, siRNA). The conventional strategy to prepare the lipoplex is the use of cationic liposomes, although the strong electrostatic interaction between the liposome and RNA has been reported to prevent the release of RNAs at the target cells (Xu *et al.*, 1996; Barreau *et al.*, 2006). Based on the present results, the domain size is one of key factors for design the RNA recognition. Because the phase states of liposome membranes are sensitive to the surrounding environment (temperature, *etc.*), it is also possible to design the "catch-and-release" strategy of the target genes, by utilizing the heat stress, for example. Not only polynucleotides but also polypeptides, proteins, and enzymes can be recognized by designed liposomes (Yoshimoto *et al.*, 2000; Tuan *et al.*, 2008; Umakoshi *et al.*, 2012). Utilization of the "*Bio-Inspired*" membranes will develop innovative chemical and biochemical processes.

General Conclusions

The methodology to design the liposome membranes for recognition of biomacromolecules and control their conformation was established in order to develop innovative bio-/chemical processes. Focusing on the physicochemical properties and "microscopic" domains of liposome membranes, the key important factors required to recognize polynucleotides and polypeptides was analyzed based on the case study of single-stranded RNAs (mRNA, tRNA, HHR) and unfolded GFP peptides. It is important to design "*Bio-Inspired*" membranes, which have a flexible surface of the "platform" that can freely match with the three-dimensional structure of target molecules to be employed as building-block of the novel biofunctional materials.

In Chapter 1, the effect of liposome addition on the *in vitro* gene expression in an *E coli* cell-free translation (CFT) system was determined, in order to find out the specific interaction of lipid membrane with biomacromolecules. It was shown that GFP expression was regulated by charged liposomes at the translation and folding steps via interaction with RNA molecules and GFP polypeptides. Characterization of biomacromolecules indicates that the nascent mRNA and GFP polypeptide are unstable and are likely to interact with liposomes via electrostatic, hydrophobic, and hydrogen bonding interactions. Focusing on the POPC/Ch liposomes, the surface properties of liposome (*i.e.*, fluidity, polarity, and heterogeneity (domain)) were also shown to be key factors to regulate liposome-biomacromolecule interaction, especially for RNA molecules.

In Chapter 2, the physicochemical properties of DOPC/DPPC and DOPC/Ch binary mixture of LUVs were determined, and nano-sized ordered domains were detected using a newly-developed TEMPO quenching method. Analysis of membrane fluidity and polarity revealed that the DOPC/DPPC binary mixture of LUVs formed immiscible "microscopic"

segregated regions. These nano-sized ordered domains were detected by using the TEMPO quenching method, and average domain sizes of 13.9, 36.2, ~13.2, and ~35.5 Å were determined for DOPC/DPPC (50/50), DOPC/DPPC (25/75), DOPC/Ch (70/30) and DOPC/DPPC/Ch (40/40/20), respectively. It can be possible to design the nano-domains that can recognize a target biomacromolecule with a surface structure of membrane that fits to the shape (*i.e.*, concavity and convexity with domains). Present findings may be a key to understanding self-assembled systems, and to designing "*Bio-Inspired*" membranes. The detection of nano-domains formed on lipid membranes also aids in understanding the function of biomembranes. It is therefore important to understand the structure and function of lipid membranes in biological systems, and to develop artificial biomembrane systems to regulate biomacromolecules.

In Chapter 3, the mechanism of the liposome interaction with single-stranded RNAs was investigated, focusing on their conformation and functions. An inhibitory effect on mRNA translation in the presence of cationic liposomes (CLs) was explored by using an *E. coli* CFT system by employing its mRNA as an initial template of GFP gene. The membrane fluidity and polarity were analyzed to identify the phase state of CLs. CLs in l_d phases markedly inhibited the translation of mRNA bound to membranes in an "inactive" state, while heterogeneous DOPC/DC-Ch (70/30) slightly inhibited the translation of mRNA, which was bound to membranes in an "active" state. Possible bindings site in the liposome-mRNA interaction was estimated to be at the level of phosphate [-PO_2^--] to carbonyl [-C=O-] moieties, where nucleobases (A, G, C) in mRNA interacted with lipids in CL membranes by analysis of Raman and FTIR. Cytosine residues interacted with heterogeneous liposomes; DOPC/Ch (70/30) with 13.3 Å-domain and DOPC/DC-Ch with 16 Å-domain. POPC/Ch (70/30) maintained mRNA conformation, resulting in an enhancement of mRNA translation. In contrast, DOPC/DOTAP (70/30) denatured the conformations of both the A-form (208 nm) and that of base stacking (265 nm) in mRNA. DOPC/DC-Ch (70/30) denatured the A-form

structure, despite the variation of lipid concentration. It is therefore concluded that heterogeneity of liposome membrane plays an important role in the regulation of the mRNA conformation and its function. Characterization and design of lipid membranes is also important in the research fields of synthetic cell biology, liposome-based drug delivery systems, and biomacromolecular engineering. Utilizing the behaviors of lipid membranes, further improvements can be achieved in the regulation of liposome-RNA interactions and the RNA functions. The key of liposome membrane design for the biomacromolecular recognition can be understood as "co-induction" of multiple interactions, such as (i) electrostatic interaction, (ii) hydrophobic interaction, (iii) entropic forces with the dehydration of membrane surface, (iv) hydrogen bonding interaction, (v) micro-domain formation at the contacting surface. Temperature setting is also important because of the increase of hydrophobic interaction between membranes and denatured biomacromolecules in unstable conformations. In the present study, it is shown that heterogeneous membranes containing the micro-domains can play important role on recognition of biomacromolecules.

In Chapter 4, the liposome membranes were, in practice, designed for recognition of biomacromolecules, such as polypeptides, HHR, and tRNA. In the case of HHR, the DOPE/DPPC (8/2) liposome was designed and its physicochemical properties were analyzed by using TNS and Laurdan, showing that HHR can bind at the interface regions (ε: 25 -35). Using the UV resonance Raman spectroscopic assays, it was indicated that the binding moieties of HHR were A and G. The DOPE/DPPC (8/2) liposome induced the conformational change of HHR-IC, resulting in the effectively enhanced HHR activity in the presence of Mg^{2+}. The interaction of the liposomes with HHR at A and G moieties was also observed in the "absence" of Mg^{2+}. Although the k_{obs} value was 0.23-fold lower in comparison with the values of Mg^{2+}, it is expected that that the DOPE liposome membranes can act as a platform of the recognition and folding of HHR without Mg^{2+}, and monovalent cations of the DOPE can act as a co-factor of its action center. In the case of tRNA, DOPC/SM/Ch (4/3/3) was

found to bind the stem and loop regions in tRNA, because DOPC/SM/Ch (4/3/3) liposome has l_o phase domains with a radius of 48-76 Å. These results indicate not only physicochemical properties of membranes (fluidity, polarity, heterogeneity) but also membrane structures with nano-sized domains are key factors for recognition of biomacromolecules. Based on the present findings, liposome membranes can be utilized as a platform for the recognition of biomacromolecules and controlling of their conformation and functions.

A general design scheme for the recognition of biomolecules, accompanying with their folding and functionalizing, was proposed based on the results described in this study. In early life on earth, lipid vesicles are likely to accumulate biomacromolecules on the membrane surface, and thus the life can be evolved (Ricardo *et al.*, 2009). From the viewpoint of self-assemblies, cholesterols in lipid membranes are shown to play important roles in the formation of nano-sized domains, and in the recognition of cytosine residues of polynucleotides, as well as the unstable proteins and enzymes, described in the previous research. The liposome membranes are one of optical biomimetic environments, because the surface design of membranes provides us a new insight into the biomacromolecular recognition. Utilizing of the "*Bio-Inspired*" membranes will develop innovative chemical and biochemical processes. It is therefore possible to design the liposome membrane that can recognize biomacromolecules and control their conformations, which are deeply relating to functions of biomacromolecules.

Suggestions for Future Works

To expand the findings obtained in this work, the following studies are recommended.

(1) *In vitro* Selection of Biomacromolecules on the Liposome Membrane

The basic findings obtained in this study can apply to the liposome-based separation and technology by utilizing the liposome membrane as a platform for the recognition of target biomacromolecules. Because the liposomes, as well as other molecular imprinting membranes, can induce multiple interaction forces with target biomacromolecules, the fine turning of liposome membrane, *e.g.*, surface charge density, fluidity, polarity, nano-domain, *etc.*, will provide us to develop an innovative recognition technology. It is important to design the liposome membrane that can recognize not only biomacromolecules but also small biomolecules, such as amino acid, nucleic acid monomer, and chiral species. Further studies are necessary to understand the recognition mechanism of liposome membranes for various kinds of biomolecules and biomacromolecules.

(2) Characterization of Various Kinds of Vesicles and Lipid Self-Assemblies

The vesicle formation and its characterization are important research topics in many fields: self-assembly science, drug delivery system, synthetic cells, bioreactor for chemical reaction, and so on. The fatty acid vesicles and detergent vesicles have withdrawn a lot of attention because of their lower cost as compared with phospholipid vesicles, and their dynamic behaviors. The methodology for the characterization of liposome membranes, described as the membrane characterization scheme in **Chapter 2**, can also be applied to characterize such vesicles. The fluorescent probes, TNS and Laurdan, can be utilized to monitor the water-lipid interface regions; Raman spectroscopic assay enables us to directly

monitor the behaviors of lipid molecule, such as the packing density of lipid membrane and the phase transition. The Cartesian diagram can visualize the heterogeneity of membrane, and the TEMPO quenching method can detect the nano-sized ordered domains in the membrane. These studies will provide us a deeper understanding for the self-assembly mechanism.

(3) Design of Novel Chemical Processes Utilizing the Interface Region of Liposome Membranes

The interface region of liposome membrane can be utilized as a platform for the recognition of biomacromolecules. There are various kinds of chemical reactions which require the transfer of products across the hydrophobic and hydrophilic phases. The quaternary ammonium ion is known as a catalyst for the migration of a reactant from one phase into another phase where reaction occurs (phase-transfer catalyst, PTC). It is expected that the PTC process with liposome membrane can be realized to achieve faster reactions, obtain higher conversions or yields, make fewer byproducts, eliminate the need for expensive or dangerous solvents that will dissolve all the reactants in one phase, eliminate the need for expensive raw materials and/or minimize waste problems. Although the mechanism of These studies will contribute to the investigation of the reaction mechanism at the interface regions between the hydrophobic and hydrophilic environment.

Nomenclatures

A_{260}/A_{280}	= purity of isolated RNA	[-]
E/M ratio	= excimer-to-monomer intensity ratio of Pyrene	[-]
G	= correction factor	[-]
GP_{340}	= general polarization calculated at exciting light at 340 nm	[-]
ΔG	= hydrophobicity of biomacromolecules	[kJ/mol/nm^2]
HFS	= surface net hydrophobicity	[kJ/mol]
K_d	= dissociation constant	[M]
k_{obs}	= observed reaction ratio of HHR	[min^{-1}]
LH	= local hydrophobicity	[-]
N	number of lipid molecules in a domain	
	$= S / [48 \times (x_{,DPPC}/(x_{,DPPC} + x_{,Ch}) + 40 \times (x_{,Ch}/(x_{,DPPC} + x_{,Ch})]$	[-]
$N_{rel.}$	= relative number of lipid molecules in a domain compared with DPPC	
	$= N_{liposome}/N_{DPPC}$	[-]
P	= fluorescence polarization of probes embedding in bilayers	[-]
$1/P$	= membrane fluidity	[-]
$Q_{liposome}$	remaining fluorescence of DPH	[-]
R	= packing density of lipid membrane	[-]
S	= calculated domain area	[Å^2]
X	radius of ordered domain	
	$= [R_{DPH} + R_{TEMPO}] \times [(Q_{liposome} - Q_{DOPC}) / (Q_{DPPC} - Q_{DOPC})]$	[Å]
z	= surface net charge of biomacromolecules	[C/nm^2]
$\Delta\nu$	= shift of FTIR peak	[cm^{-1}]
ρ	= hydrogen bonding desolvation	[-]

List of Abbreviations

ATPS	aqueous two-phase partition system
CAB	carbonic anhydrase
CFT	cell-free translation
Ch	cholesterol
CL	cationic liposome
DC-Ch	3β-[N-(N',N'-dimethylaminoethane)-carbamoyl]cholesterol
Dex	dextran
DMPC	1,2-dimethyl-*sn*-glycero-3-phosphocholine
DOPC	1,2-dioleoyl-*sn*-glycero-3-phosphocholine
DOPE	1,2-dioleoyl-*sn*-glycero-3-phosphoethanolamine
DPH	1,6-diphenyl-1,3,5-hexatriene
DPPC	1,2-dipalmitoyl-*sn*-glycero-3-phosphocholine
DPPE	1,2-dipalmitoyl-*sn*-glycero-3-phosphoethanolamine
DOTAP	1,2-dioleoyl-3-trimethylammonium propane
DSTAP	1,2-distearoyl-3-trimethylammonium propane
DSPC	1,2- distearoyl-*sn*-glycero-3-phosphocholine
E. coli	*Escherichia coli*
Em	emission wavelength
Ex	excitation wavelength
GdnHCl	guanidine HCl
GFP	green fluorescent protein
Laurdan	6-lauroyl-2-dimethylaminonaphthalene
l_d	liquid disordered
l_o	liquid ordered

LUV	large unilamellar vesicle
HHR	hammerhead ribozyme
MG	molten globule
MLV	multilamellar vesicle
NTP	nucleotide triphosphate
PAGE	polyacrylamide gel electrophoresis
PEG	polyethylene glycol
POPC	1-palmitoyl-2-oleoyl-*sn*-glycero-3-phosphocholine
POPG	1-palmitoyl-2-oleoyl-*sn*-glycero-3-phosphogrycerol
Pyrene	1-pyrene-dodecanoic acid
RTS-Kit	Rapid Translation System RTS 100 *E. coli* HY Kit
SA	stearyl amine
SDS	sodium dodecyl sulfate
SGI	SYBR Green I
SGII	SYBR Green II
SM	sphingomyelin
s_o	solid disordered
TEMPO	(2,2,6,6-tetramethylpiperidin-1-yl)oxyl
TNS	6-(p-toluidino)naphthalene-2-sulfonate
tRNA	transfer RNA

References

Abraham, D. J.; Leo, A.; Leo, J. Extension of the fragment method to calculate amino acid zwitterion and side chain partition coefficients. *Proteins*, **2**, 130-152 (1987).

Ahmed, S. N.; Brown, D. A.; London, E. On the origin of sphingolipid/cholesterol-rich detergent-insoluble cell membranes: physiological concentrations of cholesterol and sphingolipid induce formation of a detergent-insoluble, liquid-ordered lipid phase in model membranes. *Biochem.*, **36**, 10944–10953 (1997).

Albertsson, P.-Å. Partition of cell particles and macromolecules in polymer two-phase systems. *Adv. Protein Chem.*, **24**, 309-341 (1970).

Auffinger, P.; Westhof, E. RNA hydration: Three nanoseconds of multiple molecular dynamics simulations of the solvated tRNA(Asp) anticodon hairpin. *J. Mol. Biol.*, **269** (3), 326-341 (1997).

Bailor, M.H.; Musselman, C.; Hansen, A. L.; Gulati, K.; Patel, D. J.; Al-Hashimi, H. M. Characterizing the relative orientation and dynamics of RNA A-form helices using NMR residual dipolar couplings. *Nat. Prot.*, **2** (6), 1536-1546 (2007).

Bakht, O.; Pathak, P.; London, E. Effect of the structure of lipids favoring disordered domain formation on the stability of cholesterol-containing ordered domains (lipid rafts): Identification of multiple raft-stabilization mechanisms. *Biophys. J.*, **93** (12), 4307-4318 (2007).

Banchelli, M.; Berti, D.; Baglioni, P. Molecular recognition drives oligonucleotide binding to nucleolipid self-assemblies. *Angew. Chem. Int. Ed.*, **46** (17), 3070-3073 (2007).

Barreau, C.; Dutertre, S.; Paillard, L.; Osborne, H. B. Liposome-mediated RNA transfection should be used with caution. *RNA*, **12** (10), 1790-1793 (2006).

Batenjany, M. M.; Wang, Z.Q.; Huang, C. -H.; Levin, I. W. Bilayer packing characteristics of mixed chain phospholipid derivatives: Raman spectroscopic and differential scanning

calorimetric studies of 1-stearoyl-2-capryl-sn-glycero-3-phosphocholine (C(18): C(10)PC) and 1-stearoyl-2-capryl-sn-glycero-3-phospho-N-trimethylpropanolamine (C(18): C(10) TMPC). *Biochim. Biophy. Acta Biomembranes*, **1192** (2), 205-214 (1994).

Benevides, J. M.; Overman, S. A.; Thomas Jr., G. J. Raman, polarized Raman and ultraviolet resonance Raman spectroscopy of nucleic acids and their complexes. *J. Raman Spectr.*, **36** (4), 279-299 (2005).

Billinghurst, B. E.; Oladepo, S. A.; Lonow, G. R. pH-Dependent UV resonance raman spectra of cytosine and Uracil. *J. Phys. Chem. B*, **113** (20), 7392-7397 (2009).

Boggs, J. M. Lipid intermolecular hydrogen bonding: Influence on structural organization and membrane function. *Biochim. Biophys. Acta Rev. Biomembranes*, **906** (3), 353-404 (1987).

Boots, J. L.; Canny, M. D.; Azimi, E.; Pardi, A. Metal ion specificities for folding and cleavage activity in the Schistosoma hammerhead ribozyme. *RNA*, **14** (10), 2212-2222 (2008).

Borocci, S.; Ceccacci, F.; Galantini, L.; Mancini, G.; Monti, D.; Scipioni, A.; Venanzi, M. Deracemization of an axially chiral biphenylic derivative as a tool for investigating chiral recognition in self-assemblies, *Chirality*, **15** (5), 441-447 (2003).

Brezesinski, G.; Möhwald, H. Langmuir monolayers to study interactions at model membrane surfaces. *Adv. Colloid Interf. Sci.*, **100-102** (SUL.), 563-584 (2003).

Brown, A. C.; Towles, K. B.; Wrenn, S. P. Measuring raft size as a function of membrane composition in PC-based systems: Part II - Ternary systems. *Langmuir*, **23** (22), 11188-11196 (2007).

Brown, D. A.; London, E. Functions of lipid rafts in biological membranes. *Ann. Rev. Cell Dev. Biol.*, **14**, 111-136 (1998).

Bui, H. T.; Umakoshi, H.; Suga, K.; Tanabe, T.; Shimanouchi, T.; Kuboi, R. Cationic liposome inhibits gene expression in an E. coli cell-free translation system. *Membrane*, **34** (3), 146-151 (2009).

Bui, H. T.; Umakoshi, H.; Ngo, K. X.; Nishida, M.; Shimanouchi, T.; Kuboi, R. Liposome membrane itself can affect gene expression in the Escherichia coli cell-free translation system. *Langmuir*, **24** (19), 10537-10542 (2008).

Bui, H. T.; Umakoshi, H.; Suga, K.; Nishida, M.; Shimanouchi, T.; Kuboi, R. Negatively charged liposome as a potent inhibitor of post-translation during in vitro synthesis of green fluorescent protein. *Biochem. Eng. J.*, **46** (2), 154-160 (2009).

Caldorera-Moore, M.; Peas, N. A. Micro- and nanotechnologies for intelligent and responsive biomaterial-based medical systems. *Adv.Drug Deliv. Rev.*, **61** (15), 1391-1401 (2009).

Campos, A. M.; Abuin, E. B.; Lissi, E. A. Effect of a linear (1-octanol) and a branched (2,6-dimethyl-4-heptanol) alkanol upon the properties of dipalmitoylphosphatidylcholine large unilamellar vesicles. *Coll. Surf. A: Physicochem. Eng. Aspects.*, **100**, 155-163 (1995).

Carmona, P.; Rodriguez-Casado, A.; Molina, M. Conformational structure and bindingmode of glyceraldehydes-3-phosphate dehydrogenase to tRNA studied by Raman and CD spectroscopy. *Biochim. Biophys. Acta*, **1432**, 222-233 (1999).

Cerritelli, S.; Velluto, D.; Hubbell, J. A. PEG-SS-S: Reduction-sensitive disulfide block copolymer vesicles for intracellular drug delivery. *Biomacromol.*, **8** (6), 1966-1972 (2007).

Cevc, G. Membrane electrostatics. *Biochim. Biophys. Acta Rev. on Biomembranes*, **1031** (3), 311-382 (1990).

Chabaud, P.; Camplo, M.; Payet, D.; Serin, G.; Moreau, L.; Barthélémy, P.; Grinstaff, M. W. Cationic nucleoside lipids for gene delivery. *Bioconj. Chem.*, **17** (2), 466-472 (2006).

Chen, I. A.; Salehi-Ashtiani, K.; Szostak, J. W. RNA catalysis in model protocell vesicles. *J. Am. Chem. Soc.*, **127** (38), 13213-13219 (2005).

Chen, I. A.; Szostak, J. W. A kinetic study of the growth of fatty acid vesicles. *Biophys. J.*, **87** (2), 988-998 (2004).

Clark, C. L.; Cecil, P. K.; Singh, D.; Gray, D. M. CD, absorption and thermodynamic analysis of repeating dinucleotide DNA, RNA and hybrid duplexes [d/r(AC)]12·[d/r(GT/U)]12 and the influence of phosphorothioate substitution. *Nucl. Acids Res.*, **25** (20), 4098-4105 (1997).

Collawn, J. F.; Bebök, Z. Chapter 1 Structure and Functions of Biomembranes. *Curr. Topics Membranes*, **61**, 1-21 (2008).

Conn, G. L.; Draper, D. E. RNA structure. *Curr. Opin. Struc. Biol.*, **8** (3), 278-285 (1998).

Critchpield, F. E.; Gibson Jr., J. A.; Hall, J. L. Dielectric constant for the dioxane-water system from 20 to 35°. *J. Am. Chem. Soc.*, **75** (8), 1991-1992 (1953).

Curtis, E. A.; Bartel, D. P. The hammerhead cleavage reaction in monovalent cations. *RNA*, **7** (4), 546-552 (2001).

De Almeida, R. F. M.; Fedorov, A.; Prieto, M. Sphingomyelin/phosphatidylcholine/cholesterol phase diagram: Boundaries and composition of lipid rafts. *Biophys. J.*, **85** (4), 2406-2416 (2003).

De Almeida, R. F. M.; Loura, L. M. S.; Fedorov, A.; Prieto, M. Lipid rafts have different sizes depending on membrane composition: A time-resolved fluorescence resonance energy transfer study. *J. Mol. Biol.*, **346** (4), 1109-1120 (2005).

de Lange, M. J. L.; Bonn, M.; Müller, M. Direct measurement of phase coexistence in DC/cholesterol vesicles using Raman spectroscopy. *Chem. Phys. Lipids*, **146** (2), 76-84 (2007).

De Meyer, F.; Smit, B. Effect of cholesterol on the structure of a phospholipid bilayer. *Proc. Nat. Acad. Sci. U. S. A.*, **106** (10), 3654-3658 (2009).

Edelman, G. M.; Mcclure, W. O. Fluorescent probes and the conformation of proteins. *Accoun. Chem. Res.*, **1** (3), 65-70 (1968).

Eggeling, C.; Ringemann, C.; Medda, R.; Schwarzmann, G.; Sandhoff, K.; Polyakova, S.; Belov, V. N.; Hein, B.; von Middendorff, C.; Schönle, A.; Hell, S.W. Direct observation of

the nanoscale dynamics of membrane lipids in a living cell. *Nature*, **457** (7233), 1159-1162 (2009).

Eisenberg, M.; Gresalfi, T.; Riccio, T.; McLaughlin, S. Adsorption of monovalent cations to bilayer membranes containing negative phospholipids. *Biochem.*, **18** (23), 5213-5223 (1979).

Enoki, S.; Maki, K.; Inobe, T.; Takahashi, K.; Kamagata, K.; Oroguchi, T.; Nakatani, H.; Tomoyori, T.; Kuwajima, K. The equilibrium unfolding intermediate observed at pH 4 and its relationship with the kinetic folding intermediates in green fluorescent protein. *J. Mol. Biol.*, **361** (5), 969-982 (2006).

Enoki, S.; Saeki, K.; Maki, K.; Kuwajima, K. Acid denaturation and refolding of green fluorescent protein. *Biochem.*, **43**, 14238-14248 (2004).

Ferrari, D.; Peracchi, A. A continuous kinetic assay for RNA-cleaving deoxyribozymes, exploiting ethidium bromide as an extrinsic fluorescent probe. *Nucl. Acids Res.*, **30** (20), e112 (2002).

Fischer, A.; Franco, A.; Oberholzer, T. Giant vesicles as microreactors for enzymatic mRNA synthesis. *Chembiochem*, **3**, 409-417 (2002).

Florián, J.; Baumruk, V.; Leszczyński, J. IR and Raman spectra, tautomeric stabilities, and scaled quantum mechanical force fields of protonated cytosine. *J. Phys. Chem.*, **100** (13), 5578-5589 (1996).

Fox, C. B.; Uibel, R. H.; Harris, J. M. Detecting phase transitions in phosphatidylcholine vesicles by raman microscopy and self-modeling curve resolution . *J. Phys. Chem. B*, **111** (39), 11428-11436 (2007).

Frauenfeld, J.; Gumbart, J.; Sluis, E. O. V. D.; Funes, S.; Gartmann, M.; Beatrix, B.; Mielke, T.; Berninghausen, O.; Becker, T.; Schulten, K.; Beckmann, R. Cryo-EM structure of the ribosome-SecYE complex in the membrane environment. *Nat. Struc. Mol. Biol.*, **18** (5), 614-621 (2011).

Fukuda, H.; Arai, M.; Kuwajima, K. Folding of green fluorescent protein and the Cycle3 mutant. *Biochem.*, **39**, 12025-12032 (2000).

Giatrellis, S.; Nounesis, G. Nucleic acid-lipid membrane interactions studied by DSC. *J. Pharm. Bioall. Sci.*, **3** (1), 70-76 (2011).

Giel-Pietraszuk, M.; Barciszewski, J. A nature of conformational changes of yeast tRNAPhe: High hydrostatic pressure effects. *Int. J. Biol. Macromol.*, **37** (3), 109-114 (2005).

Gregoire, C. J.; Gautheret, D.; Loret, E. P. No tRNA3Lys Unwinding in a complex with HIVNCp7. *J. Biol. Chem.*, **272**(40), 25143-25148 (1997).

Gromelski, S.; Brezesinski, G. DNA condensation and interaction with zwitterionic phospholipids mediated by divalent cations. *Langmuir*, **22** (14), 6293-6301 (2006).

Guo, W.; Kurze, V.; Huber, T.; Afdhal, N. H.; Beyer, K.; Hamilton, J. A. A solid-state NMR study of phospholipid-cholesterol interactions: Sphingomyelin-cholesterol binary systems. *Biophys. J.*, **83** (3), 1465-1478 (2002).

Guo, X.; Cui, B.; Li, H.; Gong, Z.; Guo, R. Facilitation effect of oligonucleotide on vesicle formation from single-chained cationic surfactant - Dependences of oligonucleotide sequence and size and surfactant structure. *J. Polymer Sci. Part A: Polymer Chem.*, **47** (2), 434-449 (2009).

Guo, Z.; Rüegger, H.; Kissner, R.; Ishikawa, T.; Willeke, M.; Walde, P. Vesicles as soft templates for the enzymatic polymerization of aniline. *Langmuir*, **25** (19), 11390-11405 (2009).

Hammann, C.; Lilley, D. M. J. Folding and activity of the hammerhead ribozyme. *ChemBioChem*, **3** (8), 690-700 (2002).

Hannon, G. J. RNA Interference. *Nature*, **418** (6894), 244-251 (2002).

Hayashi, K.; Shimanouchi, T.; Kato, K.; Miyazaki, T.; Nakamura, A.; Umakoshi, H. Span 80 vesicles have a more fluid, flexible and " wet" surface than phospholipid liposomes. *Colloid Surf. B*, **87** (1), 28-35 (2011).

Heberle, F. A.; Wu, J.; Goh, S.L.; Petruzielo, R. S.; Feigenson, G. W. Comparison of three ternary lipid bilayer mixtures: FRET and ESR reveal nanodomains. *Biophys. J.*, **99** (10), 3309-3318 (2010).

Hirsch-Lerner, D.; Barenholz, Y. Hydration of lipoplexes commonly used in gene delivery: Follow-up by laurdan fluorescence changes and quantification by differential scanning calorimetry. *Biochim. Biophys. Acta – Biomembranes*, **1461** (1), 47-57 (1999).

Ichimori, H.; Hata, T.; Matsuki, H.; Kaneshina, S. Effect of unsaturated acyl chains on the thermotropic and barotropic phase transitions of phospholipid bilayer membranes. *Chem. Phys. Lipids*, **100**, 151-164 (1990).

Ishikawa, K.; Sato, K.; Shima, Y.; Urabe, I.; Yomo, T. Expression of a cascading genetic network within liposomes. *FEBS Lett.*, **576**, 387-390 (2004).

Janas, T.; Janas, T.; Yarus, M. Specific RNA binding to ordered phospholipid bilayers. *Nucl. Acids Res.*, **34**, 2128-2136 (2006).

Jeon, J. -H.; Monne, H. M. -S.; Javanainen, M.; Metzler, R. Anomalous diffusion of phospholipids and cholesterols in a lipid bilayer and its origins. *Phys. Rev. Lett.*, **109** (18), 188103 (2012).

Johnson, N. P.; Baase, W. A.; Von Hiel, P. H. Low energy CD of RNA hairpin unveils a loop conformation required for λN antitermination activity. *J. Biol. Chem.*, **280** (37), 32177-32183 (2005).

Juhasza, J, Davisa, J. H.; Sharomb, F. J. Fluorescent probe partitioning in GUVs of binary phospholipid mixtures: Implications for interpreting phase behavior. *Biochim. Biophys. Acta – Biomembranes*, **1818** (1), 19-26 (2011).

Kato, A.; Shindo, E.; Sakaue, T.; Tsuji, A.; Yoshikawa, K. Conformational transition of giant DNA in a confined space surrounded by a phospholipid membrane. *Biophys. J.*, **97** (6), 1678-1686 (2009).

Kato, A.; Tsuji, A.; Yanagisawa, M.; Saeki, D.; Juni, K.; Morimoto, Y.; Yoshikawa, K. Phase

separation on a phospholipid membrane inducing a characteristic localization of DNA accompanied by its structural transition. *J. Phys. Chem. Lett.*, **1** (23), 3391-3395 (2010).

Kato, A.; Yanagisawa, M.; Sato, Y.T.; Fujiwara, K.; Yoshikawa, K. Cell-Sized confinement in microspheres accelerates the reaction of gene expression. *Scientif. Rep.*, **2**, 283 (2012).

Kikuchi, I. S.; Viviani, W.; Carmona-Ribeiro, A. M. Nucleotide insertion in cationic bilayers. *J. Phys. Chem. A*, **103** (40), 8050-8055 (1999).

Kiskowski, M. A.; Kenworthy, A. K. In silico characterization of resonance energy transfer for disk-shaped membrane domains. *Biophys. J.*, **92** (9), 3040–3051 (2007).

Klein, E.; Ciobanu, M.; Klein, J.; MacHi, V.; Leborgne, C.; Vandamme, T.; Frisch, B.; Pons, F.; Kichler, A.; Zuber, G.; Lebeau, L. "HFP" fluorinated cationic lipids for enhanced lipoplex stability and gene delivery. *Bioconj. Chem.*, **21** (2), 360-371 (2010).

Klein, E.; Leborgne, C.; Ciobanu, M.; Klein, J.; Frisch, B.; Pons, F.; Zuber, G.; Scherman, D.; Kichler, A.; Lebeau, L. Nucleic acid transfer with hemifluorinated polycationic lipids. *Biomater.*, **31** (17), 4781-4788 (2010).

Kobs, G. Isolation of RNA from plant, yeast, and bacteris. *Promega Notes*, **68**, 28 (1998).

Korner, D.; Benita, S.; Albrecht, G.; Baszkin, A. Surface properties of mixed phospholipid-stearylamine monolayers and their interaction with a non-ionic surfactant (poloxamer). *Colloid Surf. B*, **3**, 101-109 (1994)

Korostelev, A.; Trakhanov, S.; Laurberg, M.; Noller, H. F. Crystal structure of a 70S ribosome-tRNA complex reveals functional interactions and rearrangements. *Cell*, **126** (6), 1065-1077 (2006).

Koynova, R.; Tenchov, B. Cationic phospholipids: Structure-transfection activity relationships. *Soft Matt.*, **5** (17), 3187-3200 (2009).

Kuboi, R.; Mawatari, T.; Yoshimoto, M. Oxidative refolding of lysozyme assisted by negatively charged liposomes: Relationship with lysozyme-mediated fusion of liposomes. *J. Biosci. Bioeng.*, **90**, 14-19 (2000).

Kuboi, R.; Umakoshi, H. Analysis and separation of amyloid β-peptides using aqueous two-phase systems under stress conditions - From aqueous two-phase system to liposome membrane system. *Solv. Extr. Res. Dev. Jpn.*, **13**, 9-21 (2006).

Kuboi, R.; Yano, K.; Komasawa, I. Evaluation of surface properties and partitioning of proteins in aqueous two-phase extraction systems. *Solv. Extr. Res. Dev. Jpn.*, **1**, 42-52 (1994).

Kucerka, N.; Pencer, J.; Sachs, J.N.; Nagle, J.F.; Katsaras, J. Curvature effect on the structure of phospholipid bilayers. *Langmuir*, **23**, 1292-1299 (2007).

Kurihara, K.; Tamura, M.; Shohda, K.-I.; Toyota, T.; Suzuki, K.; Sugawara, T. Self-reproduction of supramolecular giant vesicles combined with the amplification of encapsulated DNA. *Nat. Chem.*, **3** (10), 775-781 (2011).

Kuruma, Y.; Stano, P.; Ueda, T.; Luisi, P. L. A synthetic biology aroach to the construction of membrane proteins in semi-synthetic minimal cells. *Biochim. Biophys. Acta-Biomembranes*, **1788** (2), 567-574 (2009).

Kurz, A.; Bunge, A.; Windeck, A. -K.; Rost, M.; Flasche, W.; Arbuzova, A.; Strohbach, D.; Muller, S.; Liebscher, J.; Huster, D.; Herrmann, A. Lipid-anchored oligonucleotides for stable double-helix formation in distinct membrane domains. *Angew. Chem. Int. Ed.*, **45** (27), 4440-4444 (2006).

Lanir, A.; Yu, N. T. A Raman spectroscopic study of the interaction of divalent metal ions with adenine moiety of adenosine 5'-triphosphate. *J. Biol. Chem.*, **254** (13), 5882-5887 (1979).

Laso, M. R. V.; Zhu, D.; Sagliocco, F.; Brown, A. J. P.; Tuite, M. F.; McCarthy, J. E. G. Inhibition of translational initiation in the yeast Saccharomyces cerevisiae as a function of the stability and position of hairpin structures in the mRNA leader. *J. Biol. Chem.*, **268**, 6453–6462 (1993).

Lentz, B. R.; Barenholz, Y.; Thompson, T. E. Fluorescence depolarization studies of phase transitions and fluidity in phospholipid bilayers. 2 Two-component phosphatidylcholine

liposomes. *Biochem.*, **15**, 4529-4537 (1976)

Lentz, B. R. Use of fluorescent probes to monitor molecular order and motions within liposome bilayers. *Chem. Phys. Lipids*, **64** (1-3), 99-116 (1993).

Leontis, N. B.; Stombaugh, J.; Westhof, E. The non-Watson-Crick base pairs and their associated isostericity matrices. *Nucl. Acids Res.*, **30** (16), 3497-3531 (2002).

Lilley, D. M. J. Structure, folding and mechanisms of ribozymes. *Curr. Opin. Struc. Biol.*, **15** (3 SPEC. ISS.), 313-323 (2005).

Lingwood, D.; Simons, K. Lipid rafts as a membrane-organizing principle. *Science*, **327** (5961), 46-50 (2010).

Liu, S.; Lu, G. Interaction of cationic vesicle with ribonucleotides (AMP, ADP, and ATP) and physicochemical characterization of DODAB/ribonucleotides complexes. *Biophys. Chem.*, **127** (1-2), 19-27 (2007).

Liu, Y.; Nagle, J. F. Diffuse scattering provides material parameters and electron density profiles of biomembranes. *Phys. Rev. E. Statistical, Nonlinear, and Soft Matter Physics*, ***69*** (41), 040901-1-040901-4 (2004).

Lobo, B. A.; Rogers, S. A.; Choosakoonkriang, S.; Smith, J. G.; Koe, G.; Middaugh, C. R. Differential scanning calorimetric studies of the thermal stability of plasmid DNA complexed with cationic lipids and polymers. *J. Pharm. Sci.*, **91** (2), 454-466 (2002).

Lonez, C.; Vandenbranden, M.; Ruysschaert, J. -M. Cationic liposomal lipids: From gene carriers to cell signaling. *Prog. Lipid Res.*, **47** (5), 340-347 (2008).

Luckey, M. Membrane Structural Biology With Biochemical and Biophysical Foundations. *Cambridge University Press*, New York, U.S.A. (2008).

Luisi, P. L. Chemical aspects of synthetic biology. *Chem. Biodivers.*, **4** (4), 603-621 (2007).

Macdonald, R. C.; Rakhmanova, V. A.; Choi, K. L.; Rosenzweig, H. S.; Lahiri, M. K. O-ethylphosphatidylcholine: A metabolizable cationic phospholipid which is a serum-compatible DNA transfection agent. *J. Pharm. Sci.*, **88** (9), 896-904 (1999).

Madore, E.; Florentz, C.; Giege, R.; Lapointe, J. Magunesium-dependent alternative foldings of active and inactive Escherichia coli tRNAGlu revealed by chemical probing. *Nucl. Acids Res.*, **27** (17), 3583-3588 (1999).

Marrink, S. J.; De Vries, A. H.; Mark, A. E. Coarse grained model for semiquantitative lipid simulations. *J. Phys. Chem. B*, **108** (2), 750-760 (2004).

Marsden, S.; Nardelli, M.; Linder, P.; McCarthy, J. E. G. Unwinding single RNA molecules using helicases involved in eukaryotic translation initiation. *J. Mol. Biol.*, **361** (2), 327-335 (2006).

Marty, R.; N'soukpoe-Kossi, C. N.; Charbonneau, D. M.; Kreplak, L.; Tajmir-Riahi, H. -A. Structural characterization of cationic lipid-tRNA complexes. *Nucl. Acids Res.*, **37** (15), 5197-5207 (2009).

Mathlouthi, M.; Seuvre, A. M.; Koenig, J. L. F.T.-I.R. and laser-raman spectra of guanine and guanosine. *Carbohydrate Res.*, **146** (1), 15-27 (1986).

Michanek, A.; Kristen, N.; Höök, F.; Nylander, T.; Sparr, E. RNA and DNA interactions with zwitterionic and charged lipid membranes - A DSC and QCM-D study. *Biochim. Biophys. Acta – Biomembranes*, **1798** (4), 829-838 (2010).

Michanek, A.; Yanez, M.; Wacklin, H.; Hughes, A.; Nylander, T.; Sparr, E. RNA and DNA association to zwitterionic and charged monolayers at the air-liquid interface. *Langmuir*, **28** (25), 9621-9633 (2012).

Milani, S.; Berti, D.; Dante, S.; Hauss, T.; Baglioni, P. Intercalation of single-strand oligonucleotides between nucleolipid anionic membranes: A neutron diffraction study. *Langmuir*, **25** (7), 4084-4092 (2009).

Morozkin, E. S.; Laktionov, .; Rykova, E. Y.; Vlassov, V. V. Fluorometric quantification of RNA and DNA in solutions containing both nucleic acids. *Analyt. Biochem.*, **322** (1), 48-50 (2003).

Muñoz-Úbeda, M.; Rodríguez-Pulido, A.; Nogales, A.; Martín-Molina, A.; Aicart, E.;

Junquera, E. Effect of lipid composition on the structure and theoretical phase diagrams of DC-Chol/DOPE-DNA lipoplexes. *Biomacromol.*, **11** (12), 3332-3340 (2010).

Murtas, G.; Kuruma, Y.; Bianchini, P.; Diaspro, A.; Luisi, P. L. Protein synthesis in liposomes with a minimal set of enzymes . *Biochem. Biophys. Res. Comm.*, **363** (1), 12-17 (2007).

Nagatomo, S.; Nagai, M.; Kitagawa, T. A new way to understand quaternary structure changes of hemoglobin upon ligand binding on the basis of UV-resonance Raman evaluation of intersubunit interactions. *J. Am. Chem. Soc.*, **133** (26), 10101-10110 (2011).

Navarro, J. -A.; Flores, R. Characterization of the initiation sites of both polarity strands of a viroid RNA reveals a motif conserved in sequence and structure. *EMBO J.*, **19** (11), 2662-2670 (2000).

Ngo, K. X.; Umakoshi, H.; Shimanouchi, T.; Sugaya, H.; Kuboi, R. Chitosanase displayed on liposome can increase its activity and stability. *J. biotechnol.*, **146** (3), 105-113 (2010).

Niu, S.; Gopidas, K. R.; Turro, N. J.; Gabor, G. Formation of premicellar clusters of 2-p-toluidinonaphthalene-6-sulfonate with cationic detergents. *Langmuir*, **8** (5), 1271-1277 (1992).

Noireaux, V.; Libchaber, A. A vesicle bioreactor as a step toward an artificial cell assembly. *Proc. Nat. Acad. Sci. U. S. A.*, **101** (51), 17669-17674 (2004).

Nozaki, Y.; Tanford, C. The solubility of amino acids and two glycine peptides in aqueous ethanol and dioxane solutions. *J. Biol. Chem.*, **246** (7), 2211-2217 (1971).

Oberholzer, T.; Neirhaus, K. H.; Luisi, P. L. Protein expression in liposomes. *Biochem. Biophys. Res. Comm.*, **261**, 238-241 (1999).

Onda, M.; Yoshihara, K.; Koyano, H.; Ariga, K.; Kunitake, T. Molecular recognition of nucleotides by the guanidinium unit at the surface of aqueous micelles and bilayers. A comparison of microscopic and macroscopic interfaces. *J. Am. Chem. Soc.*, **118** (36), 8524-8530 (1996).

Orendorff, C. J.; Ducey Jr., M. W.; Pemberton, J. E. Quantitative correlation of Raman

spectral indicators in determining conformational order in alkyl chains. *J. Phys. Chem. A*, **106** (30), 6991-6998 (2002).

Otto, P.; Kephart, D.; Bitner, R.; Huber, S.; Volkerding, K. Separate isolation of genomic DNA and total RNA from single samples using the SV total RNA isolation system. *Promega Notes*, **69**, 19 (1998).

Parasassi, T.; De Stasio, G.; Ravagnan, G.; Rusch, R.M.; Gratton, E. Quantitation of lipid phases in phospholipid vesicles by the generalized polarization of Laurdan fluorescence. *Biophys. J.*, **60** (1), 179-189 (1991).

Parasassi, T.; Gratton, E. Membrane lipid domains and dynamics as detected by Laurdan fluorescence. *J. Fluoresc.*, **5** (1), 59-69 (1995).

Parasassi, T.; Krasnowska, E. K.; Bagatolli, L.; Gratton, E. Laurdan and prodan as polarity-sensitive fluorescent membrane probes. *J. Fluoresc.*, **8** (4), 365-373 (1998).

Patel, D. J.; Suri, A. K. Structure, recognition and discrimination in RNA aptamer complexes with cofactors, amino acids, drugs and aminoglycoside antibiotics. *Rev. Mol. Biotechnol.*, **74** (1), 39-60 (2000).

Pathak, P.; London, E. Measurement of lipid nanodomain (Raft) formation and size in sphingomyelin/POPC/cholesterol vesicles shows TX-100 and transmembrane helices increase domain size by coalescing preexisting nanodomains but do not induce domain formation. *Biophys. J.* **101** (10), 2417-2425 (2011).

Patil, S. D.; Rhodes, D. G. Conformation of oligodeoxynucleotides associated with anionic liposomes. *Nucl. Acids Res.*, **28** (21), 4125-4129 (2000).

Peetla, C.; Stine, A.; Labhasetwar, V. Biophysical interactions with model lipid membranes: Alications in drug discovery and drug delivery. *Mol. Pharm.*, **6** (5), 1264-1276 (2009).

Pillot, T.; Goethals, M.; Vanloo, B.; Talussot, C.; Brasseur, R.; Vandekerckhove, J.; Rosseneu, M.; Lins, L. Fusogenic properties of the C-terminal domain of the Alzheimer β- amyloid peptide. *J. Biol. Chem.*, **271** (46), 28757-28765 (1996).

Ptak, M.; Eqret-Charlie, M.; Sanson, A.; Bouloussa, O. A NMR study of the ionization of fatty acids, fatty amines and N-acylamino acids incorporated in phosphatidylcholine vesicles. *Biocim. Biophys. Acta*, **600**, 387-397 (1980).

Ricardo, A.; Szostak, J. W. Origin of life on earth. *Scientif. Am.*, **301** (3), 54-61 (2009).

Šachl, R.; Humpolíčková, J.; Štefl, M.; Johansson, L. B.; Hof, M. Limitations of electronic energy transfer in the determination of lipid nanodomain sizes. *Biophys. J.*, **101** (11), L60-L62 (2011).

Sasaki, M.; Nakasato, I.; Sugiura, H.; Fujita, H.; Sakata, T. Estimation of an index of hydrophobicity of DNA interior using 5-methoxypsoralen as a fluorescent probe. *Photochem. Photobiol.*, **46** (4), 551-555 (1987).

Sawasaki, T.; Ogasawara, T.; Morishita, R.; Endo, Y. A cell-free protein synthesis system for high-throughput proteomics. *Proc. Nat. Acad. Sci. U. S. A.*, **99** (23), 14652-14657 (2002).

Schmidt, M. L.; Ziani, L.; Boudreau, M.; Davis, J. H. Phase equilibria in DOPC/DC: Conversion from gel to subgel in two component mixtures. *J. Chem. Phys.*, **131** (17), 175103 (2009).

Shih, P.; Pedersen, L. G.; Gibbs, P. R.; Wolfenden, R. Hydrophobicities of the nucleic acid bases: Distribution coefficients from water to cyclohexane. *J. Mol. Biol.*, **280** (3), 421-430 (1998).

Shimanouchi, T.; Oyama, E.; Vu, H. T.; Ishii, H.; Umakoshi, H.; Kuboi, R. Monitoring of membrane damages by dialysis treatment: Study with membrane chip analysis. *Desalination Water Treat.*, **17** (1-3), 45-51 (2010).

Shimanouchi, T.; Sasaki, M.; Hiroiwa, A.; Yoshimoto, N.; Miyagawa, K.; Umakoshi, H.; Kuboi, R. Relationship between the mobility of phosphocholine headgroups of liposomes and the hydrophobicity at the membrane interface: A characterization with spectrophotometric measurements. *Colloid. Surf. B*, **88** (1), 221-230 (2011).

Shimanouchi, T.; Shimauchi, N.; Nishiyama, K.; Vu, H. T.; Yagi, H.; Goto, Y.; Umakoshi, H.;

Kuboi, R. Characterization of amyloid β fibrils with an aqueous two-phase system: Implications of fibril formation. *Solv. Extr. Res. Dev. Jpn.*, **17**, 121-128 (2010).

Shimanouchi, T.; Shimauchi, N.; Ohnishi, R.; Kitaura, N.; Yagi, H.; Goto, Y.; Umakoshi, H.; Kuboi, R. Formation of spherulitic amyloid β aggregate by anionic liposomes. *Biochem. Biophys. Res. Comm.*, **426** (2), 165-171 (2012).

Singh, J. S. FTIR and Raman spectra and fundamental frequencies of 5-halosubstituted uracils: 5-X-uracil (X = F, Cl, Br and I). *Spectrochim. Acta - Part A: Mol. Biomol. Spectr.*, **87**, 106-111 (2012).

Spirin, A. S.; Baranov, V. I.; Ryabova, L. A.; Ovodov, S. Y.; Alakhov, Y. B. A continuous cell-free translation system capable of producing polypeptides in high yield. *Science*, **242**, 1162-1164 (1988).

Spirin, A. S. High-throughput cell-free systems for synthesis of functionally active proteins. *Trend. Biotechnol.*, **22** (10), 538-545 (2004).

Stano, P.; Carrara, P.; Kuruma, Y.; Pereira De Souza, T.; Luisi, P. L. Compartmentalized reactions as a case of soft-matter biotechnology: Synthesis of proteins and nucleic acids inside lipid vesicles. *J. Mater. Chem.*, **21** (47), 18887-18902 (2011).

Stephanos, J. J.; Farina, S. A.; Addison, A. W. Iron ligand recognition by monomeric hemoglobins. *Biochim. Biophys. Acta- Prot. Struc. Mol. Enzymol.*, **1295** (2), 209-221 (1996).

Strobel, S. A.; Cochrane, J. C. RNA catalysis: ribozymes, ribosomes, and riboswitches. *Curr. Opin. Chem. Biol.*, **11** (6), 636-643 (2007).

Strulson, C. A., Molden, R. C., Keating, C. D., Bevilacqua, P. C. RNA catalysis through compartmentalization. *Nat. Chem.*, **4** (11), 941-946 (2012).

Suga, K.; Tanabe, T.; Tomita, H.; Shimanouchi, T.; Umakoshi, H. Conformational change of single-stranded RNAs induced by liposome binding. *Nucl. Acids Res.*, **39** (20), 8891-8900 (2011).

Sugaya, H.; Umakoshi, H.; Fadzil, K. B. M. A.; Tuan, Q.; Shimanouchi, T.; Kuboi, R.. Preparation of superoxide dismutase LIPOzyme in hollow fiber membrane module. *Desalination Water Treat.*, **17** (1-3) , 281-287 (2010).

Swartz, J. Developing cell-free biology for industrial alications. *J. Industr. Microbiol. Biotechnol.*, **33** (7), 476-485 (2006).

Tachibana, R.; Harashima, H.; Ishida, T.; Shinohara, Y.; Hino, M.; Terada, H.; Baba, Y.; Kiwada, H. Effect of cationic liposomes in an in vitro transcription and translation system. *Biol. Pharm. Bull.*, **25** (4), 529-531 (2002).

Tanaka, Y.; Kasai, Y.; Mochizuki, S.; Wakisaka, A.; Morita, E. H.; Kojima, C.; Toyozawa, A.; Kondo, Y.; Taki, M.; Takagi, Y.; Inoue, A.; Taira, K. Nature of the chemical bond formed with the structural metal ion at the A9/G10.1 motif derived from hammerhead ribozymes. *J. Am. Chem. Soc.*, **126** (3), 744-752 (2004).

Taran, V. D.; Wick, R.; Walde, P. A 1H nuclear magnetic resonance method for investigating the phospholipase D-catalyzed hydrolysis of phosphatidylcholine in liposomes. *Analyt. Biochem.*, **240**, 37-47 (1996).

Thomas, C. F.; Luisi, P. L. RNA selectively interacts with vesicles depending on their size. *J. Phys. Chem. B*, **109** (30), 14544-14550 (2005).

Tocanne, J. F.; Teissie, J. Ionization of phospholipids and phospholipid-suorted interfacial lateral diffusion of protons in membrane model systems. *Biochim. Biophys. Acta*, **1031**, 111-142 (1990).

Troutier, A. -L.; Véron, L.; Delair, T.; Pichot, C.; Ladavière, C. New insights into self-organization of a model lipid mixture and quantification of its adsorption on spherical polymer particles. *Langmuir*, **21** (22), 9901-9910 (2005).

Tsuji, A.; Yoshikawa, K. Real-time monitoring of RNA synthesis in a phospholipid-coated microdroplet as a live-cell model. *ChemBioChem*, **11** (3), 351-357 (2010).

Tuan, L. Q.; Umakoshi, H.; Shimanouchi, T.; Kuboi, R. Liposome-recruited activity of

oxidized and fragmented superoxide dismutase. *Langmuir*, **24**, 350-354 (2008).

Tzareva, B. N. V. Ribosome-messenger recognition in the absence of the Shine-Dalgarno interactions. *FEBS Lett.*, **337** (2), 189-194 (1994).

Umakoshi, H.; Morimoto, K.; Ohama, Y.; Nagami, H.; Shimanouchi, T.; Kuboi, R. Liposome modified with Mn-porphyrin complex can simultaneously induce antioxidative enzyme-like activity of both superoxide dismutase and peroxidase. *Langmuir*, **24**, 4451-4455 (2008).

Umakoshi, H.; Nishida, A. Modulation of yeast hexokinase on bio-inspired membranes. *Biochem. Eng. J.*, **69**, 138–143 (2012).

Umakoshi, H.; Tuan, L. Q.; Shimanocuhi, T.; Kuboi, R. Role of liposome on recognition and folding of oxidized and fragmented superoxide dismutase for its re-activation. *Biochem. Eng. J.*, **46** (3), 313-319 (2009).

Umakoshi, H.; Yoshimoto, N.; Yoshimoto, M.; Shimanouchi, T.; Kuboi, R. Characterization of surface properties of microbial transglutaminase using aqueous two-phase partitioning method. *Solv. Extr. Res. Dev. Jpn.*, **15**, 111-115 (2008).

Veatch, S. L.; Keller, S. L. Miscibility phase diagrams of giant vesicles containing sphingomyelin. *Phys. Rev. Lett.*, **94** (14), 148101 (2005).

Viard, M.; Gallay, J.; Vincent, M.; Meyer, O.; Robert, B.; Paternostre, M. Laurdan solvatochromism: Solvent dielectric relaxation and intramolecular excited-state reaction. *Biophys. J.*, **73** (4), 2221-2234 (1997).

Walde, P. Phospholipid membranes as regulators of localized activity. *Chem. Biol.*, **17** (9), 922-923 (2010).

Walde, P. Building artificial cells and protocell models: Experimental aroaches with lipid vesicles. *BioEssays*, **32** (4), 296-303 (2010).

Xu, L.; Anchordoquy, T. J. Cholesterol domains in cationic lipid/DNA complexes improve transfection. *Biochim. Biophys. Acta – Biomembranes*, **1778** (10), 2177-2181 (2008).

Xu, Y.; Szoka Jr., F. C. Mechanism of DNA release from cationic liposome/DNA complexes used in cell transfection. *Biochem.*, **35** (18), 5616-5623 (1996).

Yeagle, P. The Structure of Biological Membranes, 2nd Ed. *CRC Press* (2005).

Yoo, J. -W.; Irvine, D. J.; Discher, D. E.; Mitragotri, S. Bio-inspired, bioengineered and biomimetic drug delivery carriers. *Nat. Rev. Drug Discov.*, **10** (7), 521-535 (2011).

Yoshimoto, M. Studies on protein refolding process and stress-responsive functional materials using liposomes. PhD thesis, Osaka University (1999).

Yoshimoto, M.; Kuboi, R.; Yang, Q.; Miyake, J. Immobilized liposome chromatography for studies of protein-membrane interactions and refolding of denatured bovine carbonic anhydrase. *J. Chromatogr. B*, **712**, 59-71 (1998).

Yoshimoto, M.; Miyazaki, Y.; Umemoto, A.; Walde, P.; Kuboi, R.; Nakao, K. Phosphatidylcholine vesicle-mediated decomposition of hydrogen peroxide. *Langmuir*, **23**, 9416-9422 (2007).

Yoshimoto, M.; Shimanouchi, T.; Umakoshi, H.; Kuboi, R. Immobilized liposome chromatography for refolding and purification of protein. *J. Chromatogr. B: Biomed. Sci. Alicat.*, **743** (1-2), 93-99 (2000).

Yoshimoto, N. Study on interactively-induced function of Aβ and liposome under stress condition. PhD thesis, Osaka University (2005).

Yoshimoto, N.; Tasaki, M.; Shimanouchi, T.; Umakoshi, H.; Kuboi, R. Oxidation of cholesterol catalyzed by amyloid β-peptide (Aβ)-Cu complex on lipid membrane. *J. Biosci. Bioeng.*, **100** (4), 455-459 (2005).

Yoshimoto, N.; Yoshimoto, M.; Yasuhara, K.; Shimanouchi, T.; Umakoshi, H.; Kuboi, R. Evaluation of temperature and guanidine hydrochloride-induced protein-liposome interactions by using immobilized liposome chromatography. *Biochem. Eng. J.*, **29** (3), 174-181 (2006).

Yu, W.; Sato, K.; Wakabayashi, M.; Nakaishi, T.; Ko-Mitamura, E. P.; Shima, Y.; Urabe, I.

Yomo, T. Synthesis of functional protein in liposome. *J. Biosci. Bioeng.*, **92**, 590-593 (2001).

Yuan, C.; Furlong, J.; Burgos, P.; Johnston, L. J. The size of lipid rafts: An atomic force microscopy study of ganglioside GM1 domains in sphingomyelin/DOPC/cholesterol membranes. *Biophys. J.*, **82** (5), 2526-2535 (2002).

Zardeneta, G.; Horowitz, P. M. Detergent, liposome, and micelle-assisted protein refolding. *Analyt. Biochem.*, **223** (1), 1-6 (1994).

Zhelyaskov, V.; Yue, K. T. A Raman study of the binding of Fe(III) to ATP and AMP. *Biochem. J.*, **287** (2), 561-566 (1992).

Zimmer, M. Green fluorescent protein (GFP): Alications, structure, and photophysical behavior. *Chem. Rev.*, **102**, 759-781 (2002).

Zimmerman, S. B.; Trach, S. O. Estimation of macromolecule concentrations and excluded volume effects for the cytoplasm of Escherichia coli. *J. Mol. Biol.*, **222** (3), 599-620 (1991).

Zier, H.; Brunner, H.; Bernhagen, J.; Vitzthum, F. Investigations on DNA intercalation and surface binding by SYBR Green I, its structure determination and methodological implications. *Nucl. Acids Res.*, **32** (12), e103 (2004).

Zohra, F. T.; Chowdhury, E. H.; Nagaoka, M.; Akaike, T. Drastic effect of nanoapatite particles on liposome-mediated mRNA delivery to mammalian cells. *Analyt. Biochem.*, **345** (1), 164-166 (2005).

Zohra, F. T.; Chowdhury, E. H.; Tada, S.; Hoshiba, T.; Akaike, T. Effective delivery with enhanced translational activity synergistically accelerates mRNA-based transfection. *Biochem. Biophys. Res. Comm.*, **358** (1), 373-378 (2007).

Zou, S.; Scarfo, K.; Nantz, M. H.; Hecker, J. G. Lipid-mediated delivery of RNA is more efficient than delivery of DNA in non-dividing cells. *Int. J. Pharm.*, **389** (1-2), 232-243 (2010).

List of Publications

[Papers]

1. Hiroshi Umakoshi, Keishi Suga, Huong Thi Bui, Masato Nishida, Toshinori Shimanouchi, Ryoichi Kuboi, Charged Liposome Affects the Translation and Folding Steps of *in vitro* Expression of Green Fluorescent Protein, *J. Biosci. Bioeng.*, **108** (5), 450-454 (2009).

2. Huong Thi Bui, Hiroshi Umakoshi, Keishi Suga, Tomoyuki Tanabe, Kien Xuan Ngo, Toshinori Shimanouchi, Ryoichi Kuboi, Cationic Liposome can Interfere mRNA Translation in an *E. coli* Cell-Free Translation System, *Biochem. Eng. J.*, **52** (1), 38-43 (2010).

3. Hiroshi Umakoshi, Masato Nishida, Keishi Suga, Huong Thi Bui, Toshinori Shimanouchi, Ryoichi Kuboi, Characterization of Green Fluorescent Protein Using Aqueous Two-Phase Systems, *Solv. Extr. Res. Dev. Jpn.*, **16**, 145-150 (2009).

4. Keishi Suga, Hiroshi Umakoshi, Hibiki Tomita, Tomoyuki Tanabe, Toshinori Shimanouchi, Ryoichi Kuboi, Liposomes Destabilize tRNA during Heat Stress, *Biotechnol. J.*, **5** (5), 526-529 (2010).

5. Keishi Suga, Tomoyuki Tanabe, Hibiki Tomita, Toshinori Shimanouchi, Hiroshi Umakoshi, Conformational Change of Single-Stranded RNAs Induced by Liposome Binding, *Nucl. Acids Res.*, **39** (20), 8891-8900 (2011).

6. Hiroshi Umakoshi, Tomoyuki Tanabe, Keishi Suga, Huong Thi Bui, Toshinori Shimanouchi, Ryoichi Kuboi, Oxidative Stress can Affect the Gene Silencing Effect of DOTAP Liposome in an *in vitro* Translation System, *Int'l. J. Biol. Sci.*, **7** (3), 253-260 (2011).

7. Keishi Suga, Hibiki Tomita, Seishiro Tanaka, Hiroshi Umakoshi, Hydrophobic Properties of tRNA with Varied Conformations Evaluated by an Aqueous Two-Phase System, *Int'l. J. Biol. Sci.*, **8** (8), 1188-1196 (2012).

[Proceedings]

1. Keishi Suga, Hibiki Tomita, Seishiro Tanaka, Toshinori Shimanouchi, Hiroshi Umakoshi, Cell-free Protein Expression on Liposome Surface, *Proc. 1st Int'l. Symp. on Multiscale Multiphase Process Engineering (MMPE)*, Kanazawa, Japan, October (2011).

2. Keishi Suga, Hibiki Tomita, Seishiro Tanaka, Toshinori Shimanouchi, Hiroshi Umakoshi, Characterization of Surface Properties of DNA and RNA Using Aqueous Two-Phase System, *Proc. 9th Int'l. Conf. on Separation Science and Technology (ICSST11)*, Jeju, Korea, November (2011).

[Review Paper]

1. Hiroshi Umakoshi, Toshinori Shimanouchi, Keishi Suga, A "Membranome"– Based Approach toward "Bio–Inspired Membrane", *Membrane*, **37** (6), 264-269 (2012) (in Japanese)

[Related Papers]

1. Huong Thi Bui, Hiroshi Umakoshi, Keishi Suga, Masato Nishida, Toshinori Shimanouchi, Ryoichi Kuboi, Negatively Charged Liposome as a Potent Inhibitor of Post-Translation during *in vitro* Synthesis of Green Fluorescent Protein, *Biochem. Eng. J.*, **46** (2), 154-160 (2009).

2. Huong Thi Bui, Hiroshi Umakoshi, Keishi Suga, Tomoyuki Tanabe, Toshinori Shimanouchi, Ryoichi Kuboi, Cationic Liposome Inhibits Gene Expression in an *E. coli* Cell-Free Translation System, *Membrane*, **34** (3), 146-151 (2009).

Acknowledgements

The author is greatly indebted to Prof. Dr. Hiroshi Umakoshi (Division of Chemical Engineering, Graduate School of Engineering Science, Osaka University), for his excellent guidance and helpful advice and supports throughout this work. The author is thankful to Prof. Dr. Masahito Taya and Prof. Dr. Takayuki Hirai (Division of Chemical Engineering, Graduate School of Engineering Science, Osaka University) for a number of valuable comments and criticism during the completion of this thesis. The author is deeply grateful to Assoc. Prof. Dr. Toshinori Shimanouchi (Graduate School of Environment and Life Science, Okayama University) for his valuable comments, supports, helpful advices and discussion throughout this work.

The author is also greatly thankful to Prof. Dr. Ryoichi Kuboi (San Francisco Center for Education and Research, Osaka University) for a number of valuable comments and discussion in research group on Membrane Stress Biology. The author would like to express one's thankfulness to Prof. Dr. K. Ohgaki, Prof. Dr. K. Jitsukawa, Prof. Dr. Y. Okano, Prof. Dr. M. Nakano, Prof. Dr. N. Nishiyama, and all the staff of Division of Chemical Engineering, Graduate School of Engineering Science, Osaka University for their kind cooperation during my research. The author is also thankful to Prof. Dr. K. Kaneda (Research Center for Solar Energy Chemistry, Osaka University), Prof. Dr. K. Ueyama (Kogakuin University), Prof. Dr. Y. Inoue (Osaka University).

The author wishes to thank to Prof. Dr. P. Walde (ETH, Zurich), Prof. Dr. T. Tsuchido (Kansai University), Prof. Dr. K. Murofushi (Ochanomizu University), Prof. Dr. S. Ichikawa (University of Tsukuba), Prof. Dr. K. Kato (Ehime University), Assoc. Prof. Dr. M. Yoshimoto (Yamaguchi University), Assist. Prof. Dr. N. Yoshimoto (Yamaguchi University), Prof. Dr. H. Nakamura (Nara National College of Technology), Prof. Dr. K. Morigaki (Kobe University), Assoc. Prof. Dr. K. Shiomori (Miyazaki University), Assoc. Prof. Dr. S. Morita (Wakayama National College of Technology), Dr. H. Sugaya (Toray Industries, Inc.), Dr. Y. Yamada (Kao Corporation) for their comments and suggestions during this work. The author also thankful to Prof. Dr. M. Konno (Tohoku University), Prof. Dr. Y. Kobayashi (Ibaraki University), Prof. Dr. T. Nagamune (University of Tokyo), Prof. Dr. M. Goto (Kyusyu University), Prof. Dr. S. Nakao (Kogakuin University), Prof. Dr. H. Matsuyama (Kobe University), Prof. Dr. M. Kamihira (Kyusyu University), Prof. Dr. S. Takeoka (Waseda University), Prof. T. Oshima (Miyazaki University), Prof. Dr. A. Kumar (Indian Institute of Technology Kanpur), Prof. Dr. M. D. Amiridis (University of South Carolina), Prof. Dr. C. Williams (University of South Carolina), Prof. Dr. B. Higgins (University of California, Davis) for their valuable comments and discussion.

Special thanks are given to following colleagues for their experimental collaboration: Dr. L. Q. Tuan (Nong Lam University), Dr. H. T. Bui (Inst. Post Harvest), Dr. K. X. Ngo (University of Geneva), Dr. H. Ishii (Tohoku University), Dr. V. T. Huong (Hanoi National University of Education), Dr. K. Hayashi. The author also thankful to D. Ishikawa, A. Hiroiwa, M. Nishida, K. Nishiyama, T. Matsumoto, K. Morimoto, E. Oyama, N. Shimauchi, K. Murata, N. Yasuda, H. Yoshioka, R. Onishi, T. Tanabe, N. Kitaura, H. Tomota, A. Nishida, Y. Manno, P. Kiattisak, T. Ishigami, T. Tatsui, S. Tanaka, T. Yokoi, H. Mohammed, R. Teel, K. Sugita, J. Chinzaka, T. Hinoyama, N. Maruyama, F. Iwasaki, T. Katsura, M. Kiriishi, D. Kondo, Y. Takaya, T. Bando, M. Hirose and all the member in Bio-Inspired Chemical Engineering Laboratory. The author would like to express one's thankfulness to Ms. Keiko Fukumoto for her kind support during this work.

The author would like to thank his parents Yoshitsugu Suga and Mana Suga, and his sister Midori Suga for their continuous encouragements and kind support throughout this work.

The author gratefully acknowledges the financial support of this work by the fellowship of the Japan Society for the Promotion of Science (JSPS) and Global COE program "Global Education and Research Center for Bio-Environmental Chemistry".